– *An international journal for New Concepts in Geoplasma Tectonics* –

NCGT JOURNAL

Volume 8, Number 2, August 2020. ISSN 2202-0039.
Editor-in-Chief: Louis HISSINK (louis.hissink@bigpond.com)

CONTENTS

Please feel free to contact the CEO of the, Mr. Bruce Leybourne, at mail@ievpc.org.
For contact, correspondence, or inclusion of material in the NCGT Journal please use the following methods: *NEWCONCEPTSINGLOBAL TECTONICS.* 1. E-mail: louis.hissink@bigpond.com.com; 2. Mail, air express, etc., 33 Fields Road, Tanja, NSW 2550, Australia (files in MS Word or ODT format, and figures in gif, bmp or tif format) as separate files; 3. Telephone, +61 419 283 775. *DISCLAIMER*: The opinions, observations and ideas published in this journal are the responsibility of the contributors and do not necessarily reflect those of the Editor and the Editorial Board. *NCGT Journal* is a refereed quarterly international online journal and appears in March, June, September and December. For Mac computer users, this journal in pdf format must be opened with Acrobat or Acrobat Reader. *ISSN number*; ISSN 2202-0039.

From The Editor

This issue is late due to the reduction in the rate of submissions received, an understandable situation given the economic disruption of the covid-19 pandemic and related events, natural and political. I have thus received five papers and one short communication, plus an addendum for a previous paper.

An interesting paper from M.H. Asadiyan on river and earth meandering makes a cosmological link to tectonics. L and V Gordienko further report on their work of upper-mantle geophysics while Straser and the Italian team report on precursor signals using electromagnetics and radio direction monitoring. G. G. Kochemsasov compares the Moon and Mars regolith layer development from a novel trembling mechanisn. F.Tsunoda forwarded a short communication In addition I have reviewed a new book, The Hidden History of Earth Expansion.

The enormous social changes underway globally from the policy reactions to the covid-19 pandemic, whether unintended or not, has led to significant social uncertainty. There is apparently a global movement to reset the world's economies, flagged by various UN IPCC and WEF representatives over the last decade or so. It is possible this policy started during the 1970's following the Club Of Rome's report on an inferred future human population crisis. The goal of this economic reset is to reshape almost everything, principally to mitigate climate change.

I am not sure what this will mean for the NCGT Journal but as I have already experienced some mild censoring of climate change heresy as a former editor of the Australian Institute of Geoscientists Newsletter, I suspect this journal will be targeted at the appropriate time. This may mean our online internet portals could be possibly closed, and publication of the journal restricted to a private mailing list. Interested readers should contact the editor.

We are living in interesting times.

Louis A.G. Hissink M.Sc. IEEE MAIG(rtd)

River Meandering and Earth Meandering

Muhammad Hassan Asadiyan Falahiyeh
Emeritus member of Payam-e Noor University, Ahwaz/Iran

asadiyan@pnu.ac.ir

Abstract

Earth dynamics is a subject that has not yet been completely clarified. While working on our doctoral dissertation at Shiraz University, we found several remarkable conclusions. These conclusions came after a 15 years journey through the earth's morphology. The first one is that: *rivers meandering and Earth meandering are two sides of one coin;* i.e. understanding of one can help to understand the other. The second find is that: *geodynamics is driven by rotation and gravitation*. The third find is that: *geodynamics is made up of two components, Dahw(spiralling) and Tahw(spreading)*. All the geomorphological evidence suggests that the spiraling of layers on the Earth's surface originated from a galactic spiral field which once flared up in the center of the Earth. The first D/T cell arms emerged from Mecca (Geodynamic Pole, (GP)) and reached the current location in the poles after billions of years of spiraling and after the construction of oceans and continents. Earth's layers tend to circulate from most friction region (fire ring) and South Pole toward least friction region (GP) via E-W and S-N cycloidal paths. Reduction in the Earth's rotation and position of GP in the space could be responsible for Earth polarization and Magnetic Polarization. Spiraling of layers follow harmonic forms (like O, S, Ƨ, 8, Ω, ∞..). Based on the first scientific conclusion, we used measurable quantities in the river to calculate friction in the Earth which about 0.00188 which is tangent of 0.1078 degree.

Introduction

You may be surprised to learn that even the great Albert Einstein gave time to the problem of meanders. In the report delivered in 1926 at a meeting of the Russian Academy of Sciences [1], he compared the motion of river water to swirling of water in a glass. The analogy allowed him to explain why rivers choose the twisted paths.

Based on this, and in order to understand the nature of meandering in rivers and its connection with tectonics, we considered the ***Jarrahi*** River in southwestern Iran as a case study. The result of this study was an article published in 2010 [2], in which the concept of Spiral Tectonics/ST was first proposed. Dahw and Tahw [3] two components of ST. In this regard Global Wrench Tectonics [4] said- internal degassing in association with vertical mass transfer, instigating changes of the planet's moments of inertia but ST said- change in the position of GP in the space, rearranged position of oceans and continents accordingly (i.e. balance in gravitation). Wax-model [5] is a lab evidence for spiral tectonics. The first point in the area that caught our attention was morphology similar to the Möbius Strip, which makes balance between two different horizons (Figure 2). The next case is the observation of polygonal morphology. Polygonal faulting is the result of Möbius twisting at Earth surface (Figure 2, top right corner).The Möbius is made up of couple of sigmoid: (compression) and (tension). S rotates counter clockwise and Ƨ rotates clockwise. Using the concepts presented in [6], we calculated the friction in the river of ***Jarrahi*** and the Earth, which appeared to be very close to each other. In this article, we try to give the exact address of the concepts and convey the desired goals by using the explanation of the figures. I consider geomorphology as firm basement and build my concept confidently over it.

Fig. 1/a

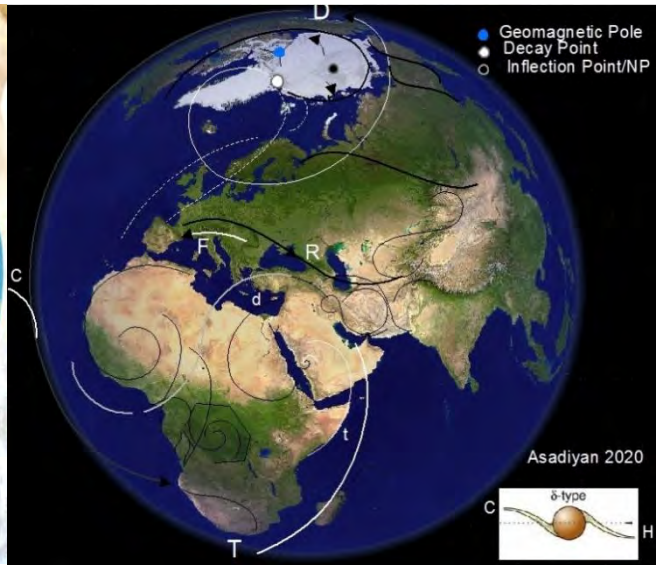

Fig. 1/b

In Fig.1/a, we could consider the Earth is a large shear globe that is characterized by African-Blast. The indicator blast is δ-type, with its right arm leading to the Himalayan (H) and it's left arm to the Caribbean Sea 'c'. The left arm is also connected to Scotia through Mid Atlantic Ridge/MAR and the right arm is connected to the Decay Point (DP) through Mid Continental Ridge/MCR (Ural Mountains). The two are morphologically similar, except that in MCR the ***spiral*** component is predominant and in MAR the ***spreading*** component is predominant. This difference has occurred due to the deviation of the Geodynamic Pole/GP to the north. The study area is located between the forward field (F) and retard field (R). The forward arm F starts from the wide African-Apex and leads to the North Pole and the Retard arm R starts from the narrow Mediterranean Apex to the South Pole. Difference in Apex-Form is referred to angle of interference between F-Field and R-Field. The Earth's axis is located at a critical divergent point. The DP (white spot) is located at a convergent critical point between Spitsbergen and Greenland. In terms of tectonics, highly dahwed Greenland is synthetic with Eurasia and highly thawed Spitsbergen synthetic with the America. The left-arm of global spiral leads to the right-arm of local spiral of the North Pole. The Earth's axis is located in the middle of Catastrophic Region (CR). *The eccentricity of the polar spiral is equal to the size of the earth's tilt angle (TA).* TA equals twice the distance of decay length/D. it seems deviation of GP from equator is also 2D. According to the f_c=h/2D [4], the friction is inversely proportional to the D, and the friction is maximized when it reaches zero (that is, the sun's orbital plane coincides with the Earth's rotating plane).

Fig. 1/b, shows the reverse spiral movement of the continents on both sides of the DP. The counter clockwise global spiral has now become the cw spiral at the North Pole after billions of years of twisting, starting with Mecca and terminated in DP, respectively. Most large seas are located in an area of spreading between Möbius e and f. Rocky Mountains and the Himalayas are inversely polarized with respect to the Sea of Japan and Sea of Bermuda (with respect to TA-axis). TP stands for tectonic pose and TT stands for tectonic tail.

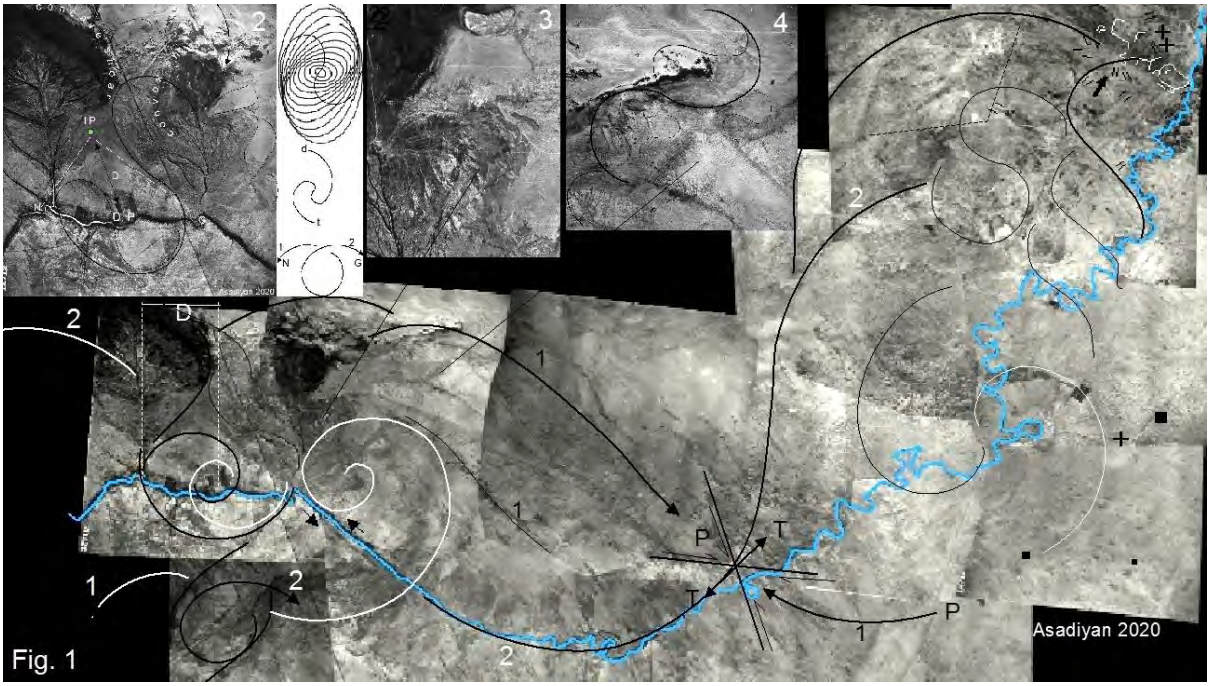

Fig 2

Fig. 2/1: This is the output of the Earth's laboratory. You can see the Jarrahi River that oscillates between counter clockwise cyclones-couple. Tuning of this pair of cyclones, caused the proximity of wings, hence the OX-BOW between them closed about 50 years ago. The river flows from Ramhormoz and Aghajari foothills in the northeast and terminates in Shadegan Delta in the southwest. Our research area is located in between two global forward and retard arms. These two boundaries are tectonically balance with a Transfer Möbius. The left wing is a right twist sigmoid (**Fig. 3/a**). The OX-BOW is created right at the cross point and indicates the relation between meandering and torsional tectonics. The P/T model is also created at the cross point. The pressure 'P' is created along the forward component (1) and the tension 'T' is created along the retard component (2). The line that runs close to the 'DP' is the Bandar Imam railway to Ahwaz, which was built before 1955 imaging. 'DP' is the center of the central bar located at a critical distance from N-G cycloid (**Fig. 2.2**). The center of the central bar has been degraded due to severe interference between the joints of the two forward and retard fields. The right bank collapse of the Al-Hamidi-Pond with a sharp apex (similar to the Möbius of the Mediterranean) with twisted and stepped water ways , and the left bank falling of the Al-Mansoura-Pond with the wide Apex (similar to the Möbius of Africa), and spiky joints resembling pine coniferous leaves. The morphological difference between the two zones is due to the dominance of one field over another. In the Al-Hamidi, pressure and twisting are dominant, but in the Al-Mansoura, expansion and tension are dominant.

Fig. 2.2, all the elements seen in this photograph are also shown in **Fig.1/b**. In fact this is a Quasi-Planet in local scale. Green point is Inflection Point (IP) of Jarrahi which is cross point of GorGor-continuation (G) and Nahr-Alshiekh-continuation (N). Interestingly these extensions are completely perpendicular and made two side of Fibonacci-Rectangle. N-G is chord of right triangle. Location of Decay Point (DP) is satisfied in Fibonacci-Proportion. Based on the Earth-Shape we inferred: one arm must be longer the other (middle sketch). Right part is galactic model of rotation. In this photograph, you can see an ellipse, which we named it a polarized ellipse. The polarized ellipse is formed by the passage of two back and forth fields '1' and '2' against each other. Passing of the two field is a Möbius, which white-loop in the area shows the part related to "Dahw" ((the action that unrolled the earth and shaped it like an egg during the procedures of its creation)) , and the grey-loop in the area shows the part related to "Tahw" ((the action that caused the earth to spread and expand during the procedures of its creation)). On Earth's scale these two parts are facing each other one to

the east and the other to the west, but on a local scale the two parts are within a polarized ellipse. The "Dahw" part resembles the continental part and the rest of the ellipse represents the oceanic part of the Earth, which appears as an ellipse on a small scale.

This model has been used to calculate river friction. The ring shown next to **Fig. 2.2**, shows the two arms of a cycloid, arm No.2 is parallel to the river in "GORGOR" (G) and arm No.1 is parallel to the river in "NAHR-ALSHEIKH" (N). By extending accompanied by reverse rolling of forward and retard of 1/2-arms , in one hand spreading occurs in the ponds, in the other hand the "N-G" ring becomes smaller ((this the "DAHW" part)). If this circular traction continues to reach 360 degrees, the concave and convex shores will cross and eventually facing each other's (Same as the morphology of E/W Pacific's shores). Due to the interference of the back and forth acting fields, the ridge between them became similar to Aleutian trench. The significant conclusion to be withdrawn here is that: *the Earth's circumference is a cosmic cycloid*.

The straight tributary in the middle of Al-Mansoura Pond is a critical line from which the spiky drains are diverted in two directions and serve as the local axis. The distance "D" in this image is about 600 meters. Based on the formula f_c=h/2D and assuming an average depth of 3 meters for the Jarrahi river, "f_c " will be about 0.0020. On the other hand assuming 1200 km of distance "D" on earth and 4.5 km average depth of the oceans, "f_c " of the Earth will be about 0.00187. Notice that the figures are very close to each other. The figures indicate the accuracy of the evidence. Decay length is a fundamental distance from which all scales are integer orders of this distance. [4].

Fig. 2.3, is a part of a larger image which is very similar to Möbius. Interestingly, on a large scale, the Tunisian tectonics exactly follows this pattern. This phenomenon tells us that a single pattern dominates earth's phenomena. The "Dahw" shaped part along with the "Diapirism" and the "Tahw" shaped part along with the "Grabens" **Fig. 3/b**. the distribution of "Diapirism" in NE Iran also follow this pattern.

Fig. 2.4, is an interesting example of the collision of two reciprocating fields and folding in the sedimentary environment of the present era. The fine system of the joints is created by the interference of these two fields and a new fold is driven on it. The angle between them depends on the local axis tilt, the local tilt itself depends on the tilt of the earth axis and this is a significant finding in tectonic.

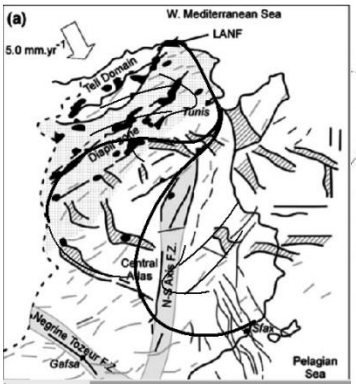

Fig 3/a

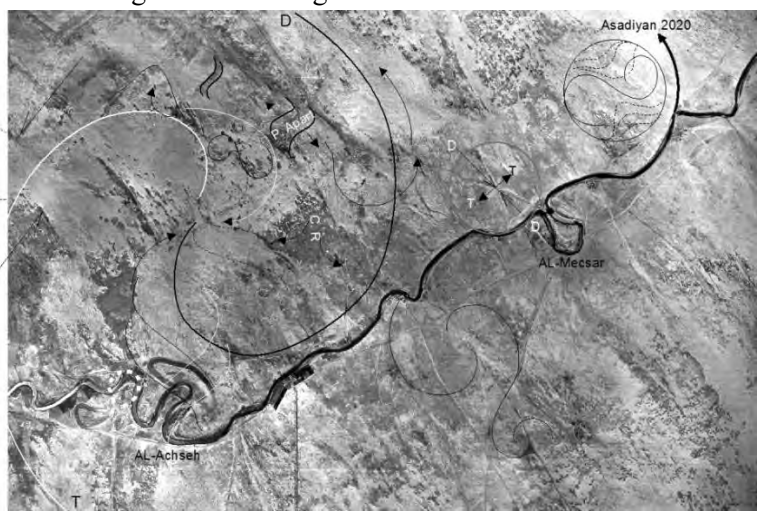

Fig 3/b

Fig. 3/a helps us to better understand the formation of spiral elements (such as the Möbius ring, the orthogonal P-T pattern, the couple cyclone, the catastrophic zones or shadow zone in the microtectonics, the pull apart basin, and the recumbent of the layers). Here you see a galaxy-like cell whose center and circumference rotate in opposite directions (like model shown in **Fig, 2.2**). Notice how the layers are inverted at the central bar.

Take a good look at the inter-arm regions; you will see a typical sample of Pull Apart basin which opens in E-W direction, created by D-arm pure shear. You will see also a beautiful layer-bending flexure along N-S direction, created by T-arm simple shear. So, we can say *certain structure formed in the particular part of spiral*. Where the layer is rotated 180 degrees, a P/T pattern or Pressure/Tension pattern is created. Where the eastern wing of Transform-Möbius has been pushed over the western wing, the Ox-bow has been created. (The Ox-Bow is called "Al-mexar" in our local language). The reason for closing is due to crossing of F/R-arms in the cross point. The two orthogonal Ox-Bow of Al-Achseh (a local name for a place in the river) indicate that the two F/R-components are orthogonal. At the present time the "Tahw"-component which is represented by white Sigmoid is predominant. The Ox-Bow Lake you see west of Al-Achseh is actually a wing of the transform Möbius-Strip, caused by the interference of two reciprocating wave fronts (the model is shown in the upper right corner).

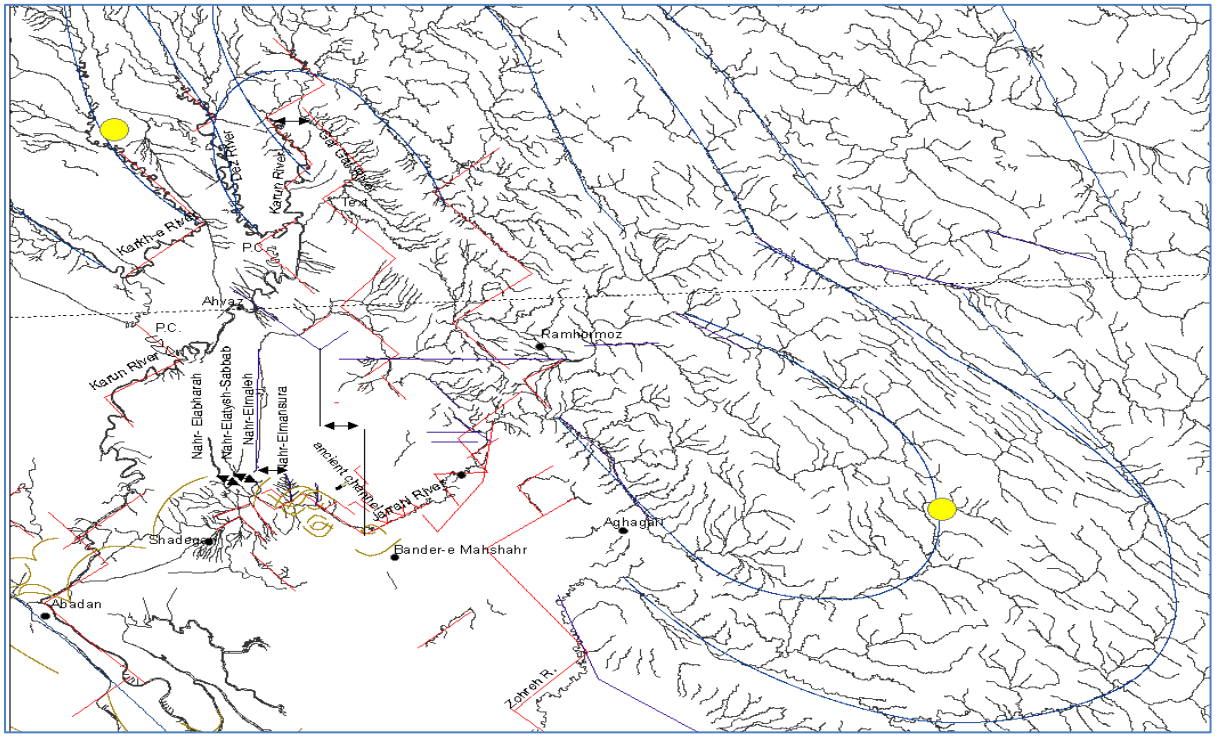

Fig. 4

Fig. 4 shows part of the Karkheh, Karun, Jarrahi and Zohreh drainage basin. These basins are created by the Möbius twist and take on a general shape similar to ∞ (it is also similar to a bird whose beak is towards Abadan), the forward segment runs from above and the backward segment runs from below Ramhormoz. The upward continuation of the Jarrahi River also passes through its center (point of S/2-intersection), which is why its Delta has an interesting symmetry. The subsidence took place at the intersection point matches with Ramhormoz's alluvial fan. Due to the shifting of NW-wing toward the geodynamic pole, it has expanded more than the SE-wing. As a result of this expansion, it seems the Gor-Gor, Karun, Dez, and Karkheh rivers in the northern part of the region was a one river and later have been partitioned and migrated to the west. But Zohre and Jarrahi rivers on the other side of the intersection are in the opposite sense. Red lines are orthogonal faults created by two reciprocating components. East-Migration of Karkheh and Tigris from the Choghazanbil-Temple and Waset (Iraqi city), can be justified in this regard. The double arrow lines indicate the separation of the networks due to expansion.

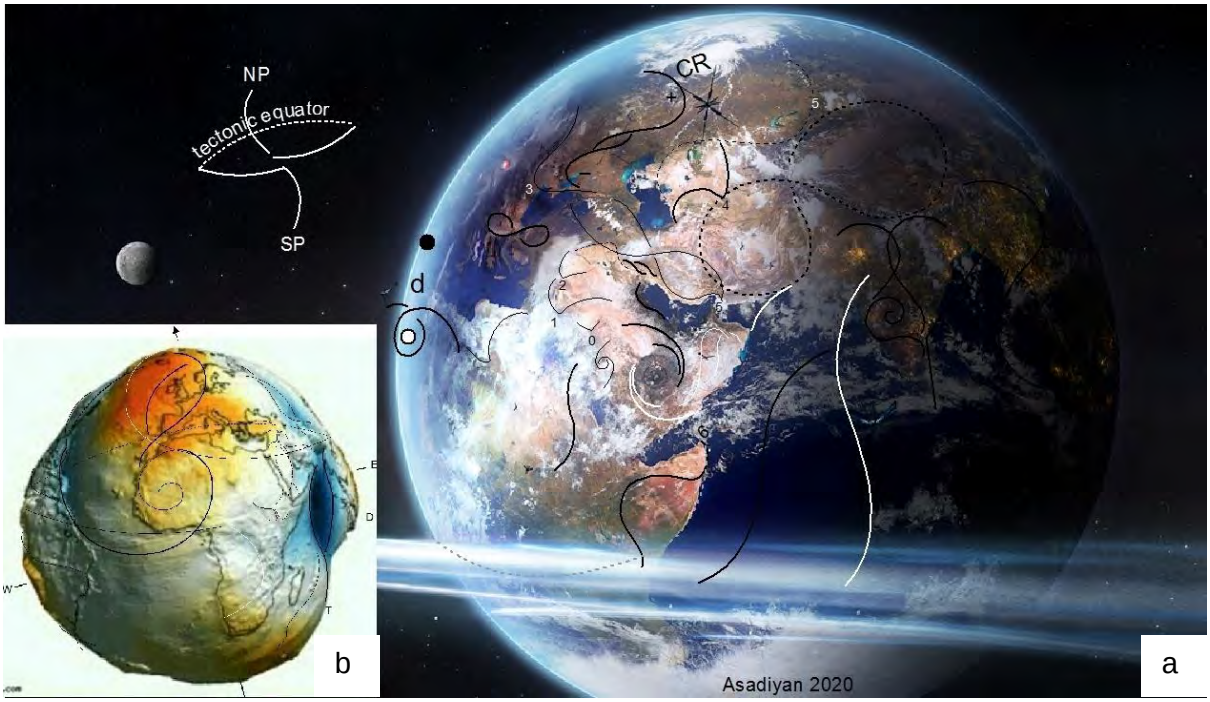

Fig. 5

Fig. 5/a, right, you see the Arabian-Cylinder which has a nice symmetry in the Earth. The cross section of this cylinder is completely like cross section of the Earth. Notice the bending-direction in the both side of the Persian Gulf and Caspian Sea. In the PG bending occurred in NS-direction but in the CS in EW-direction. Why the north shore of the Black Sea bended ruggedly but the north shore of the Caspian Sea bended smoothly? As previous said, this is referred to angle-difference and rotation-difference between forward component and retard component. The tectonic equator is great circle of double-cone cycloid passed through Himalaya and Bermuda. TE emerged from Nazca and growth toward the GP then tailed toward N-pole and S-pole. When start/end of TE converges in GP, the mouth of the Indian-Ocean also closed. It seems the N-tail is longer and circulates faster than the S-tail. It seems the thickness of lithosphere (D) is equal the lenght-difference between these two arms and satisfied in this relation (0.618-0.382=2D). Interestingly 2D is integer order of Mecca-Equator distance (about 2383.36 Km). As we go toward the Earth-Center the 2D decreases (i.e. increase in symmetry). It seems the Earth structuralized within two period of spiraling, in the first period core and mantel structuralized and in the second period the rest of the Earth is structuralized. Broad Apex and Narrow Apex of N-Africa formed due to interference of 1/2-arm of African cycloids with two distinct points: Decay Point (white) in the center and Inflection Point (black) in Catastrophic Zone. The distance between DP and IP is named primary Decay Length (d). D related to secondary period.

In Fig. 5/b, left, you see the actual shape of the Earth. Most smooth region (Arabia) located between most high land (Green Land) and most low ocean (Indian), why these nice arrangements take place. The only model which responsible for these figures is cosmic cycloid (tectonic equator/TE) which shown in the Fig. 5/a.

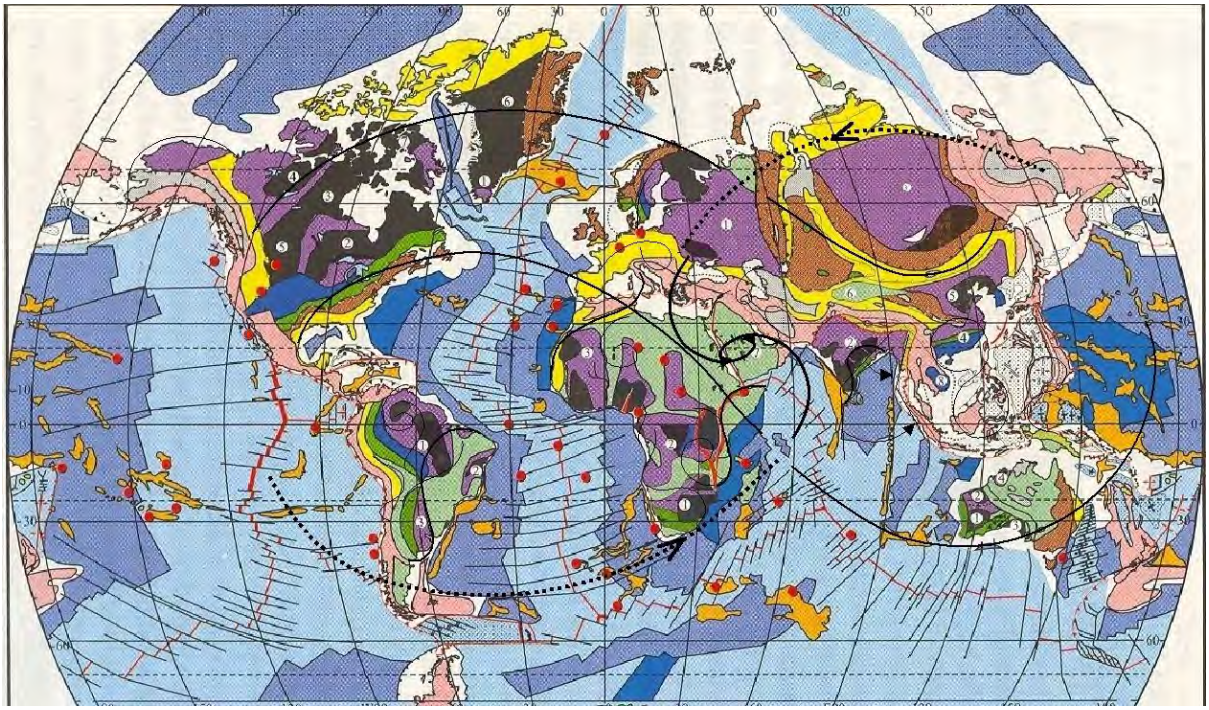

Fig. 6

The Earth meanders like river between concave shore (West Pacific) and convex shore (East Pacific) along Earth-Möbius (2 is forward segment and S is retard segment). Material meandered from high friction region (fire ring) toward least friction region (Geodynamics Pole/GP). EM collects the whole continents in one side and abandons Pacific on the other side. The EM arises from the inner core and emerges from Mecca (GP). The EM up down the whole Earth. The EM polarised within an ellipse. We see many harmony in the EM, for example, Mecca located in the cross point of forward segment and retard segment. Gulf of Bengal with vertical opening formed in the SE of GP but Iceland with horizontal opening formed in NW of GP. MAR formed in the Retard Loop but MCR formed in the Forward Loop. FL and RL bounded by polarised ellipse. Broad Apex and Narrow Apex of N-Africa highly tighten by cross point.

Discussion,

The linkage between RM and EM is quite difficult and need deep image from small scale to big scale. In the context we mentioned friction as a fundamental parameter, here this question arises: how we could apply this parameter for Earth Meandering, in the cup of tea experiment [1], it is clearly understood how tea-leaves accumulate in the center of the glass. For EM two arguments could be arising: 1- the angular velocity of the Earth during the Earth's history gradually decreases so circular path occurred inside the Earth due to friction-difference between center and circumstance of the Earth. 2-tiltness of the Earth in the space applies momentum-difference between NP and SP and accordingly applies friction-difference between NP and SP as well as between fire-ring and GP (may be 1 and 2 together).

Certainly the position of GP isn't fixing but varies with position of the Earth in the space. It seems once a time the GP coincide with SP, but as a universe extended it is rolled back along spiral path until reach the current position in the center of continents. During this long time whole the Earth up down and polarized with respect to E-W and N-S. Crossing of S-segment and 2-segment of Earth-Möbius release high friction-thermal, in inner core pressure is dominants so we have solidification but in CZ like outer core tension is dominants so we have melting.

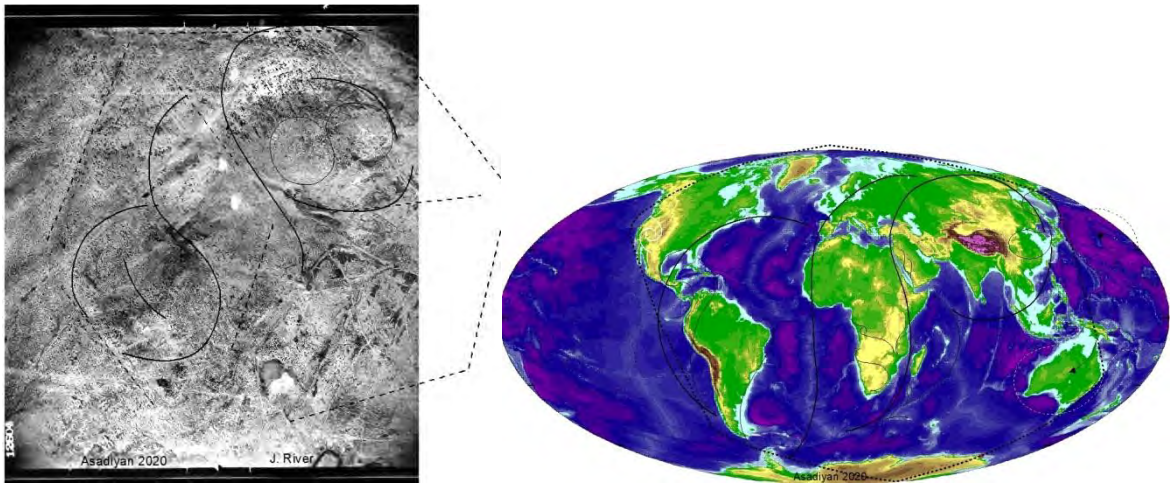

Fig. 7/a, and 7/b, show relation of polygonal faulting with Mobius-Deformation into two scales.

7/a shows corner part of Fig. 2, historical hill of Tel-Alasvad located in the cross point of local Mobius. Corner of this figure shows part of Jarrahi River. Triple junction separate three different geological faces, one horizontal and the others vertical. North –eye of local Mobius in the horizontal face embrace smaller Mobius. Fig. 7/b, like Fig. 6 dotted lines shows polygonal form of the continents which embraces Global-Mobius.

References,

[1] Aslamazov, L. G., Varlamov, A. A., 2001. The wonders of physics, World Scientific.

[2] Asadiyan, M. H, and Zamani, A., 2010. Could Dahw/Tahw dissolve problems of Plate Tectonics? Asian Journal of Earth Sciences 2(3): 190-212.

[3] The Holy Quran, 79/30 and 91/6.

[4] Storetvedt, K.M., 2003. Global Wrench Tectonics, Bergen, Fagbokforlaget, 397p.

[5] Katz1, R. F. and Ragnarsson, R., 2004. Tectonic microplates in a wax model of sea-floor spreading, New Journal of Physics, Volume 7.

[6] Edwards, B. F. and Smith, D. H., 2002. River meandering dynamics, Phys. Rev. E 65, R046303.

VELOCITY STRUCTURE OF THE UPPER MANTLE

Lyudmila Gordienko and Vadim Gordienko
Institute of Geophysics, National Academy of Sciences, Kiev, Ukraine
tectonos@igph.kiev.ua

Abstract: The authors have constructed models featuring seismic P-wave velocity distribution in the upper mantle beneath oceanic, continental and transition regions, such as mid-ocean ridges (MOR), basins, trenches, island arcs, and back-arc troughs (BAT), Atlantic transitional zones, flanking plateaus (FP)of MORs, platforms, geosynclines, rifts, recent activation zones The models are in agreement with the deep-seated processes in the tectonosphere as predicted in terms of the advection-polymorphism hypothesis (APH). The models for areas island arcs and coastal ridges are like those for alpine geosynclines disturbed by recent activation. The models for mid-ocean ridges and back-arc troughs are identical. They fit the pattern of recent heat-and-mass transfer in the case of rifting, which, given the basic crust with continental thickness, leads to oceanization. The model for the basin reflects the effect of thermal anomalies smoothing beneath mid-ocean ridges or back-arc troughs about 60 million years later. The model for the trench and flanking plateau reflects the result of lateral heating of the mantle's upper layers beneath the quiescent block from the direction of the island arc and basin (trench) and MOR and basin (FP).

Keywords: Oceans, continents, transition regions, upper mantle, velocity models.

INTRODUCTION

A generalization of the geological and geophysical information pertaining to continents, oceans and ocean- to-continent transition zones that was performed, in particular, by (Gordienko, 2012, 2015 and others), reveals that the said information is insufficient to ensure well-grounded verification of hypothetical schemes of the deep-seated processes in the tectonosphere of the regions in question. In this specific case, we are talking about schemes conforming to the advection-polymorphism hypothesis. The situation may be rectified, to a certain extent, with the help of velocity models constructed for the upper mantle beneath those regions, which are known for their often-elevated seismicity and are equipped with a rather extensive earthquake monitoring system. Even the construction of one-dimensional P-wave velocity (V_p) distribution with depth, although not reflecting sufficient detail, could enable us to gain insight into the main patterns of heat-and-mass transfer in the upper mantle. Of particularly great interest would be a comprehensive set of such models for seismically unstable mid-ocean ridges (MOR), oceanic basins, deep-water trenches, island arcs (in these authors' opinion, also coastal ridges as their equivalents), and back-arc troughs (BAT), alpine rifts and geosynclines, platforms and zones recent activation.

Velocity profiles constructed for many such regions have been reported in publications, but that information tends to be inconsistent (see below) or is limited to a priori concepts, such as, for example, on the absence of velocity variations with regard to the AK135 model (Gudmundsson et al., 1998; and others) at depths of the upper mantle's lower portion, and so on.

The most promising, in our opinion, is an operation being planned for island arcs, alpine rifts and geosynclines with the use of particularly dense seismic observation networks. Hypocenters of many earthquakes beneath territories and offshore expanses in those regions are located at relatively shallow depths in the mantle's upper horizons. They may provide valuable material for the constructions being planned. Yet, we are also aware of possible complications due to the extremely irregular distribution of seismic wave velocities in the subcrustal portion of the tectonosphere (Nizkous et al., 2006; and others). Despite these reservations, however, the goal may still be achieved.

In the authors' opinion, island arcs are not oceanic formations proper: They are Alpine geosynclines like those on continents. This conclusion is also corroborated by seismological data (Gordienko, 2016; and

others). Yet, the arcs are part of a system of structures in the active zone of continent-to-ocean transition. Back-arc troughs are often located closer to the continent and their crust is in a state of nearly complete oceanization. For that reason, we added island arcs to the list of regions separately to be explored. After we study them and gain experience, it will be easier to proceed to the construction of mantle models for other regions.

We have constructed models featuring seismic P-wave velocity distribution in the upper mantle beneath oceanic, continental and transition regions, such as mid-ocean ridges (MOR), basins, trenches, island arcs, and back-arc troughs (BAT), Atlantic transitional zones, flanking plateaus (FP) of MORs, platforms, geosynclines, rifts, recent activation zones.
A detailed bibliography on regions covered by studies was presented in the authors' earlier publications over past eight years (Gordienko et al., 2012, 2015a, b, 2016a, b, c, d, 2017a, b, 2018a, 2020 and others).

A PRIORI DATA ON VELOCITY PROFILES FOR THE UPPER MANTLE

Continents, oceans and active margins have been covered fairly well by seismological studies (Chu et al., 2012; Feng et al., 2007; Fukao, 1977; Gontovaya et al., 2006; Gudmundsson et al., 1988; Hansen et al., 2001; Jiang et al, 2009; Kennett et al., 1993;Pavlenkova et al., 1993, 2006: Romanowicz , 2003; Tectonosphere…, 1992; Walck, 1995; Zhao et al., 1999 and others). There are, however, quite significant differences between models for regions of the same type that are described in the publications listed above. This is largely because individual authors adopt a priori concepts on the velocity structure of the upper mantle. For a geological interpretation of velocity profiles to be accurate, they must be presented in absolute values of V_P. For that reason, we ignored models based on anomalous values if the authors failed to provide information on the relevant profiles.

Two groups of models can be identified: The first group always displays a sharp velocity contrast at a depth of about 400 km; this element is absent from the second group (**Fig. 1**).

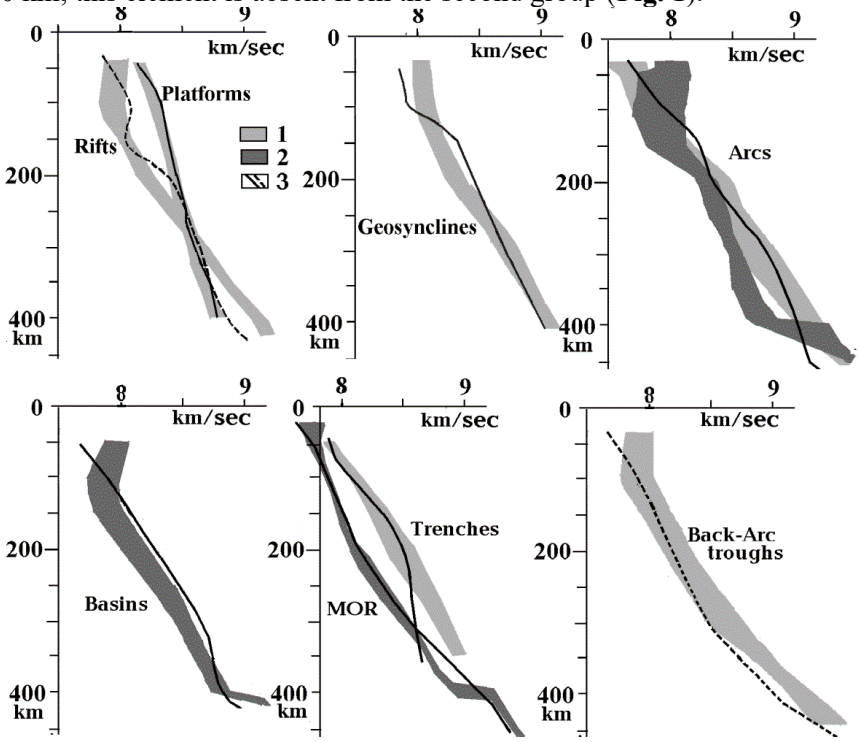

Fig. 1. Velocity models for regions with different endogenous regimes.
1 – without a surge in V_P at the depth of about 400 km; 2 – with a surge in V_P;
3 – velocity profiles for the upper mantle constructed during this study

Our data represent an average for several profiles; an average value ± average deviation from it are shown for each depth. Information for different regions varies depending on the number of models used, and we cannot claim that we have reviewed all the available data. It is rather a matter of detecting prevalent trends. The average values preset for all depths in the upper mantle beneath regions are similar. Therefore, in selecting an estimated travel time graph matching observed ones, it is possible to use a single first-approximation model.

Apart from seismic data, petrological data too, those obtained by A. Ringwood (1981), provide a substantiation for placing an interface at the depth of 410 km. This depth is not infrequently incorporated a priori into velocity models for the mantle. The petrological evidence points to the beginning of a polymorphic transformation of mantle rocks at approximately that depth (at the temperature of about 1,600ºC). Considering the hypothetical composition of the olivine undergoing transformation, it must be assumed that the process spreads over a considerable depth interval (the PT-conditions). According to estimates (Brown et. al., 1981; Irifune, 1987; and others), based on experimental data, the thickness of the layer, in which olivine-α transforms into modified spinel (olivine-β) and the transition of pyroxenes into garnets is completed, amounts to about 60 km. A. Ringwood's estimate is 100 km, but in his interpretation, it is apparently a depth range for two transitions culminating in the formation of olivine-γ (specifically, spinel with olivine composition).

The value of the vertical temperature gradient used in the evaluation of the depth of the polymorphic transition appears to be close to the actual gradient, but the quoted absolute temperature (T) values and the technique used for their determination (Brown et al., 1981 and Ringwood, 1981) are at variance with our thermal models for the upper mantle (Gordienko, 2012, 2015; and others). The very fact of the dissimilar velocity profiles being recorded in the same region shows that it is impossible to get an unambiguous solution to the inverse geophysical problem given dissimilar approaches resorted to by different authors. Researchers who studied this specific issue (Zhao et al., 1999, for example), point out that seismic evidence can be made consistent with dissimilar V_p patterns within the depth interval in question. The depth of the velocity contrast in the models in question has been assumed to equal approximately 400 km. At the same time, studies conducted with the specific goal of determining that depth (i.e., under the assumption that the interface exists), suggest a depth of about 430 km or somewhat larger (Flanagan et al., 1999, Pavlenkova et al., 2006).

The reliability of such information improves with an increase in detail and accuracy of accounting for the overlying strata (Flanagan et al., 1999; Melbourne, 1998), but in practical terms, the depth variations (about 10 km) are smaller than the errors in their determination (about 15 km). From this perspective, it might be useful to compare obtained results with the data of deep seismic probing based on nuclear explosions in Northern Eurasia (Pavlenkova et al., 2006). In this case, the interface imaging technique enables us to make the most of the information on velocities in the crust and upper mantle. The depths, as determined by the two methods, coincide with an accuracy of up to a few kilometers.

Thus, the depth at which polymorphic transition most probably started must be about 430-435 km. This result is also in close agreement with that established with the help of a thermal model for the upper mantle beneath a quiescent platform. At somewhat larger depths, the velocity must increase with a larger gradient, but not discontinuously.

The study (Gordienko, 2018) has shown an approximate match between the depths for the transition zone top in various continental regions as derived from experimental and estimated data. As far as oceans are concerned, the situation remains uncertain due to differences between the experimental data as reported by different authors. For that reason, we largely limited our modelling to the upper mantle.

Our crustal model (for island and continent seismic stations) was based on the data from publications (Belyaevsky, 1981, Continental…, 1995, Jerlih, 2011, Mooney et al., 2002, Nizkous et al.., 2006, Pavlenkova et al., 1993, 2006, Tectonosphere …, 1992, Udintsev, 1987, and others). Crustal thickness in first-approximation models is limited to 10-40 km. It goes without saying that the adopted crustal thickness and velocity structure are the result of a compromise between the data reported by different authors. In some specific regions, certain corrections were introduced to the structure without affecting results of the calculation in any appreciable manner. The high variability of seismic P-wave velocities within the subsurface depth interval has been detected because of all sufficiently detailed studies (Nizkous et al., 2006; Pavlenkova et al., 1993; and others). The high variability is responsible for the sharp increase in the scatter of arrival times of waves from earthquakes at small angular distances. The corresponding segments of travel time graphs were simply ignored, and the graphs started from about 3° after which the scatter of arrival time acquired a stable character. Accordingly, velocity profiles were constructed, as a rule, starting from depths of about 50 km.

FACTUAL EVIDENCE USED

Tectonic classification of oceans and active margins is often based on an adopted hypothesis regarding deep-seated processes. In view of the extremely limited information on the geological history of oceans, the authors tried to avoid such an approach. In most cases, we used purely morphological indications and information on recent seismicity. Upheavals accompanied by earthquakes were attributed to mid-ocean ridges; vast basins were classified as regions of the same type regardless of local topography or manifestations of recent magmatism that complicate the general picture; marginal trenches and BATs were identified according to the sharp variation of depths. Island arcs and coastal ridges of Kamchatka, as well as of Northern, Central, and Southern Americas constituted an exception. They were viewed as undergoing the very beginning of the post geosynclinals stage of evolution, in many cases complicated by recent activation (Gordienko, 2012, 2016). Within their boundaries, the latest folding of the thick strata (usually confined to troughs at the outer – oceanic – side of the island), aged from Oligocene to Pliocene, occurred at the Pliocene/Pleistocene interface. It cannot be ruled out that folding in arcs situated further west is older. In the case of continents, we managed to identify with more certainty zones with prevailing dissimilar endogenous conditions. The relevant data were reported in the authors' earlier publications (Gordienko et al., 2012, 2015a, b, 2016a, b, c, d, 2017a, b, 2018a, 2020 and others).

Fig. 2 shows location of seismic stations whose data were used in this study (International…, 2014). The regions covered by studies differ significantly both in terms of the volume of collected evidence (the number of earthquakes) and coverage of the existing structures of the same type. This is associated with the availability of information, as well as with the size and location of the structures. A composite numerical characterization of the data is about 200 seismic stations and 40,000 earthquakes.

The most comprehensive evidence was collected for island arcs and coastal ridges in the Pacific and Indian oceans. The large spatial extent of the structures and the abundance of earthquakes contributed to our efforts. Trenches, FP and zones recent activization of platforms were among the least explored objects. The small width of such structures, which are twisted in plan, hampered the choice of sites for seismic recording stations and of shallow earthquakes that might alleviate the construction of a velocity model specifically for the trench not affected by adjacent basins or island arcs. For that reason, the mean velocity model for the trenches turned out to be much less substantiated than for arcs. The maximum depth to which the Vp pattern was plotted was also smaller. The situation is somewhat better in the case of back-arc troughs: We managed to construct a model for depths reaching the lower portion of the upper mantle. Mid-ocean ridges are delineated relatively well, while oceanic basins, platforms and rifts – not so well. Hopefully, in the future, the use of larger amounts of data will make it possible to update the so far obtained results. Yet even the results already at hand may be instrumental in discovering

many important characteristics of the mantle's velocity structure beneath regions with different endogenous regimes.

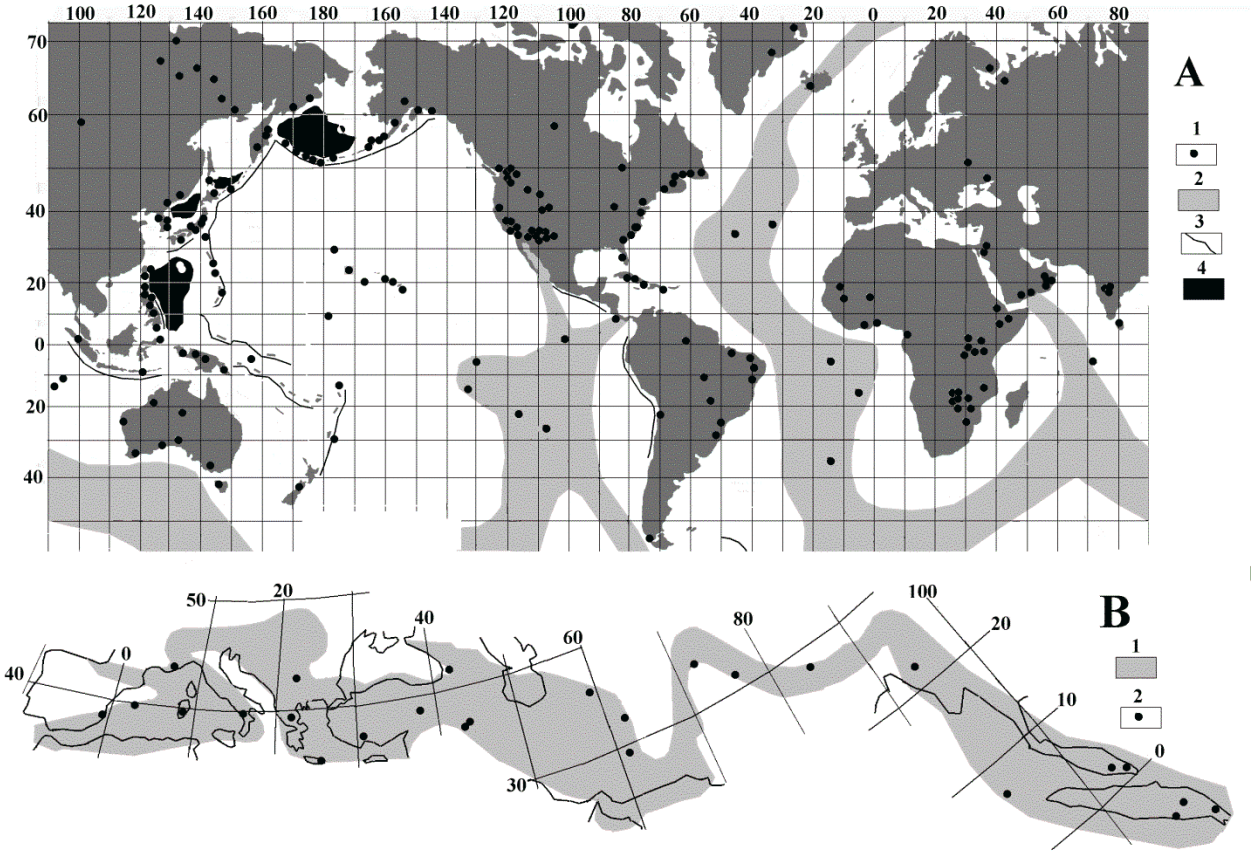

Fig. 2. Seismic stations whose data were used for plotting traveltime graphs.
A: 1—seismic stations, 2—mid-ocean ridges, 3 –trenches, 4 – back-arc troughs covered by studies.
B: 1 – alpine geosyncline Tetis , 2 - seismic stations

COMPUTATION TECHNIQUE

The estimated traveltime graph was plotted on the basis of the SEIS-83 modelling program worked out by I. Psencik and V. Cerveny. Maximum necessary depths that the rays could reach were attained at approximately 25° offset distances and with traveltimes of about 300 sec (**fig. 3**). For comparison with the estimated travel time graph, we used information on traveltimes from a publication by the (International…, 2014). We only used those data on the earthquakes whose epicenters were in regions covered by study. The depths (H) of the hypocenters used in the analysis of the earthquakes reached 50-55 km. All of them were converted to a single H value approximately matching the depth of the M. discontinuity. Corrections to the arrival times of waves were revised in the process of construction of a velocity structure within the depth range between the actual depth of the hypocenter and the depth of the M discontinuity.

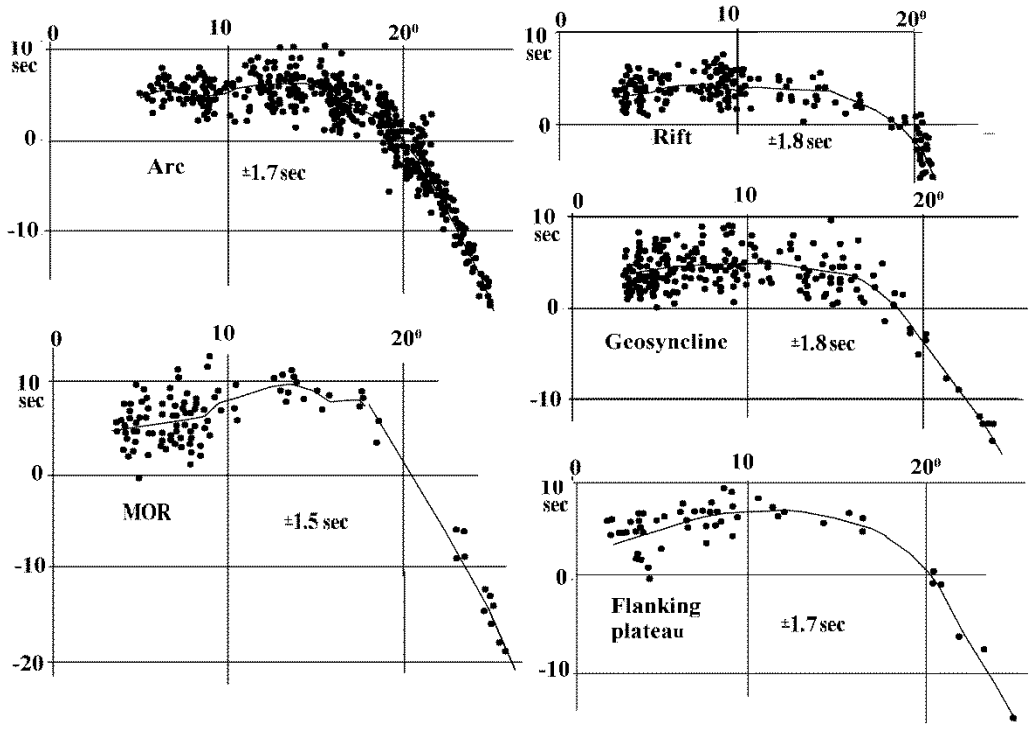

Fig. 3. Reduced observed travel time graphs recorded at seismic stations in some studied regions.

For convenience of comparison between estimated and observed traveltime graphs, we plotted their reduced versions for seismic P-wave velocities in upper mantle rocks amounting to 8.2 km/sec. Smooting of observed arrival times was performed using a sliding window at 3-4 degrees. The resulting point on the traveltime graph was placed inside the window with an allowance for the varying "cluster" of observed data; a unit step of the window amounted to 0.4°.

Deviation of dots from the median curve appears to be a fairly good characteristic of the error in the observed traveltime graph. The average deviation for all the traveltime graphs is about 2 sec. A typical value of the deviations does not exceed those obtained in similar studies (Feng et al., 2007; and others).

Averaged travel time graphs were constructed for all types of regions under study. Trenches and flanking plateaus were an exception: The insufficient amount of available material caused us to construct a single travel time graph using the data for all structures. Average deviations of individual travel time graphs from the median are not large (they reach maximum for island arcs and coastal ridges and continental rifts, but even there they amount to 1.8 sec) -- just around 1.5 sec. At the present level of available information, it is possible to conclude that a single travel time graph should be applied to the entire dataset for separate structures within regions of the same type. Given the errors, differences are inevitable. Results of comparison between observed and estimated travel time graphs can also be assessed with an account for the error. Variations in computation results, expressed in terms of time differences for dissimilar velocity structures, change significantly with the depth for which changes are introduced into the model.

In order not to overlook velocity anomalies, we will classify as appreciable all those differences between estimated and observed travel time graphs that exceed two seconds. Yet, not all velocity anomalies (conforming to deviations from the selected estimated travel time graph) recorded in the procedure can be viewed as reliable.

The majority of observed travel time graphs match estimated ones fairly well (see **Fig. 4 and 5**), i.e., we can claim that a typical velocity structure of the upper mantle beneath the features under study matches that used in the computations.

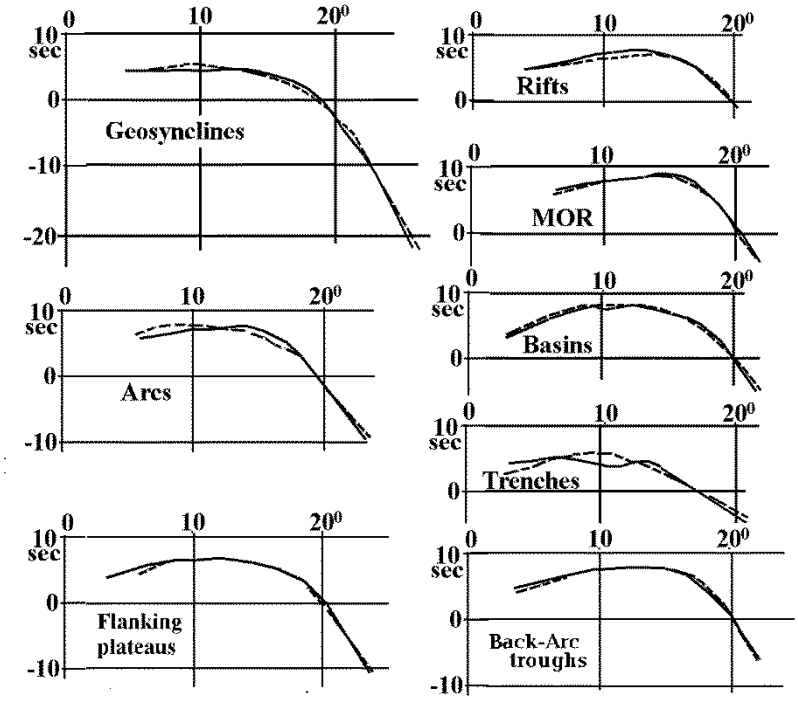

Fig. 4. Coordination between observed (solid lines) and estimated (dashed lines) travel time graphs.

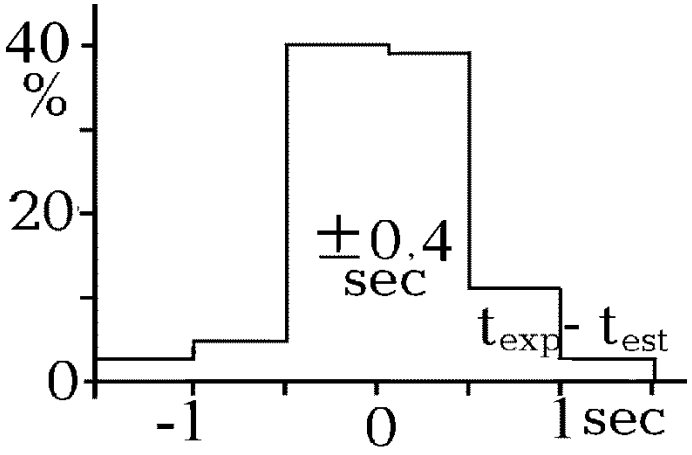

Fig. 5. Histogram showing a pattern of deviations of averaged experimental travel time graphs from estimated graphs.

Obviously, the typical differences in the travel time graphs can be fully accounted for by errors in the source material. small anomalies (0,10-0,15 km/sec), which correspond to differences in wave travel times of 2 sec, are not common.

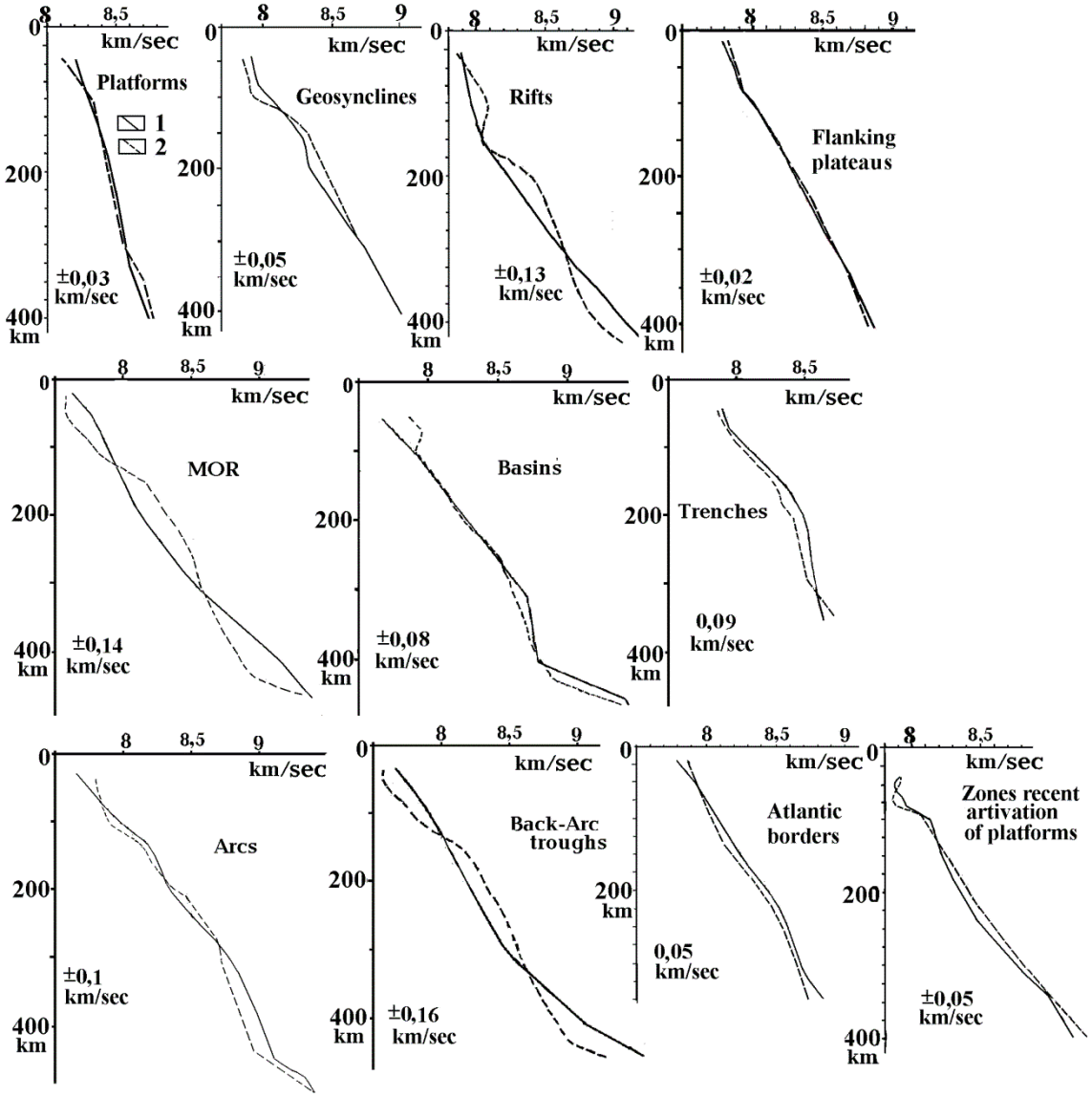

Fig. 6. Best-fit velocity models for the upper mantle beneath regions with different endogenous regimes. Velocity sections: 1- observed, 2 – estimated.

DISCUSSION OF RESULTS

The experimental and estimated velocity profiles differ by an average of ±0.08 km/sec. This corresponds to the 0.06 km/sec error value typical for each of the techniques. In the case of MOR, rifts and BATs the differences can be 1.5 to 2 times larger. Additional research for those regions is required.

Analysis of the deep-seated processes that prompted the construction of certain thermal models for the mantle and the observed V_p continues. In this paper, we will focus on velocity models proper.

Velocity patterns that we have constructed comprise symmetrical positive and negative anomalies unlike velocity patterns for parts of quiescent Precambrian platforms (**Fig. 6**). They point to the advective nature of the heat-and-mass transfer that caused those anomalies. The model for areas beneath trenches and flanking plateaus is an exception It may well be explained by the lateral aliasing effect on the platform and basin model of overheated volumes of material from the subcrustal mantle beneath island arcs and basins (trenches) and activated basins and MOR (FP). A symmetrical positive anomaly may be

positioned at depths larger than those studied beneath trenches. This points to a relatively recent large amplitude advective displacement of the upper mantle material beneath one or both adjacent regions. Geological evidence fully corroborates this assumption. Almost identical heat-and-mass transfer events took place beneath Alpine geosynclines, island arcs, and ocean basins, at any rate in the northwestern Pacific Ocean Basin and; 100 million years later, such events took place beneath arcs (Gontovaya et al., 2006; Gordienko, 2012; Tectonosphere…, 1992; and others). In all cases, they may have been complemented by single-event heat-and-mass transfer processes during recent millions of years. Studies of the upper mantle beneath trenches at the eastern periphery of the Pacific have not, unfortunately, been conducted.

Velocity structure of the area beneath the trench may point to a relatively small mass of overheated material transported to the subcrustal area beneath adjacent regions – at the level of one quantum of tectonic action (QTA). In terms of the advection-polymorphism hypothesis (APH), QTA is the minimum volume of material with a typical diameter of 50-70 km involved in displacement (Gordienko, 2012; and others). The resulting models have been cross-referenced with V_p patterns at solidus temperatures and at relevant depths. They differ somewhat for island arcs and costal ridges, on the one hand, and the rest of the ocean regions, on the other. In the former case, we assumed normal composition of the mantle beneath continents and in other cases, eclogite inclusions most probably underwent melting which caused changes in the solidus temperature and V_p values. A comparison between the mantle model beneath platforms, trenches, FP and the distribution of V_p at solidus temperatures prompts a conclusion that there is no asthenosphere there. In all other cases, it does exist, and its top portion lies at relatively shallow depths pointing to the recency of the processes in the mantle. Such depths of the partial-melting layer may only arise under the effect of Alpine or post-Alpine heat-and-mass transfer episodes. Recent post geosynclinals activation utilizes material and energy reserves of the asthenosphere that emerged precisely at the end of the cycle.

At the very bottom of the profile, the high vertical gradient in the V_p distribution beneath activation regions may signify the beginning of a polymorphic transformation of the mantle olivine. If one views this anomaly because of the sharp drop in temperature following the final advective heat-and-mass transfer episode, then the corresponding temperature hike should be at the level of 800ºC. Such an anomaly is unrealistic since it far exceeds the difference between normal platform-type temperatures and the PT conditions at the onset of the process of α-olivine transition into β-olivine. Anyway, a velocity model for such depths is rather dubious: Its noticeable changes do not affect the estimated travel time graph in any appreciable manner.

Advective transport of the upper mantle material takes place within cells whose centers occur at depths of about 220-230 kilometers. Here T and V_p are unchanged. Exceptions are trenches, Atlantic borders and FP. In these regions T are created by lateral influences. The average Vp for the remaining experimental models is 8,37 ± 0,07 km/sec, as in the reference models of the upper mantle AK135 or IASP91. There is coordination at a depth of 400 km - about 9 km/sec.

CONCLUSIONS

A rather thick of active regions asthenosphere was detected – a layer of partially molten mantle rocks with a small (approximately up to 2%) liquid phase content. A thick depth interval of active regions with abnormally low-temperature rocks has been spotted in the lower portion of the upper mantle. The extent of their cooling at the depth of 400-450 km is sufficient for triggering a polymorphic transformation of olivine.

The constructed velocity profiles vary little from region to region with the same type of endogenous conditions. This enables us to maintain that the models represent standard (typical) V_p distributions in the mantle beneath the regions, just as presumed in terms of the APH. The estimated mantle profile beneath

platform, geosyncline, island arc, trench and flanking plateau fully fits that predicted. Models of ocean basins agree with the concept to the effect that the mantle beneath them is a result of smoothing of thermal anomalies that prevailed in the mantle beneath the mid-ocean ridges or back-arc troughs.

A more detailed analysis of the nature of velocity anomalies will be performed in studies of the deep-seated processes in the mantle. Velocity profiles alongside other geophysical information will constitute major criteria for verifying the credibility of the tectogene hypothesis. Upper mantle velocity profiles can be constructed for any region of the Earth with the help of the data reported in the study and with the use of thermal models based on the advection-polymorphism hypothesis (APH). In more detailed studies, they can be used as parameters for constructing "initial reference models" (Kissling et al., 1994, p. 19635) without the need to restrict the task to focal depths of the earthquakes (Gontovaya et al., 2006, Gordienko, 2018b).

Acknowledgements: The authors wish to express special thanks to Mrs. Rita Schneider for translating this paper from Russian.

References

Belyaevsky, N.A. 1981. The structure of the Earth's crust of the continents according to geological and geophysical data. Moskow: *Nedra.* 432p. (in Russian).

Brown, J., Shankland T., 1981. Thermodynamic properties in the earth as determined from seismic profiles. *Geop. J. R. Astron. Soc*. v.66. pp. 579-596.

Chu, R., Schmandt, B., and Helmberger, Vol., 2012. Juan de Fuca subduction zone from a mixture of tomography and waveform modeling. *J.G.R.,* Vol. 117. B03304.

Continental Rifts: Evolution, Structure and Tectonics. 1995. Olsen, K., ed., Amsterdam*, Elsevier*, 492 p.

Erlikh, Je.N., 2011. Essays on the geology of island arcs, google.com*/site/geotermiakuril* (in Russian)]

Feng, M., Lee, S., and Assumpcao, M., 2007. Upper mantle structure of South America from joint inversion of waveforms and fundamental mode group velocities of Rayleigh waves. *J. G.R*. Vol. 112. B04312.

Flanagan, M. and Shearer P., 1999. A map of topography on the 410-km discontinuity from PP precursors. *Geoph. Res. Letters*. Vol. 26, no. 5, p. 549-552.

Fukao, Y., 1977. Upper mantle P-wave velocity structure on the ocean side of the Japan-Kurile Arc. *Geoph. J. R. Astr. Soc.*, Vol. 50, p. 621-642.

Gontovaya, L.I. and Gordienko, V.V., 2006. Deep-seated processes and geophysical models of the mantle for Eastern Kamchatka and Kronotsky Bay. *Geology and minerals of the World Ocean*. No. 2, p. 107-121 (in Russian).

Gordienko, V.V., 2010. On the nature of anomalous seismic P-wave velocities in the upper mantle. *Geophys. J.,* No. 3, p. 43-63 (in Russian).

Gordienko, V.V., 2012. Processes in the Earth's tectonosphere (advection-polymorphism hypothesis). Saarbrücken: *LAP.* 256 p. (in Russian).

Gordienko, V., 2015. Essential points of the advection-polymorphism hypothesis. *NCGT Journal*, v. 3, No. 2, p. 115-136.

Gordienko, V., 2016. Deep-seated processes in the tectonosphere of geosynclines. *NCGT Jounal*. v. 4. No. 1, p. 6-31.

Gordienko, V.V. 2018.Roof depth of the transition zone between the upper and lower mantle of the Earth. Doc. NASU No 4. p.60-65. (in Russian).

Gordienko, V.V., Gordienko L.Ja.,. 2012. Velocity section for the upper mantle beneath the Aleutian, Kurile and Japanese island arcs. *Geology and minerals of the World Ocean.* No 3. P. 37-46. (in Russian).

Gordienko, VV, Gordienko L.Ya. 2015a. Velocity model of the upper mantle under the island arcs and coast ridges of the Pacific Ocean. *Geology and minerals of the World Ocean*. No 3. P.69-81. (in Russian).

Gordienko, V.V., Gordienko L.Ya. 2015b. Velocity section of the upper mantle under the island arcs of the northern and western margins of the Pacific Ocean. *Geoph. journal.* No 3. p. 124-138. (in Russian).

Gordienko, V.V., Gordienko L.Ya. 2016a.Velocity model of the upper mantle of back-arc depressions. *Geology and minerals of the World Ocean*. No 2. P. 37-47. (in Russian).

Gordienko, VV, Gordienko L.Ya. 2016b. Velocity model of the upper mantle under the mid-ocean ridges. *Geology and minerals of the World Ocean.* No 1. P.33-42. (in Russian).

Gordienko, V.V., Gordienko, L.Ya., 2016c. Velocity profiles for the upper mantle beneath oceanic trenches. *Reports of the UNAS*. No 4, P. 62-68 (in Russian).

Gordienko, V.V., Gordienko L.Ya. 2016d.Velosity sections of the upper mantle of oceanic basins and deep-sea trenches. *Reports NASU*. No 4. S.62-68.

Gordienko, V.V., Gordienko L.Ya. 2017a. The deep process and P-wave velocities in the upper mantle of transition zones of the Atlantic type. *Geology and minerals of the World Ocean*. No 3. p.62-72. (in Russian).

Gordienko, V.V., Gordienko L.Ya. 2017b. Velocity models of the upper mantle of continental and oceanic rifts. *Geophysical Journal.* No 6. p.20-40. (in Russian).

Gordienko, V.V., Gordienko L.Ya. 2018a.Velosity models of the subcrustal mantle of Ukraine. *Geophysical Journal.* No 6. p.30-51. (in Russian).

Gordienko, V.V., Gordienko L.Ya. 2018b. Plate movements and earthquakes. *Geology and minerals of the oceans*. No 4. p.5-19. (in Russian).

Gordienko, V.V., Gordienko, L.Ya. 2020. A velocity model of the upper mantle of the flanking plateaus of mid-ocean ridges. *Geology and minerals of the World Ocean*. No 1.p. (in Russian).

Gudmundsson, O. and Sambridge, M., 1998. A regionalized upper mantle (RUM) seismic model. *J.G.R.* v. 102, B4. p. 7121-7126.

Hansen, R., Ratchkovski N. 2001. The Kodiak Island. Alaska Mw7 Earthquake of 6 December 1999. *Seism. Research Letters.* 72(1), p. 22-32.

Irifune, T., 1987. An experimental investigation of the pyroxene-garnet transformation in a pyrolite composition and its bearing on the constitution of the mantle. *Phys. Earth and Pl. Inter*., v. 45, p. 324-336.

International Seismological Centre, On-line Bulletin, http://www.isc.ac.uk, Internatl. Seismol. Cent., Thatcham, United Kingdom, 2014.

Jiang, G., Zhao, D., and Zhang, G., 2009. Seismic tomography of the Pacific slab edge under Kamchatka. *Tectonophysics.* v. 465. p. 190-203.

Kennett, B., Engdahl, E., and Buland R., 1995. Constraints on seismic velocities in the Earth from traveltimes, Geophys. *J. Int.,* v.122, p.108-124

Kissling, E., Ellsworth, W.L., Eberhart-Phillips, D. & Kradofler, D., 1994. Initial reference models in local earthquake tomography, *J.G.R.*, 99, p. 19635-19646.

Melbourne, T., Yelmberger D. 1998. Fine structure of the 410-km discontinuity. *J.G.R.* v.103. no. B5. pp. 10091-10102.

Mooney, W., Prodehl C., Pavlenkova N. 2002. Seismic velocity structure of the continental lithosphere from controlled source data. *International handbook of earthquake and engineering seismology*. v.81a. P. 887-910.

Nizkous, I.V., Kissling, E., Sanina, I.A., and Gontovaya L.I., 2006. Velocity properties of the lithosphere in the Kamchatka Region ocean-to-continent transition zone according to seismic tomography. *Physics of the Solid Earth.* No. 4, p. 18-29 (in Russian).

Pavlenkova, N. I., Pogrebitsky, Yu. E., and Romanyuk, T.V. 1993. Seismic-density model for the crust and upper mantle in the Southern Atlantic Region based on the data of the Angola-Brazil geotraverse. *Physics of the Solid Earth.* No.10, p. 27-38 (in Russian).

Pavlenkova, G. A. and Pavlenkova, N. I., 2006. Structure of the upper mantle beneath Northern Eurasia based on records from an experimental nuclear explosion. *Tectonophysics.* Vol. 416, p. 33-52.

Ringwood, A., 1981. Composition and petrology of the Earth's mantle. Moscow: *Nedra.* 583 pages (in Russian).

Romanowicz, B. 2003. Global mantle tomography: Progress status in the past 10 years. Annu. *Rev. Earth Planet Sci.* Vol. 31, p. 303-328.

Tectonosphere of the Asia-Pacific margin, 1992. Gordienko, V.V., Andreyev, A.A., Bikkenina, S.K., et al. Vladivostok: *FEB RAS*. 238 p. (in Russian).

Udintsev, G.B., 1987. Topography and structure of the ocean floor. Moscow, *Nauka*. 340 pages (in Russian).

Walck, M. 1985. The upper mantle beneath the north-east Pacific rim: A comparison with the Gulf of California. *Geoph. J. R. Astr. Soc.* Vol. 81, p. 43-276.

Zhao, M., Langston, C., Nyblade, A., and Owens T., 1999. Upper mantle velocity structure beneath southern Africa from modelling regional seismic data. *J.G. R*., Vol. 104, B3, p. 4783-4794.

INTERNATIONAL STUDY ITALY-MALAYSIA PRE-SEISMIC SIGNALS RECORDED BY RDF – RADIO DIRECTION FINDING MONITORING NETWORK, BEFORE EARTHQUAKES: MW 6.3, OCCURRED AT 111 KM SW OF PUERTO MADERO IN MEXICO AND MW 6.3, OCCURRED AT 267 KM NW OF OZERNOVSKIY IN RUSSIA, NOVEMBER 20, 2019.

Taha Rabeh (1), Daniele Cataldi (2), Zamri Zainal Abidin (3),
Gabriele Cataldi (4), Valentino Straser (5)

[1]National Research Institute of Astronomy and Geophysics (NRIAG), Helwan, Cairo, Egypt (EGY). taharabeh@yahoo.com
[2]Radio Emissions Project, Lariano, Rome, Italy (I). daniele77c@hotmail.it
[3]Radio Cosmology Research Lab, Department of Physics, Faculty of Science, University of Malaya, Kuala Lumpur, Malaysia (MY). zzaa@um.edu.my
[4]Radio Emissions Project, Cecchina, Rome, Italy (I). ltpaobserverproject@gmail.com
[5]Department of Science and Enviroment UPKL Brussel (B). valentino.straser@gmail.com

ABSTRACT

Through this study, the authors want to establish the existence of a possible correlation between the electromagnetic signals recorded and the occurrence of some strong earthquakes of magnitude:

1. M 6.3 - 111km SW of Puerto Madero, Mexico - 2019-11-20 04:27:05 (UTC) GPS: 13.982°N 93.130°W - 11.0 km depth.
2. M 6.3 - 267km NW of Ozernovskiy, Russia - 2019-11-20 08:26:07 (UTC) GPS: 53.163°N 153.685°E - 486.8 km depth.

In this context, the study was carried out by a close international cooperation between Italy and Malaysia, from the monitoring network developed by the Radio Emissions Project, based on the RDF technology - Radio Direction Finding, which is also part of Malaysia. The data have identified the presence of electromagnetic signals having a precise azimuth of arrival and is registered by the Italian resort of RDF – Ripa-Fagnano (AQ) (GPS: Lat. +42.265663N, Long. +13.583765E), both from the station Pontedera, (PI) (GPS: Lat. +43.672479N, Long: +10.640079E), and the equation for the RDF station Malaysia, University of Malaya (GPS: Lat: +3.120956N, Long: +101.655326E).

Keywords: RDF systems, earthquake prevision, electromagnetic signals, candidate precursors.

INTRODUCTION

It was 1890 when the British geologist John Milne, inventor of the eponymous horizontal seismograph, a professor at the Imperial College of Engineering in Tokyo and founder of the Seismological Society of Japan (SSJ), in his work entitled "*Earthquakes in connection with electric and magnetic phenomena*" (J. Milne, 1890), described some electrical phenomena magnetic and related to seismic activity. It was the first scientific publication ever in which they were described a series of electromagnetic phenomena, about one hundred years later, the international scientific community renamed as "*Electromagnetic Seismic Precursors*" or ESPs. In 2007, Gabriele Cataldi and Daniel Cataldi founded a scientific research project (Radio Emissions Project) dedicated to monitoring and study of Electromagnetic Seismic Precursors (ESPs) and, in the course of a few years, they have developed an innovative electromagnetic tracking method (G. Cataldi, 2019), who was able to provide valuable data on the pre-seismic electromagnetic anomalies, meaning by this term also electromagnetic phenomena of solar origin and those of geomagnetic nature (G. Cataldi et al., 2013-2019; D. Cataldi et al., 2014-2019; V. Straser, 2011-2012; Straser V. et al., 2014-2019). The use of the RDF system, as part of the seismic prediction, has been realized starting from March 2017, from Radio Emissions Project, through which it was possible to obtain the first important results on the registration of electromagnetic signals appeared before the occurrence of strong earthquakes (Straser et al., 2017). In this suit, the international cooperation with

Malaysia and with Radio Cosmology Research Lab, Department of Physics, Faculty of Science University of Malaya, has allowed us to further develop the monitoring capabilities of the RDF system for the identification, registration and the analysis of pre-seismic electromagnetic emissions on a global scale.

1.0 – METHODS AND DATA

1.1 – Monitoring Stations.

To carry out this study, the authors analyzed the electromagnetic signals from the three main stations:

- **First station**: Italian RDF Station Ripa-Fagnano (AQ) (Lat. + 42.265663N, Long. +13.583765E), equipped with a station monitoring continuous electromagnetic monitoring, broadband, technology implemented with RDF (Radio Direction Finding). The technology developed by the Radio Emissions Project, for the monitoring of the pre-seismic radio emissions, it is able to identify the target arrival direction (azimuth) of the electromagnetic signals picked up between the band SELF (Super-Extremely-Low-Frequency: 0 <f <3Hz) and the first portion of the band LF (Low-Frequency; 30 <f≤300kHz) reaching 96kHz (total bandwidth ≈ 96kHz; 0 <f≤96 kHz) with a resolution <1Hz, an analog-to-digital conversion 24-bit and a digital sampling to 192kHz.
- **Second Station**: Malaysian RDF station of Kuala Lumpur, (Lat. +3.123088N, Long. +101.653117E), this one equipped with a station monitoring continuous electromagnetic monitoring, broadband, technology implemented with RDF (Radio Direction Finding). The technology developed by the Radio Emissions Project, for the monitoring of the pre-seismic radio emissions, it is able to identify the target arrival direction (azimuth) of the electromagnetic signals picked up between the band SELF (Super-Extremely-Low-Frequency: 0 <f <3Hz) and the first portion of the band LF (Low-Frequency; 30 <f≤300kHz) reaching 96kHz (total bandwidth ≈ 96kHz; 0 <f≤96 kHz) with a resolution <1Hz, an analog-to-digital conversion 24-bit and a digital sampling to 192kHz.
- **Third Station:** Italian RDF station of Pontedera (PI), (Lat. +43.672479N, Long: +10.640079E), this one equipped with a station monitoring continuous electromagnetic monitoring, broadband, technology implemented with RDF (Radio Direction Finding) . The technology developed by the Radio Emissions Project, for the monitoring of the pre-seismic radio emissions, it is able to identify the target arrival direction (azimuth) of the electromagnetic signals picked up between the band SELF (Super-Extremely-Low-Frequency: 0 <f <3Hz) and the first portion of the band LF (Low-Frequency; 30 <f≤300kHz) reaching 96kHz (total bandwidth ≈ 96kHz; 0 <f≤96 kHz) with a resolution <1Hz, an analog-to-digital conversion 24-bit and a digital sampling to 192kHz.

All three stations are equipped by an antenna system, oriented on the cardinal axes, and characterized by square loops with a copper wire winding 25 and 50 coils. The signals converted by the amplification system developed by the Radio Emissions Project, it is then processed by a computer system that generates a set of dynamic spectrograms and graphs on which then has been possible to carry out the analysis.

1.2 – Case number one:

On November 16, 2019, around at 22:10 UTC, the RDF station Ripa-Fagnano (AQ), showed the appearance of electromagnetic signals of azimuth "bluish-violet" (Fig. 3), with characteristics of impulsivity in frequent appearance, located mainly between 0-2 kHz, 5-20 kHz and 40-45 kHz (Fig. 1). This first increment is then passed around at 23:20 UTC of 15 November 2019, only to reappear in a peremptory manner around 10:30 hours UTC of 16 November 2019, presenting a similar frequency distribution with respect to the first appearance, namely: between 0- 2 kHz, between 5-20 kHz (Fig. 2).

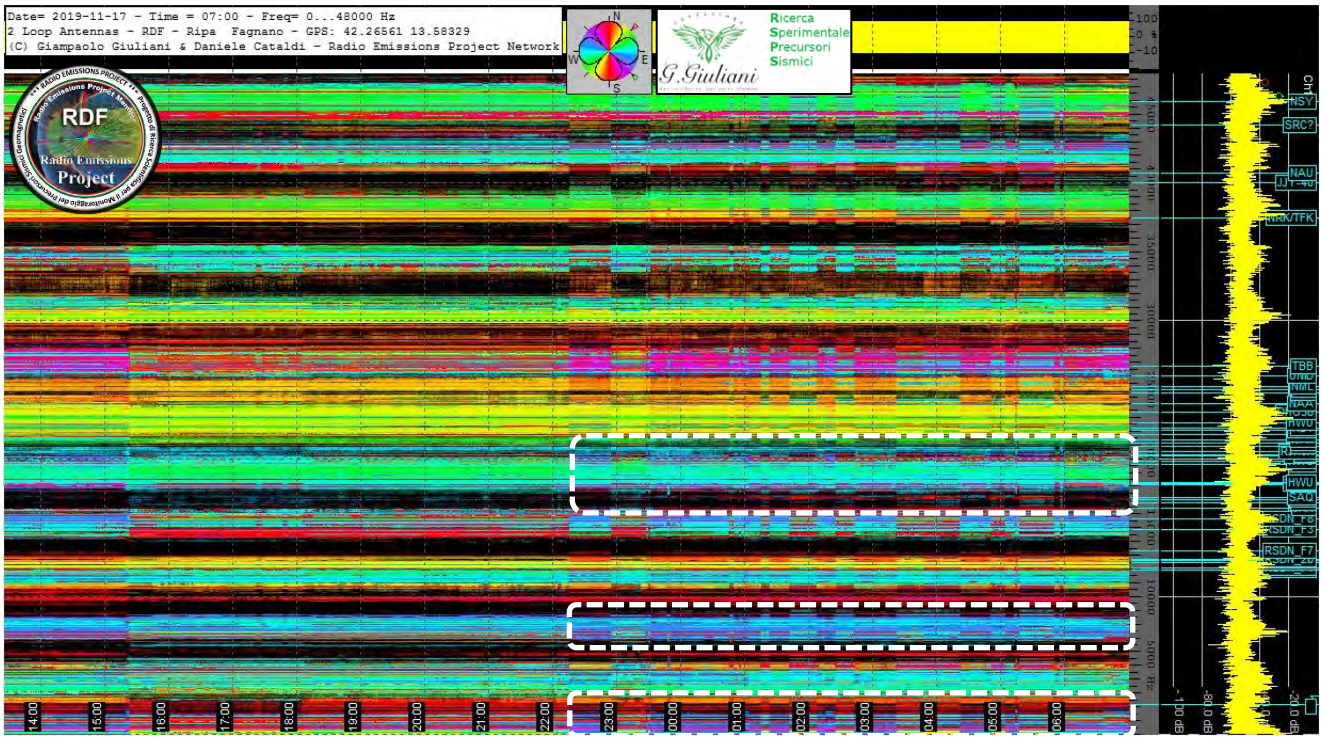

Figure 1 – Spectrogram of Radio Emissions Project, Ripa-Fagnano station (AQ), which highlights the presence of electromagnetic color signals "bluish-violet" (Fig. 3), displaced in frequency, broadband. Source: Radio Emissions Project and Permanent Foundation G. Giuliani.

All signals, clearly evident, they are presented without any notice, so detached from the normal background natural geomagnetic. The detection system of Ripa-Fagnano (AQ) has indicated the precise azimuth, bluish-violet color (Fig. 3).

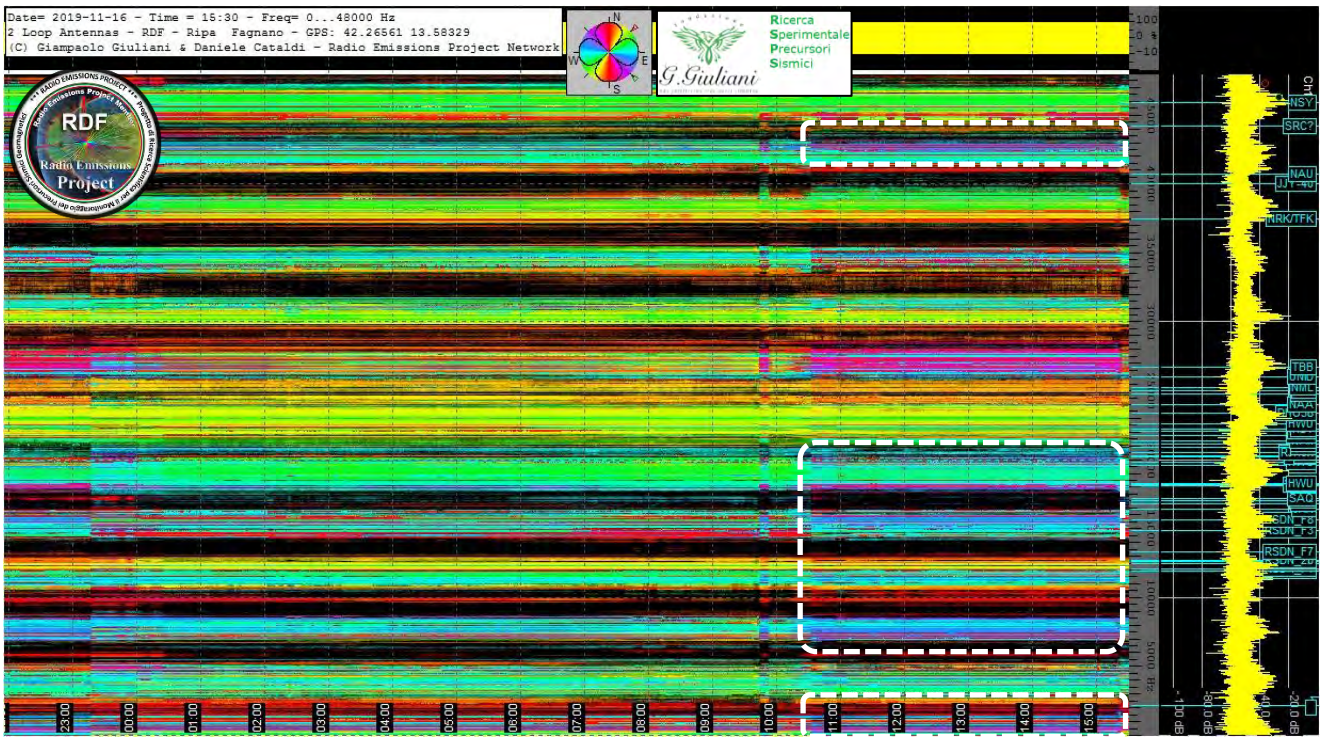

Figure 2 – Spectrogram of Radio Emissions Project, station-Ripa Fagnano (AQ), which highlights the presence of electromagnetic color signals "bluish-violet" (Fig. 3), displaced in frequency, broadband. Source: Radio Emissions Project and Permanent Foundation G. Giuliani.

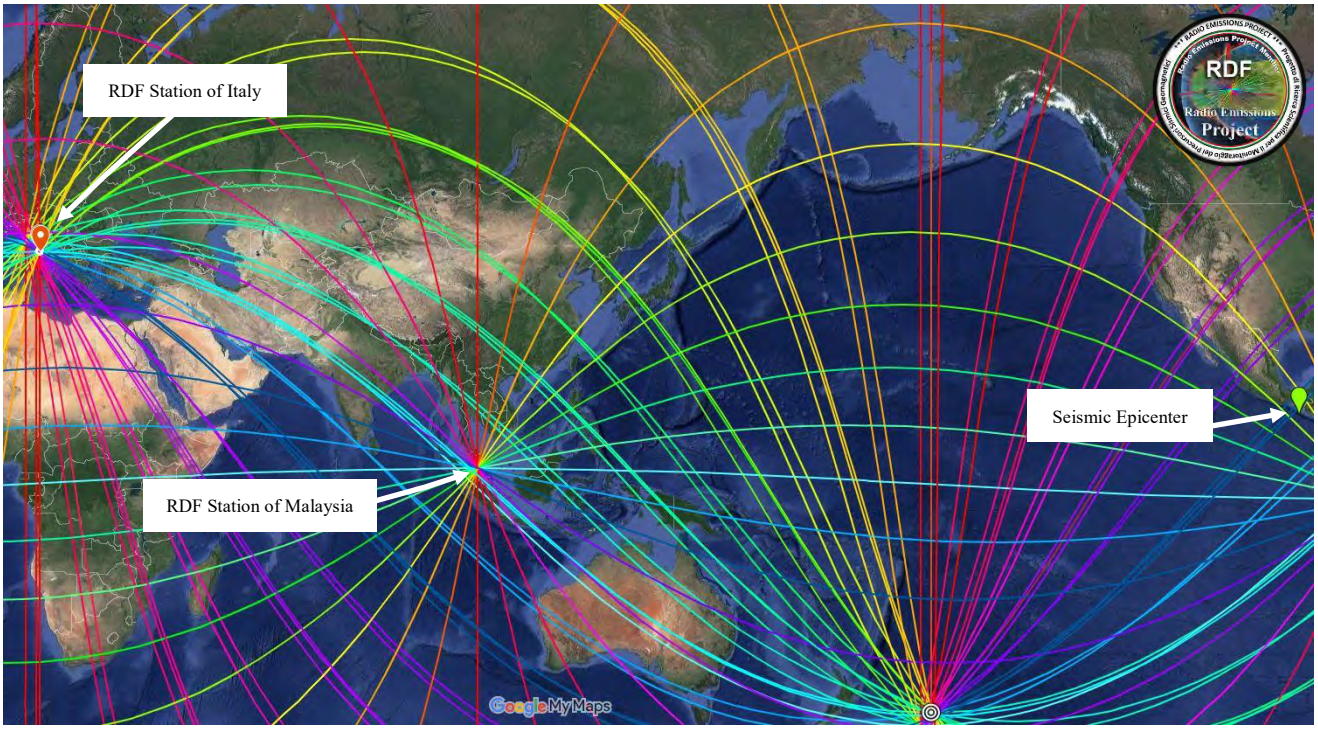

Figure 3 – World Mapping the RDF system, developed by the Radio Emissions Project, it highlights the azimuths of the various monitoring stations located on the globe and the earthquake epicenter considered in this study. Source: Radio Emissions Project, Google Maps.

In the same period the Malaysian RDF station, recorded the increases not be underestimated, including azimuth between the yellow and the green (Fig. 3). In this context, the highlighted increments and recorded by the Malaysian RDF station emphasized as such signals of the electromagnetic type had appeared without notice, and equipped with precise azimuthal characteristics

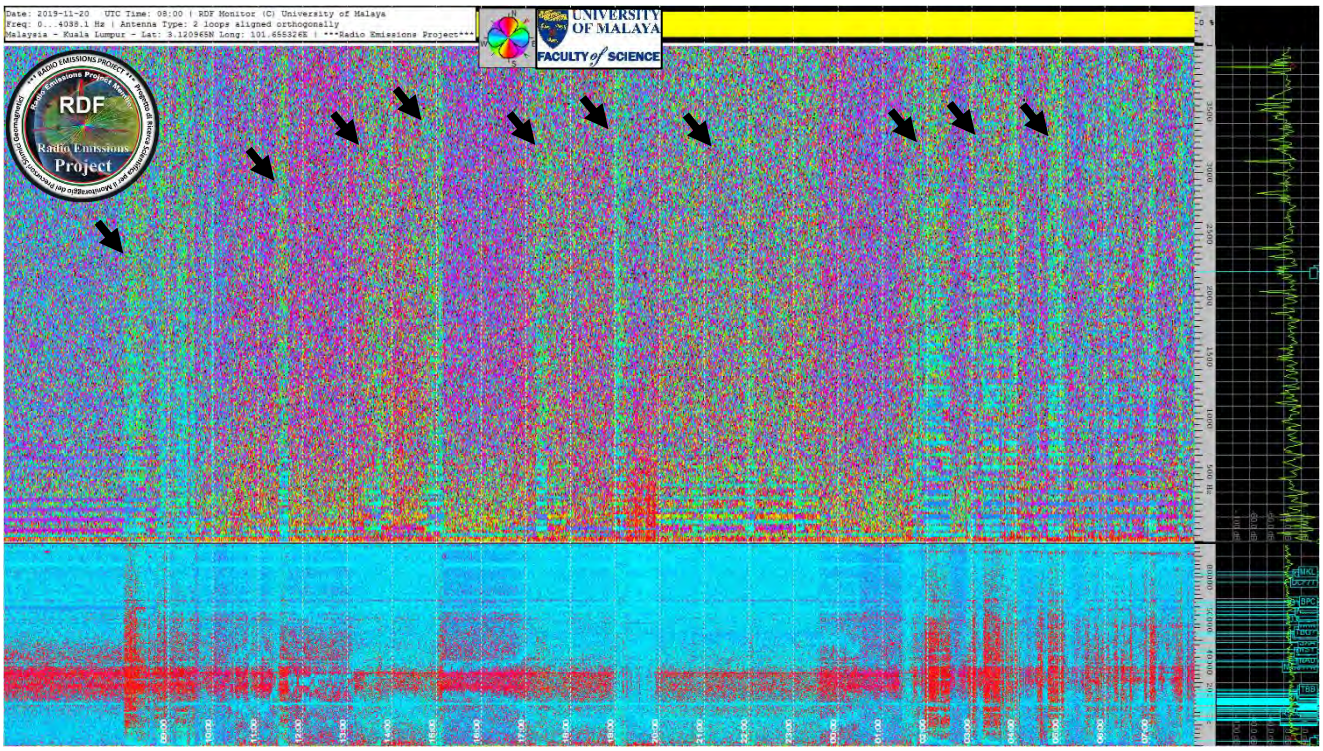

Figure 4 – Spectrogram of Radio Emissions Project, Malay house, run by the University of Malaya. It shows the presence of signals on a yellow-green azimuth (azimuth visible on the map in Fig. 3), and appeared previously to the earthquake which occurred in Massico, object of this study. Source: Radio Emissions Project Network, University of Malaya.

The increases recorded by that station (Malaysia), have appeared with impulsivity characteristics, confirming the recordings of the Italian station Ripa-Fagnano (AQ), as shown in Fig. 1 and 2. In addition

to this it has been possible to ascertain the presence of emissions located in a restricted time period, just behind the earthquake, the subject of this study. The characteristics of the signals recorded by the Malaysian RDF station are the following: the increase occurred between the hours of 11:00 UTC of 19 November 2019 02:00 UTC of 20 November 2019. The electromagnetic frequency of the recorded signals, as evidenced by the RDF system was between 0-5 kHz and 0-48 kHz increments to the entire band (Fig. 4).

1.3 – Triangulation of the received signals.

Following the appearance of such increments, highlighted by the RDF stations, it has been possible to realize a triangulation suggested by the azimuth highlighted by the detection system, in this case:

1. The first type of signal has been the one with azimuth bluish-purple, evidenced by Italian RDF station.

2. The second type of signal has been the one with yellow-green azimuth, recorded by the Malaysian RDF detection station.

Both signals, if we look at the global mapping of the RDF system (Fig. 3) intersect along the area of the center-America (Mexico), and should be to identify, with some degree of phase shift of the signal, due to the high distance of detection, well-defined area (Fig. 5). The study shows that the electromagnetic emissions have had a certain percentage of the signal phase shift in degrees, such as not having made it possible to accurately identify the real seismic epicenter. On this issue we are working to try to understand what the cause is. The main hypothesis, see the presence of electromagnetic emission is not isotropic, that is due to the particular structure of the fault and the crustal structure that is not capable of emitting an isotropic signal that is irradiated in a regular manner along each direction, but due to the characteristics the earth's crust, such emissions are partly directional.

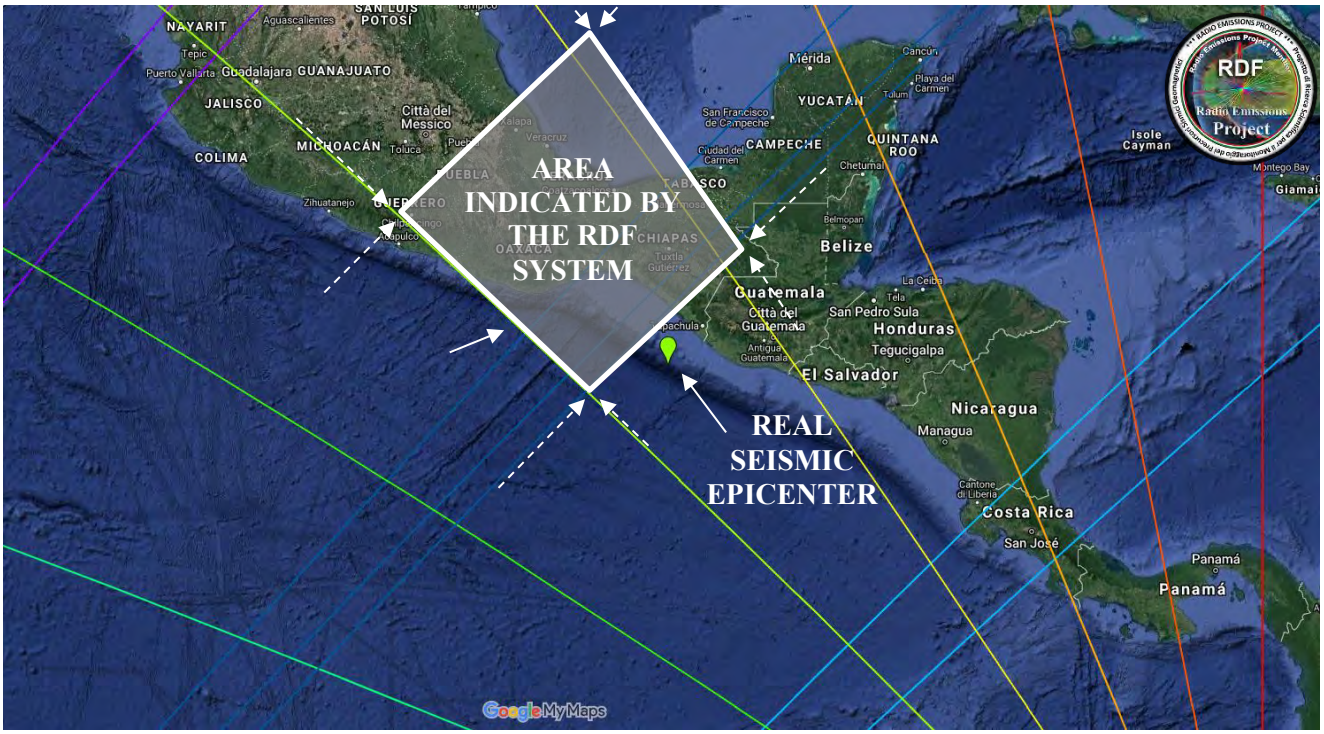

Figure 5 – World Mapping the RDF system, developed by the Radio Emissions Project, it highlights the azimuths of the various monitoring stations located on the globe and the earthquake epicenter considered in this study. In this case, the area indicated by the RDF system was highlighted in advance an area close to the epicenter earthquake. Source: Radio Emissions Project, Google Maps.

The non-homogeneity of the issuer, may in this case generate signals that are spread unevenly from the electromagnetic emission source and, therefore, can get to the monitoring station in a slightly phase-shifted in azimuth. Considering then the ionospheric variations where such signals are guided (propagation of the Earth-ionosphere cavity), also due to solar activity and weather, it is understood as

such phase shift can be frequent. In this regard it would require additional RDF stations, spread on the globe to increase the accuracy of the detection system.

1.4 - Case number two:

On the same day, it occurred a second earthquake of high intensity: 6.3 mW at 267km NW of Ozernovskiy, Russia - 11/20/2019 08:26:07 (UTC) (GPS: 53 163 153 685 ° N ° E) 486.8 km depth. Around at 00:45 UTC of 19 November 2019, one of the Italian RDF stations, this time localized in Pontedera (PI), recorded some very interesting impulsive increments (Fig. 6):

- Peak hours of 00:45 UTC - 40 kHz (mid-frequency signal).
- Peak hours of 02:50 UTC - 40 kHz (mid-frequency signal).
- Peak hours of 04:05 UTC - 40 kHz (mid-frequency signal).
- Peak hours of 06:05 UTC - 40 kHz (mid-frequency signal).
- Peak hours of 07:15 UTC - 40 kHz (mid-frequency signal).
- Peak hours of 08:20 UTC - 40 kHz (mid-frequency signal).

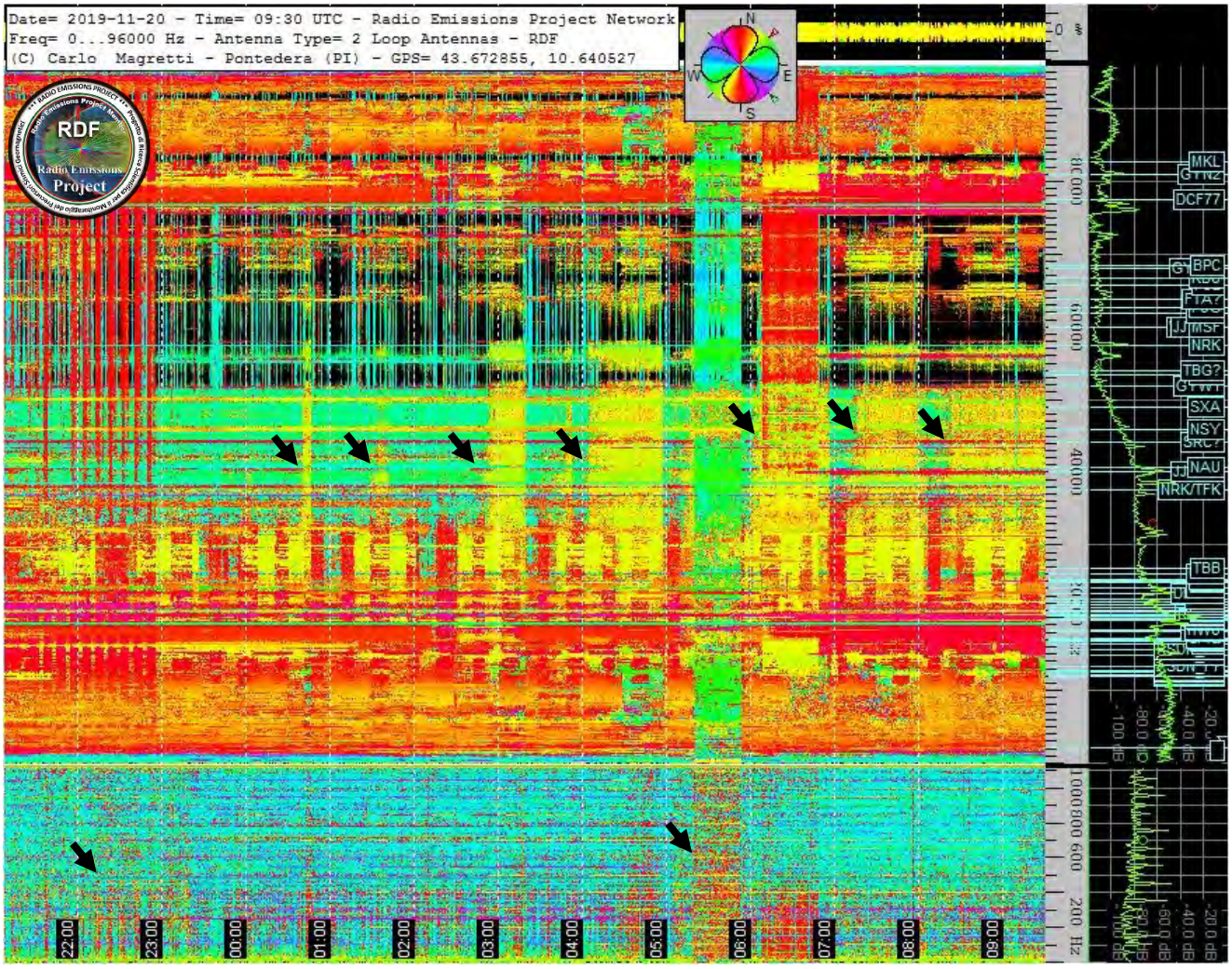

Figure 6 – Spectrogram of Pontedera RDF station (PI), in Italy, managed by Mr Carlo Magretti (collaborator of Radio emissions Project), in which one sees some net and intense electromagnetic emissions yellow (yellow azimuth), which appeared to start from hours: 00:45 UTC on 18 November 2019. Source: Radio Emissions Project Network.

Such electromagnetic increments have had an azimuth of yellow color, well detached from the natural geomagnetic bottom, while some yellowish increments have appeared in band SELF-ULF, between

22:00 UTC of 19 November 2019 the 05:20 UTC on November 20, 2019 . The researchers' hypothesis is that there was therefore important electromagnetic emissions along that azimuth. The confirmation is then arrived from the RDF station of Malaysia, when an increase of all well detached from the local geomagnetic bottom and also this impulsive type, showed the presence of electromagnetic emissions with yellowish type azimuth and orange.

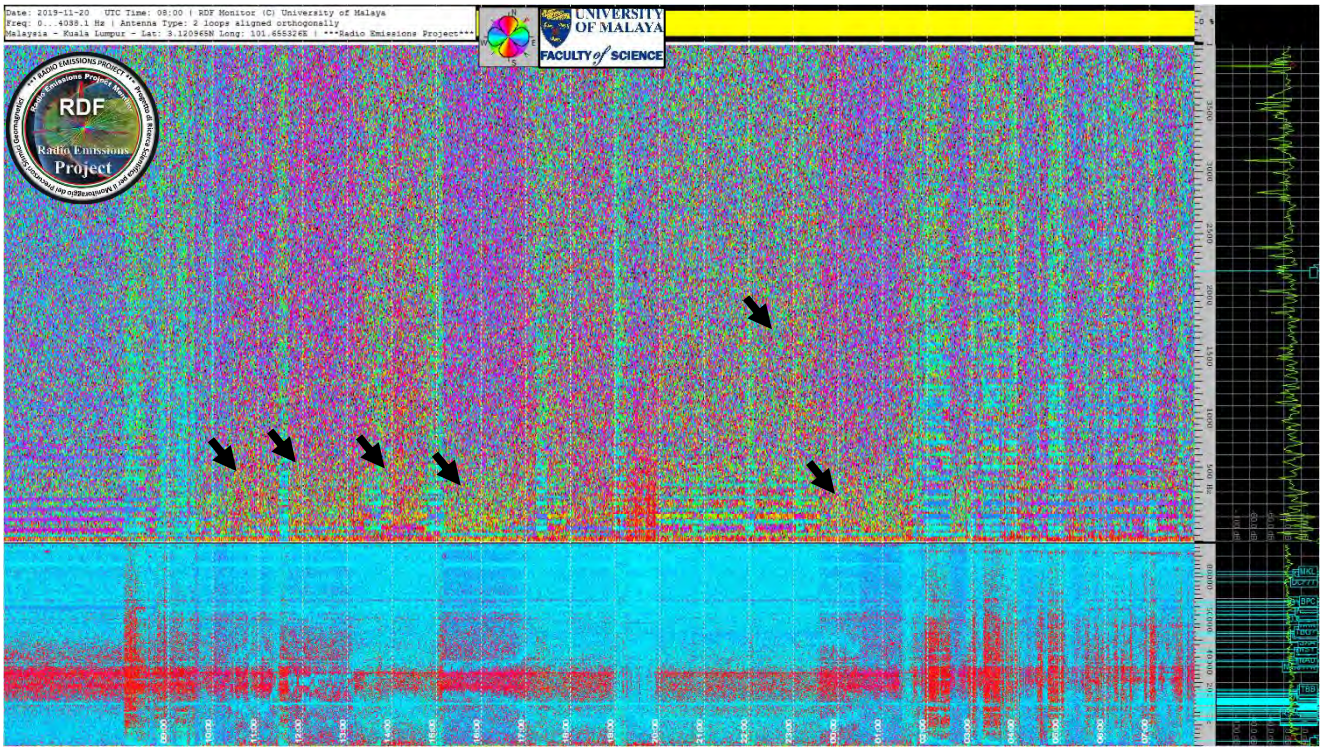

Figure 7 – Spectrogram of Kuala Lumpur RDF station, Malaysia, managed by the University of Malaya. It shows the presence of signals on azimuth yellowish-orange (as visible in Fig map 8 and 9), especially appeared within the 5 kHz and at full bandwidth (40 kHz). Source: Radio Emissions Project Network, University of Malaya.

The data confirmed that there was an act an intense electromagnetic emission of crustal origin which could identify. These increases had appeared at the following times and frequencies to the same medium:

November 19, 2019

- 10:00 UTC - by 1 kHz
- 11:50 UTC - by 1 kHz
- 13:50 UTC - by 1 kHz
- 15:10 UTC - by 1 kHz
- 17:30 UTC - by 1 kHz
- 23:15 UTC - by 1 kHz

November 20, 2019

- 02:30 UTC - by 1 kHz

Such electromagnetic surges lasting up to a few hours, they occurred sporadically to the entire band 0-40 kHz), between 10:00 UTC of 19 November 2019, and 03:00 UTC on 20 November 2019. The increase has had a sudden appearance, and it was clearly visible. The RDF system has now determined the azimuth of origin, providing useful data to the triangulation of the signals to intercept the emission area (as shown in Fig. 7).

1.5 – Triangulation of the received signals.

Triangulation was made by weaving the data of the stations of Pontedera, Pisa, Italy, and one in Kuala Lumpur, Malaysia. The data in fact could provide precise details in a azimuth reported by the RDF system, which showed an area positioned at Russia.

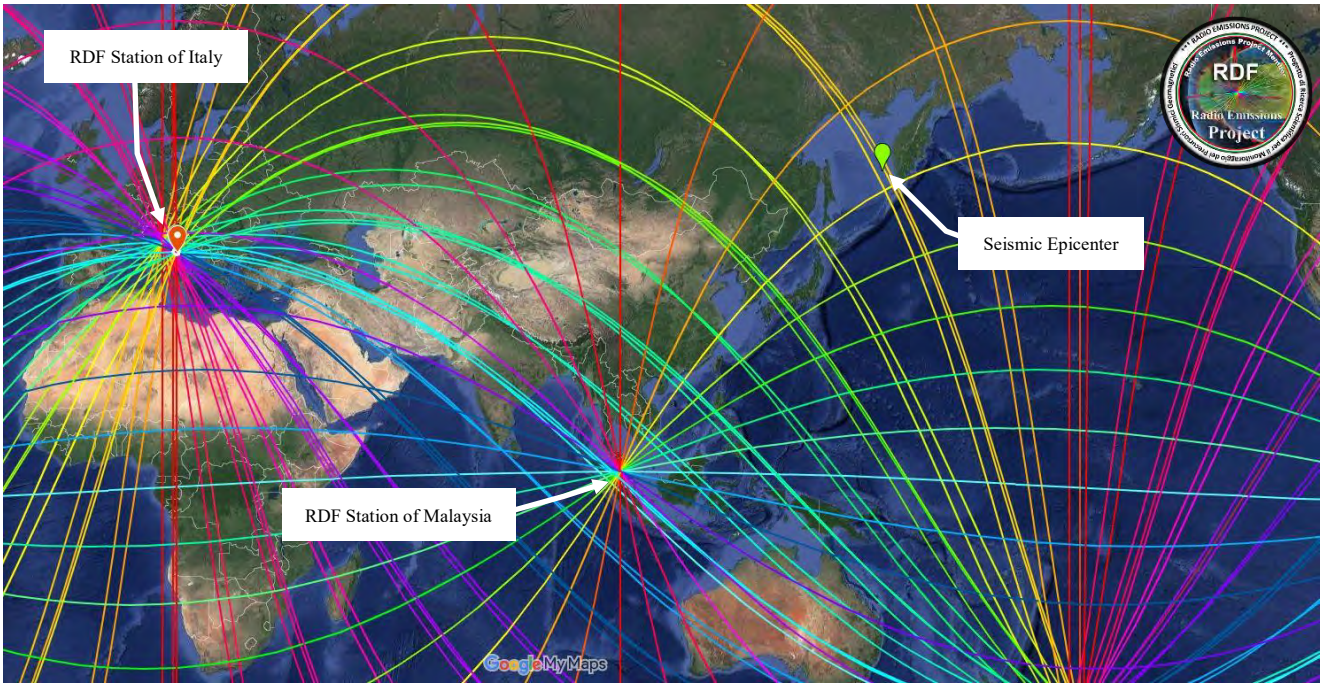

Figure 8 – World Mapping the RDF system, developed by the Radio Emissions Project. It shows the azimuths of the two stations considered in this study and the location of the epicenter earthquake. Source: Radio Emissions Project.

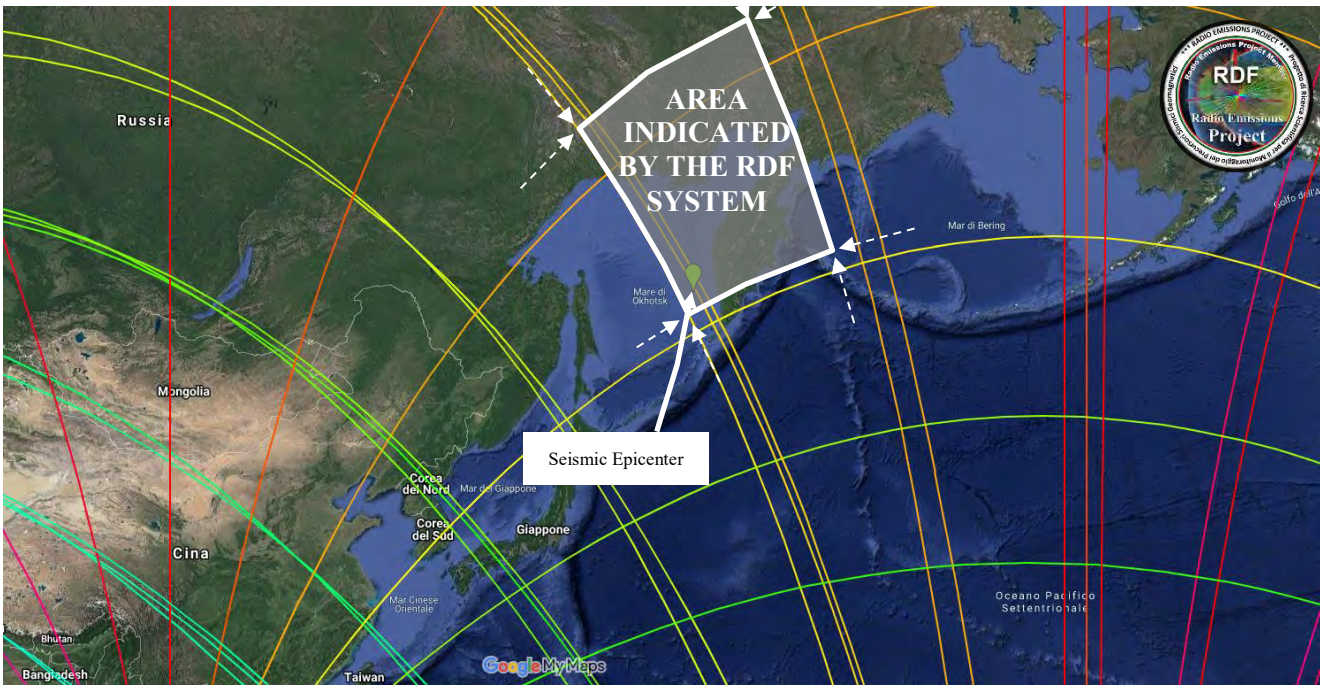

Figure 9 – World Mapping the RDF system, developed by the Radio Emissions Project. It shows the azimuths of the two stations considered in this study and the location of the epicenter earthquake. In this case the magnification sports highlights the geographic portion identified by the RDF system in triangulation. Source: Radio Emissions Project.

In this case the data supplied by RDF system as confirmed in that area could be the strong earthquake. Within a few hours, in fact, the quake occurred. Exactly at: 08:26:07 (UTC) of 20 November 2019, ie at the end of the increase reported by RDF station in Kuala Lumpur, Malaysia, and in the course of the increase reported from Pontedera RDF station (PI).

2.0 DISCUSSION

2.1 – The detection method.

The electromagnetic detection system, used in this study has the ability to detect signals coming also from a considerable distance, as compared to other survey and monitoring systems with which it is not possible to obtain such a capacity and sensitivity.

Mexican Earthquake:

- In addition 10.2 thousand kilometers away from the point of origin of the electromagnetic emissions from the Italian RDF station.
- More than 17,500 kilometers away from the point of origin of the electromagnetic emissions from the Malaysian RDF station.

Russian Earthquake:

- More than 8,600 km away from the point of origin of electromagnetic emissions, from the Italian RDF station.
- More than 7300 km away from the point of origin of the electromagnetic emissions from the Malaysian RDF station.

The use of electromagnetic amplification systems, such as those developed by the Radio Emissions Project, also allows greater highlight weaker signals compared to those present in the natural electromagnetic background which tends to cover them (electromagnetic noise). In this case the method used ensures the amplification of such signals and the recognition of their arrival azimuth.

2.2 – Prevision Hypothesis.

While it is therefore possible to obtain, as in this case, signals having a precise azimuth, it is possible to consider them in a forecasting context that has a certain precision? Of course it is, even if in order to obtain greater accuracy, which is sufficient to suggest the area within which to expect a strong earthquake, it must necessarily increase the number of RDF stations, and dislocarle on the Earth's surface.

The spatial distribution of the RDF system is just one of the essential elements in order to ensure a certain predictive accuracy, a great importance lies in the elaboration of the same signals on their ability to be triangulated and thus obtain continuous data. In this regard there is the need of having to use a computer system that carries out such work in an automated manner, indicating the azimuth of the signals and the possible area in which it can verify the earthquake.

The analysis of this study, has allowed us to emphasize the importance of the methodology based on triangulation of electromagnetic signals and on the construction of an automatic detection system, active 24h7.

2.3 - Error in azimuth

In the course of the RDF system experimentation, developed by the Radio Emissions Project, it was several times denoted a small signal localization error, especially over long distances, or in those signals coming from a distance of several hundred kilometers. In this context, the detection system has denoted the origin of the signals with an error of about 5 degrees (maximum approximation). After the initial trial was concluded by researchers that this error is generated by the phenomenon known as "Fading". The fading can be flat or constant at different frequencies, or selective or depend on the frequency, thus generating a distortion in the signal amplitude. In this case, the types of Fading identified by researchers who were able to interact with the monitoring system are the following:

1. STATIC FADING due to the absorption by oxygen and atmospheric water vapor (mostly at certain absorption peaks corresponding to the respective molecular resonances). In these bands it

is obviously not advisable to transmit any electromagnetic power. The complementary bands useful for transmission are commonly known as transmissive windows.

2. SPARKLING FADING, due to the scattering particle and characterized by low levels of attenuation and zero average over time.
3. DEEP FADING characterized by high levels of attenuation. It may be due to the presence of multiple paths (*multipath fading*) followed electromagnetic wave in its path and whose recombination in phase is random in time generating power variations in the receiver as a result of constructive or destructive interference.
4. FADING BY PRECIPITATION (eg. rain): strongly increases with the frequency of the electromagnetic wave and is depending on the intensity of precipitation.
5. EFFECT FROM FADING DUCT: anomalies in the vertical distribution of the refractive index, caused by changing weather conditions (eg. Temperature inversions), leading to the formation of 'atmospheric ducts' remains confined in which the electromagnetic signal which undergoes strong attenuations in the reflection on the walls of the duct itself.
6. FADING OF REFLECTION FROM SOIL that produces reflected waves that come in addition, with different phases, creating direct wave interference and fading random similar to multipath fading.
7. FADING FOR DIFFRACTION due to the presence of physical obstacles.

In the physical system considered, namely that the propagation of electromagnetic emissions, compared to the location of the monitoring station, must also be considered the type of electromagnetic emission generated at the level crustal (both in the fault surface that in the immediate vicinity, for piezoelectric effect and for effect of the formation of flowing charges that generate electric dipole and thus natural load-bearing).

In this context the electromagnetic emission generated at the level of the fault is susceptible to the following characteristics of the rocks capable of varying the type of issue:

1. Form and extent of the fault and the area in which it accumulates the tectonic stress and, therefore, where they accumulate the electrical particles flowing (current) capable of generating an electromagnetic field.
2. Presence of obstacles in the vicinity of the fault point of origin, as the presence of mountains.
3. Rock type and their crystal lattice.
4. Presence of water.
5. Depth emission of electromagnetic signals, with respect to the ground level.
6. Pressure and temperature of the rocks.
7. Electromagnetic permeability of the rock layers.
8. Type intrusion inside the rocks, such as ferrous or siliceous elements.

All these characteristics can affect the type of signal generated, beyond its power in kW. It is therefore a physical system that has many variables and which may determine a different electromagnetic field according to the characteristics mentioned above. These variables have been widely debated by researchers and already identified starting from 2017. In this case, the signals may propagate in different directions and thus assume the delays and variations in azimuth with respect to their initial point of origin (Straser et al., 2018).

Hence the importance, confirmed by all researchers, who resides in the installation of more RDF stations

located on the globe, which would be able to better identify the origin of these crustal emissions and thus reduce the level of error of the system.

3.0 – CONCLUSIONS

In conclusion, the researchers involved in this study, important to consider the use of such a detection system, associated with the prediction-seismic and to the study of seismogenesis, as well as to the study of solar activity (closely related).

The data highlighted by the survey stations, equipped by the RDF technology - Radio Direction Finding, have provided important information and sufficient to consider such a detection technique, useful for earthquake prediction to a certain degree. The data are still scarce in order to use this method accurately, so the researchers all agree on the need for dissemination of this technology on a global scale. It is also important to proceed in improvement of the receiving system using the best sound systems, they can provide information even more precise and sharp, starting with the system designed and developed by the Radio Emissions Project.

The data have confirmed that the recorded electromagnetic signals, can be considered of electromagnetic seismic precursors (PSE), having direct relation both temporal and azimuth with the earthquake occurred in Mexico and Russia. It was also all agree how the dislocation of other RDF stations on Earth's soil, having to be made quickly.

ACKNOWLEDGMENTS

We would like to thank the researchers and students who took part in the creation of the RDF system in Malaysia, without their irreplaceable contribution, the study would not have been possible. Between these:

- Zamri Zainal ABIDIN Sector: Radio Astronomy.
- Mohd Shazwan Mohd RADZI Sector: Solar Radio Physics.
- Abdul Aziz Ahmed SIYAD Sector: Radio Astronomy Instrumentation.
- Zainol Abidin IBRAHIM Sector: Astronomy Instrumentation.

We also thank Prof. Taha Rabeh for representing the Radio Emissions Project in the context of international research in Malaysia. Thank you all.

Daniele Cataldi and Gabriele Cataldi - Radio Emissions Project founders

REFERENCES

1. Radio Direction Finding System, a new perspective for global crust diagnosis - New Concepts in Global Tectonics Journal, v. 6, no. 2, June 2017. Valentino Straser1 Department of Science and Environment UPKL Brussels, Daniele Cataldi 2, Radio Emissions Project, Rome, Gabriele Cataldi 3, Radio Emissions Project, Rome.

2. Radio Direction Finding (RDF) - Pre-seismic signals recorded before the earthquake in central Italy on 1/1/2019 west of Collelongo (AQ) - Daniele Cataldi (1), Gabriele Cataldi (2), and Valentino Straser (3) - (1) Radio Emissions Project, Rome, Italy (daniele77c@gmail.com), (2) Radio Emissions Project, Rome, Italy (ltpaobserverproject@gmail.com), (3) - Department of Science and Environment UPKL, Brussels (valentino.straser@gmail.com) - Geophysical Research Abstracts Vol. 21, EGU2019-3124, 2019 EGU General Assembly 2019.

3. G. Cataldi. (2019). Precursori Sismici – Monitoraggio Elettromagnetico. Lulu.com. ID: 24294486, ISNB: 9780244820053.

4. G. Cataldi, D. Cataldi. (2013). Reception of Natural Radio Emissions in the ELF Band. The INSPIRE Journal, Volume 20, Spring/Summer 2013.

5. G. Cataldi, D. Cataldi. Sismicità – Gas Radon – Elettromagnetismo – Radioattività. Reti di monitoraggio ufficiali e amatoriali. Stato dell'arte nella ricerca di segnali possibili precursori sismici. Regione Autonoma Friuli Venezia Giulia, Protezione Civile. Comune di Pozzuolo Del Friuli, F.E.S.N. 2014. pp. 44-49; 97-99.

6. G. Cataldi, D. Cataldi, V. Straser. (2018). Solar wind ionic density variations related to M6+ global seismic activity between 2012 and 2018. European Geosciences Union (EGU) General Assembly 2019, Short-term Earthquake Forecast (StEF) and multy-parametric time-Dependent Assessment of Seismic Hazard (t-DASH) (NH4.3, AS4.62, EMRP2.40, ESSI1.7, Gi2.13, SM3.9), General Contribution on Earthquakes, Earth Structure, Seismology (SM1.1), Geophysical Research Abstract, Vol. 21, EGU2019-3067, 2019, Vienna, Austria.

7. G. Cataldi, D. Cataldi, V. Straser. (2017). Solar and Geomagnetic Activity Variations Correlated to Italian M6+ Earthquakes Occurred in 2016. European Geosciences Union (EGU), General Assembly 2017. Geophysical Research Abstracts Vol. 19, EGU2017-3681, 2017. Seismology (SM1.2)/Natural Hazards (NH4.7)/Tectonics & Structural Geology (TS5.5) The 2016 Central Italy Seismic sequence: overview of data analyses and source models.

8. G. Cataldi, D. Cataldi, V. Straser. (2017). Solar and Geomagnetic Activity Variations Correlated to Italian M6+ Earthquakes Occurred in 2016. European Geosciences Union (EGU), General Assembly 2017. Geophysical Research Abstracts Vol. 19, EGU2017-3681, 2017. Seismology (SM1.2)/Natural Hazards (NH4.7)/Tectonics & Structural Geology (TS5.5) The 2016 Central Italy Seismic sequence: overview of data analyses and source models.

9. G. Cataldi, D. Cataldi, V. Straser. (2017). Solar wind proton density increase that preceded Central Italy earthquakes occurred between 26 and 30 October 2016. European Geosciences Union (EGU), General Assembly 2017. Geophysical Research Abstracts Vol. 19, EGU2017-3774, 2017. Seismology (SM1.2)/Natural Hazards (NH4.7)/Tectonics & Structural Geology (TS5.5) The 2016 Central Italy Seismic sequence: overview of data analyses and source models.

10. G. Cataldi, D. Cataldi, V. Straser. (2016). Solar activity correlated to the M7.0 Japan earthquake occurred on April 15, 2016. New Concepts in Global Tectonics Journal, V. 4, No. 2, June 2016.

11. G. Cataldi, D. Cataldi, V. Straser. (2015). Solar wind proton density variations that preceded the M6,1 earthquake occurred in New Caledonia on November 10, 2014. European Geosciences Union (EGU) General Assembly 2015, Geophysical Research Abstract, Vol. 17, Vienna, Austria. Natural Hazard Section (NH5.1), Sea & Ocean Hazard - Tsunami, Harvard-Smithsonian Center for Astrophysics, High Energy Astrophysics Division, SAO/NASA Astrophysics Data System.

12. G. Cataldi, D. Cataldi, V. Straser. (2015). Solar wind ion density variations that preceded the M6+ earthquakes occurring on a global scale between 3 and 15 September 2013. European Geosciences Union (EGU) General Assembly 2015, Geophysical Research Abstract, Vol. 17, Vienna, Austria. Natural Hazard Section (NH5.1), Sea & Ocean Hazard - Tsunami, Harvard-Smithsonian Center for Astrophysics, High Energy Astrophysics Division, SAO/NASA Astrophysics Data System.

13. G. Cataldi, D. Cataldi and V. Straser. (2014). Earth's magnetic field anomalies that precede the M6+ global seismic activity. European Geosciences Union (EGU) General Assembly 2014, Geophysical Research Abstract, Vol. 16, Vienna, Austria. Natural Hazard Section (NH4.3), Electro-magnetic phenomena and connections with seismo-tectonic activity, Harvard-Smithsonian Center for Astrophysics, High Energy Astrophysics Division, SAO/NASA Astrophysics Data System.

14. G. Cataldi, D. Cataldi, V. Straser. (2014). Solar wind proton density variations that preceded the M6+ earthquakes occurring on a global scale between 17 and 20 April 2014. European Geosciences Union (EGU) General Assembly 2015, Vienna, Austria. Natural Hazard Section (NH5.1), Sea & Ocean Hazard - Tsunami, Geophysical Research Abstract, Vol. 17, Harvard-Smithsonian Center for Astrophysics, High Energy Astrophysics Division, SAO/NASA Astrophysics Data System.

15. G. Cataldi, D. Cataldi, V. Straser. (2013). Variations Of Terrestrial Geomagnetic Activity Correlated To M6+ Global Seismic Activity. EGU (European Geosciences Union) 2013, General Assembly, Geophysical Research Abstracts, Vol. 15. Vienna, Austria. Harvard-Smithsonian Center for Astrophysics, High Energy Astrophysics Division, SAO/NASA Astrophysics Data System.

16. V. Straser, D. Cataldi, G. Cataldi. (2019). Registration of Pre-Seismic Signals Related to the Mediterranean Area with the RDF System Developed by the Radio Emissions Project. International Journal of Engineering Science Invention (IJESI), www.ijesi.org. Volume 8 Issue 03 Series. March 2019. PP 26-35. ISSN (Online): 2319 – 6734, ISSN (Print): 2319 – 6726.

17. V. Straser, D. Cataldi, G. Cataldi. (2019). Radio Direction Finding (RDF) - Geomagnetic Monitoring Study of the Himalaya Area in Search of Pre-Seismic Electromagnetic Signals. Asian Review of Environmental and Earth Sciences, v. 6, n. 1, p. 16-27, 14 jun. 2019.

18. V. Straser, D. Cataldi, G. Cataldi. (2019). Electromagnetic monitoring of the New Madrid fault us area with the RDF system - Radio Direction Finding of the radio emissions project. New Concepts in Global Tectonics Journal, V7 N1, March 2019.

19. V. Straser, G. Cataldi, D. Cataldi. (2019). Namazu's Tail – RDF: a new perspective for the study of seismic precursors of Japan. Lulu publisher.

20. V. Straser, G. Cataldi, D. Cataldi. (2017). Solar and electromagnetic signal before Mexican Earthquake M8.1, September 2017. New Concepts in Global Tectonics Journal, V. 5, No. 4, December 2017.

21. V. Straser, G. Cataldi. (2015). Solar wind ionic variation associated with earthquakes greater than magnitude M6.0. New Concepts in Global Tectonics Journal, V. 3, No. 2, June 2015, Australia. P.140-154.

22. V. Straser, G. Cataldi, D. Cataldi. (2015). Solar wind ionic and geomagnetic variations preceding the Md8.3 Chile Earthquake. New Concepts in Global Tectonics Journal, V. 3, No. 3, September 2015, Australia. P.394-399.

23. V. Straser, G. Cataldi. (2014). Solar wind proton density increase and geomagnetic background anomalies before strong M6+ earthquakes. Space Research Institute of Moscow, Russian Academy of Sciences, MSS-14. 2014. Moscow, Russia.

24. V. Straser. (2012). Can IMF And The Electromagnetic Coupling Between The Sun And The Earth Cause Potentially Destructive Earthquakes? New Concepts in Global Tectonics Newsletter, no. 65, December, 2012. Terenzo PR, Italy. Society for Interdisciplinary Studies (SIS).

25. V. Straser. (2012). Intervals Of Pulsation Of Diminishing Periods And Radio Anomalies Found Before The Occurrence of M6+ Earthquakes. New Concept in Global Tectonics Newsletter, no. 65, December, 2012. Terenzo PR, Italy.

26. V. Straser. (2011). Radio Anomalies And Variations In The Interplanetary Magnetic Field Used As Seismic Precursor On A Global Scale, New Concepts in Global Tectonics Newsletter, no. 61, December, 2011. Terenzo PR, Italy.

27. V. Straser. (2011). Radio Wave Anomalies, Ulf Geomagnetic Changes And Variations In The Interplanetary Magnetic Field Preceding The Japanese M9.0 Earthquake. New Concepts in Global Tectonics Newsletter, no. 59, June, 2011. Terenzo PR, Italy.

RADIO DIRECTION FINDING (RDF) - GEOMAGNETIC MONITORING STUDY OF THE JAPANESE AREA RELATED TO PRE-SEISMIC ELECTROMAGNETIC SIGNALS

Valentino Straser
Department of Science and Environment UPKL, Brussels – (valentino.straser@gmail.com)

Daniele Cataldi
Radio Emissions Project, Rome (Italy) – (daniele77c@gmail.com)

Gabriele Cataldi
Radio Emissions Project, Rome (Italy) – (ltpaobserverproject@gmail.com)

Abstract: The study aims to present data relating to broadband electromagnetic monitoring (SELF-VLF band, 0-32000 Hz) capable of working 24/7, within the electromagnetic monitoring network with RDF (Radio Direction Finding) technology. The area monitored area for experimentation is the Japanese one, historically affected by strong and devastating earthquakes. The study found 1424 groups of radio anomalies, related to crustal diagnosis and non-destructive earthquakes. This is the first network of this type capable of working on a wide bandwidth (ELF-VLF band, 0-96000 Hz) specially designed to study the so-called "Seismic Electromagnetic Precursors" (SEPs) and the "Seismic Geomagnetic Precursors" "(SGPs). This monitoring system, based on RDF technology, has been active since 2017.

Keywords: RDF system, earthquake prediction, SELF-VLF, Japanese area, earthquake.

1 – INTRODUCTION

The system developed by the Radio Emissions Project, based on RDF - Radio Direction Finding technology, has made it possible to ascertain from 2017 the existence of strong electromagnetic signals before the occurrence of an earthquake (Straser et al., 2018; Straser et al., 2017; Straser et al., 2016; Straser et al., 2015, Cataldi et al. 2017, Cataldi et al. 2016). On 24 January 2019, monitoring began of the Japanese area, an area characterized by very strong earthquakes and high seismic risk, not least that of 11 March 2011 of magnitude Mw9 which caused extreme disasters in north-eastern Japan due to the high waves of a tsunami generated by the earthquake and the strong movements of the soil. The death toll and missing persons were estimated at over 20,000. Before this earthquake occurred, for more than 30 years on the border between the Pacific and the North American plates, no other destructive earthquakes had occurred, after that of Miyagi in 1978, it was therefore expected that there would be a strong earthquake within 30 years subsequent, with a probability of 99% and this happened (Furumura et al., 2011). This monitoring was used to ascertain the appearance of any electromagnetic signals that appeared before a possible strong earthquake, to understand if there were evident electromagnetic phenomena that could have indicated crustal energy accumulation phenomena, typical of the area subjected to electromagnetic monitoring.

2 – INSTRUMENT

2.1 – The RDF Station in Lariano (Rome, Italy)

The RDF (Radio Direction Finding) station used for this study is that of Lariano (Rome, Italy; Lat: 41.729535N, Long: 12.840968E), equipped with two Loop antennas with a diameter of 1 meter containing 50 turns each (Fig.1), aligned with each other orthogonally and with respect to the geographical poles.

It is managed by Daniele Cataldi and is equipped with a radio receiver prototype designed and built by Gabriele Cataldi which is able to detect changes in the electromagnetic field in the VLF band (0.3-96 kHz) 24/7.

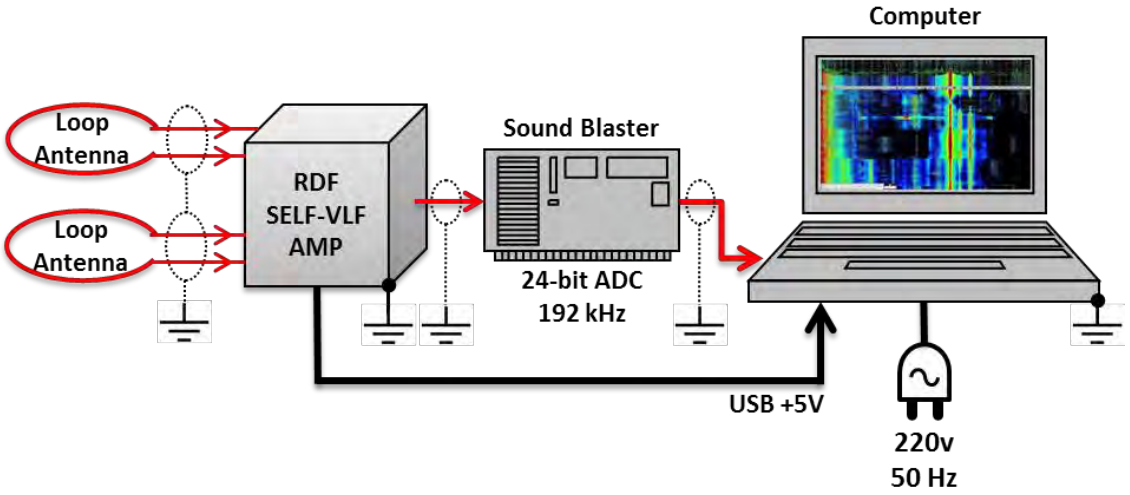

Fig. 1 - Schematization of the RDF Radio Direction Finding receiving and amplification system located in Lariano, Rome, Italy; developed by the Radio Emissions Project, and used for this study. It consists of two Loop antennas, a radio amplifier (receiver), connected to the PC's microphone socket, via the Sound Blaster.

3 – THE STUDY

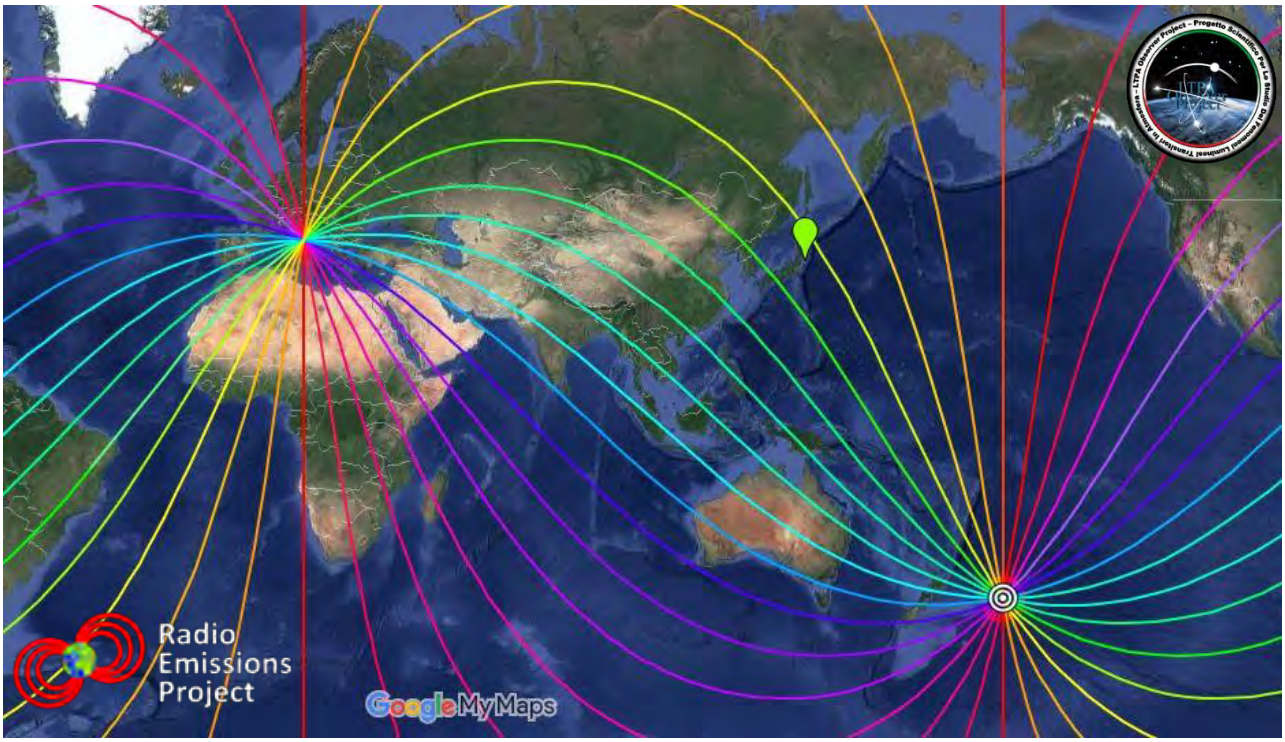

Fig. 2 – Monitoring area

On January 24, 2019, electromagnetic monitoring of the Japanese area began, as visible in Fig. 2 and 3, continuing until October 14, 2019. This electromagnetic monitoring was made possible thanks to the RDF - Radio Direction Finding station of the electromagnetic detection system of the Radio Emissions Project in Lariano, Rome, Italy.

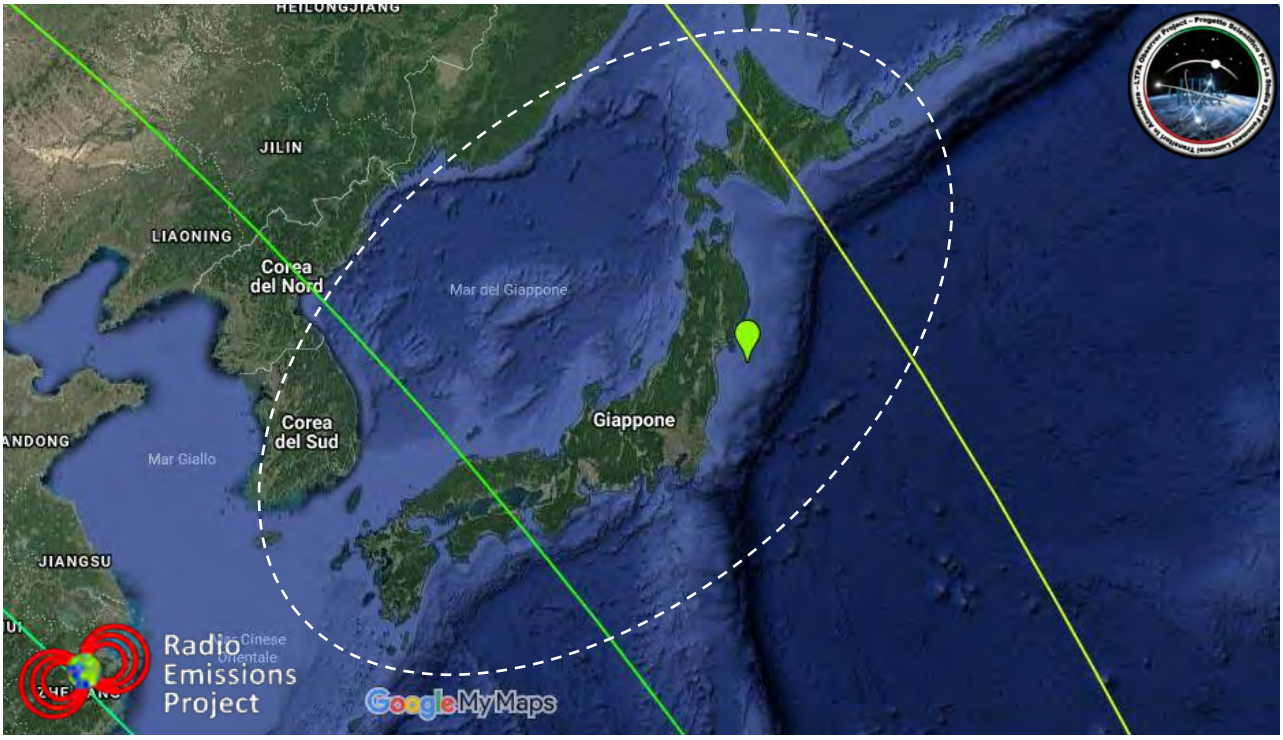

Fig. 3 - The geographical area examined and the azimuth monitored by the RDF system of Lariano, Rome, Italy and Pontedera, Pisa, Italy.

The monitored area is about 9,800 km from the RDF station (Rome, Italy), as shown in Fig. 5. This distance, considering the reception characteristics of the RDF station itself, is not to be underestimated compared to the total coverage of the station (with a radius of 20,000 km), reaching about half of the maximum coverage (in this case the experimentation took place in 2017) (Straser et al., 2018), as seen in Fig. 4

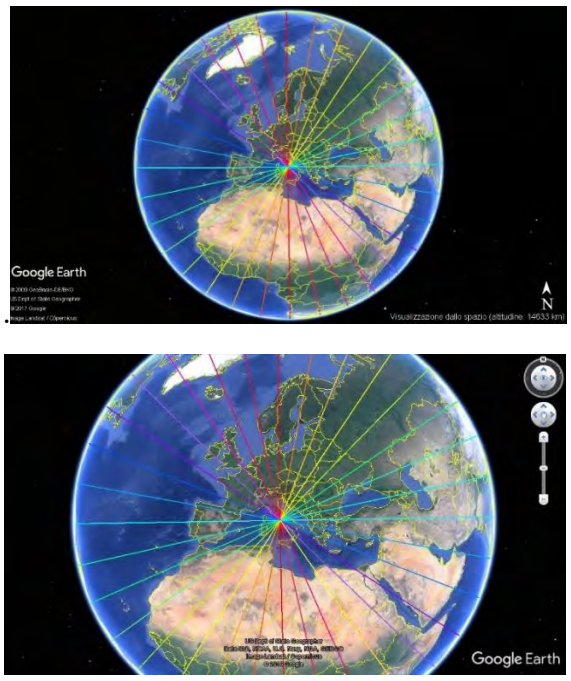

Fig. 4 - Worldwide coverage of the RDF system, developed by Daniele and Gabriele Cataldi.

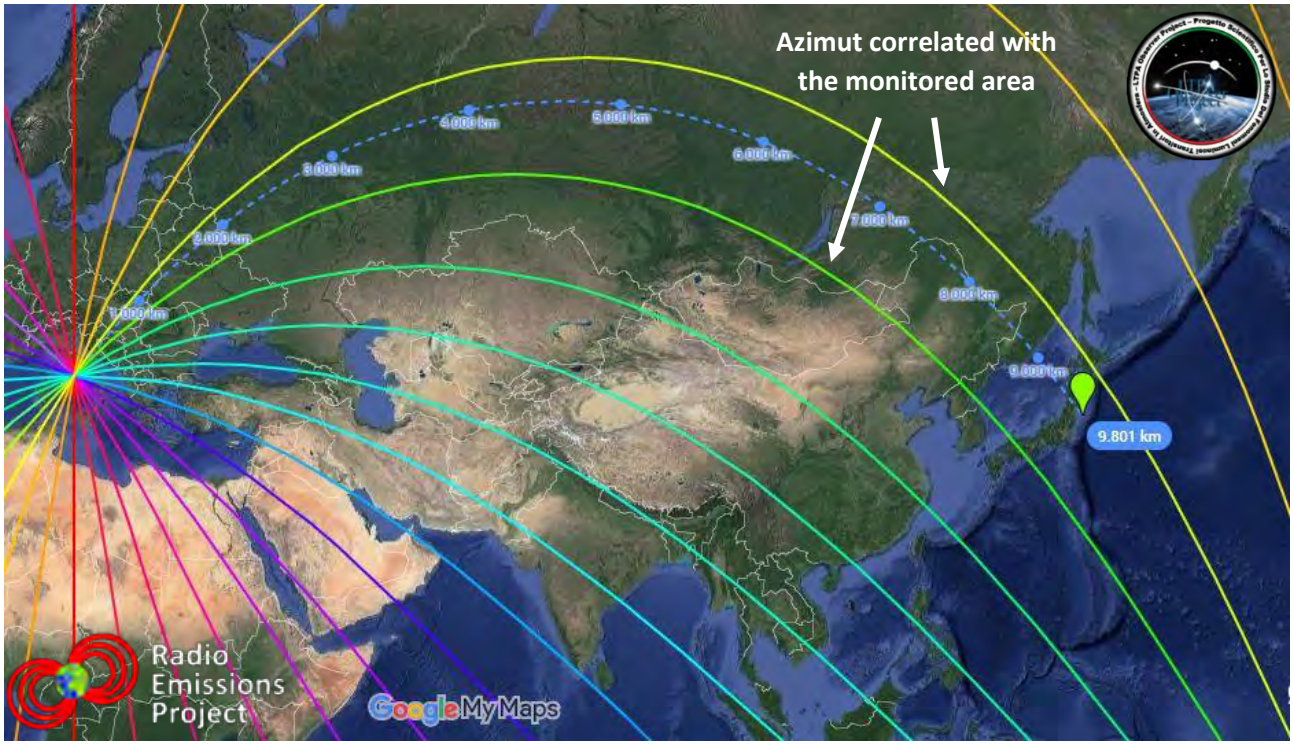

Fig. 4 - Distance between Lariano RDF station, Rome, Italy and the monitored Japanese area. Google Maps.

In this case, the monitored electromagnetic signals fall under the green and yellow azimuth, including the relative nuances, as highlighted by the colorimetric map of the RDF system in Lariano (RM) (Fig. 5). This azimuth is located in the NE - NNE direction with respect to the Italian geographical position in which the RDF monitoring station is located. This geographical area is extremely large (as visible in Fig. 3):

• Perimeter: 5,862 km

• Area: 1,983,373,034 km2

The monitoring system therefore had to keep under continuous electromagnetic control all the emissions from this large area, also considering the proximity to the ring of fire, which is a few thousand kilometers away and which appears to be a very large natural emitter of emissions electromagnetic continuous and strong intensity. The signals coming from this large area have often generated intense electromagnetic modulations, such as to cover the weak emissions coming from the Japanese territory.

This is therefore one of the important data not to be underestimated, which was however considered in this study and which represented a "limit" of the RDF system, in detecting further signals from the area under continuous monitoring data.

4 –DATA

4.1 – The Signals

The signals recorded by the RDF - Radio Direction Finding system, developed by the Radio Emissions Project, concerned pulsing or continuous increases in correspondence with the green / yellow azimuth, these signals appeared very frequently, saturating, sometimes part of the apparitions, the The entire

electromagnetic band taken into consideration (0-96 kHz of bandwidth), as shown in Fig. 6. In this case the number of dynamic spectrograms investigated and generated by the system were 447.

Sporadic signals instead appeared only at certain frequencies, whose emission characteristics are discussed in this study.

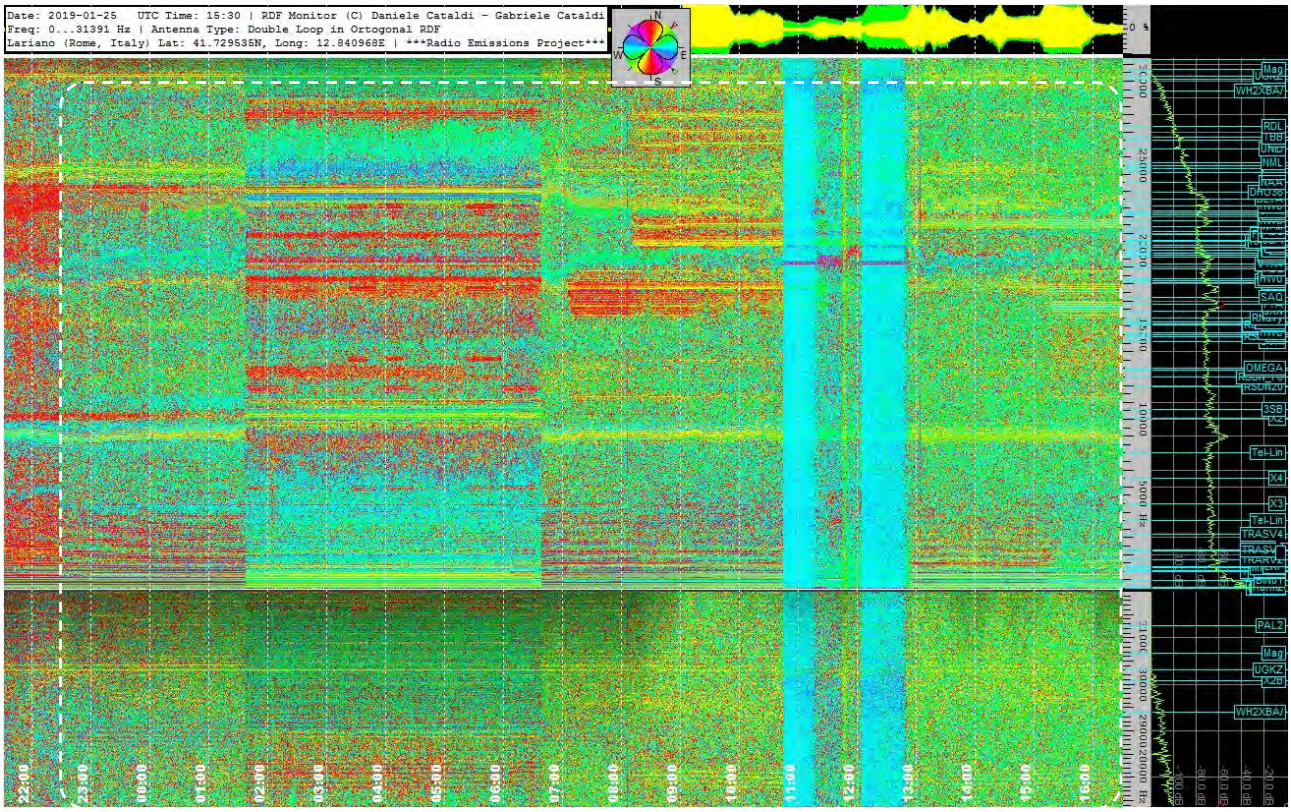

Fig. 5 - An example of the greeen/yellow signals (radio-anomaly) recorded, coming from japanese azimuth. In this case it is one of the spectrograms recorded by the RDF station in Lariano, Rome, Italy.

The study undertaken by the Radio Emissions Project through the RDF station in Lariano, Rome, Italy, highlighted some interesting characteristics of the radio anomalies recorded during the study, a study focused on the search for signals having seismic predictive characteristics in the Japanese area.

The signals considered were only those polarized with the Japanese azimuth, eliminating all the increases and electromagnetic peaks coming from other geographical areas of the earth's globe.

The first interesting data are the number of anomalies (having the same azimuth as the area under monitoring), which appeared over the weeks and months in which this study continued.

5 – THE STUDY

The total number of radio anomalies recorded during the study is 1424, each of which correlated with the Japanese azimuth. This number is associated with electromagnetic increases having different frequencies (as visible in Fig. 7, 8, 9, 10, 11, 12, 13, 14, 15, 16). The data contained in this study were extrapolated from the monitoring system developed by Daniele Cataldi and Gabriele Cataldi, which independently detected the electromagnetic emissions, providing indications on their azimuth origin (frequency polarization), in relation to the entire extension of the earth's surface and therefore taking into consideration the geographical areas of the terrestrial globe, from where these signals come.

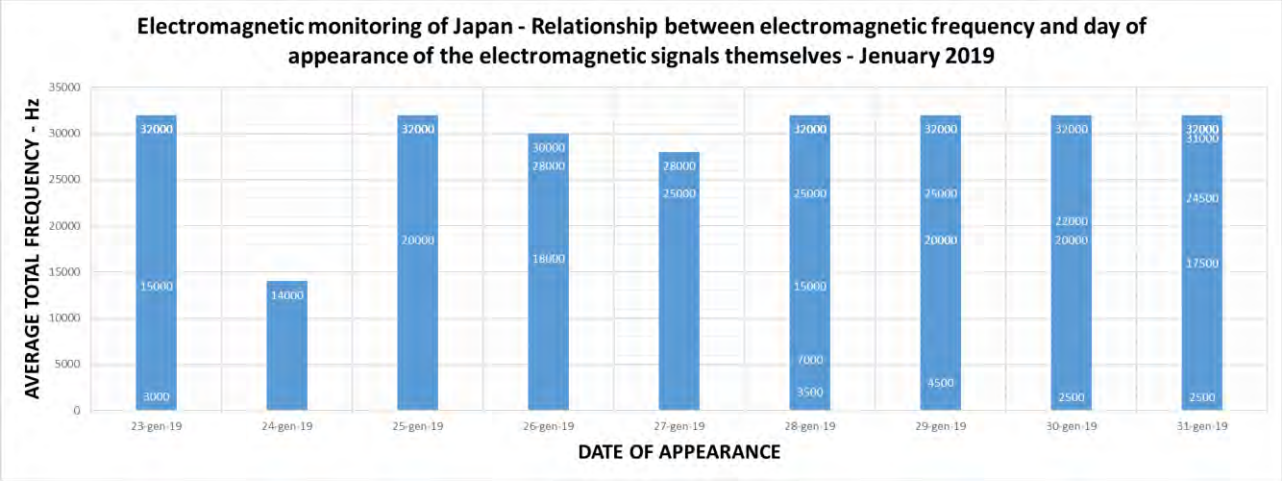

Fig. 6 - Relationship between the number of radio anomalies that appeared during the study and their frequency distribution. Source: Radio Emissions Project. January 2019.

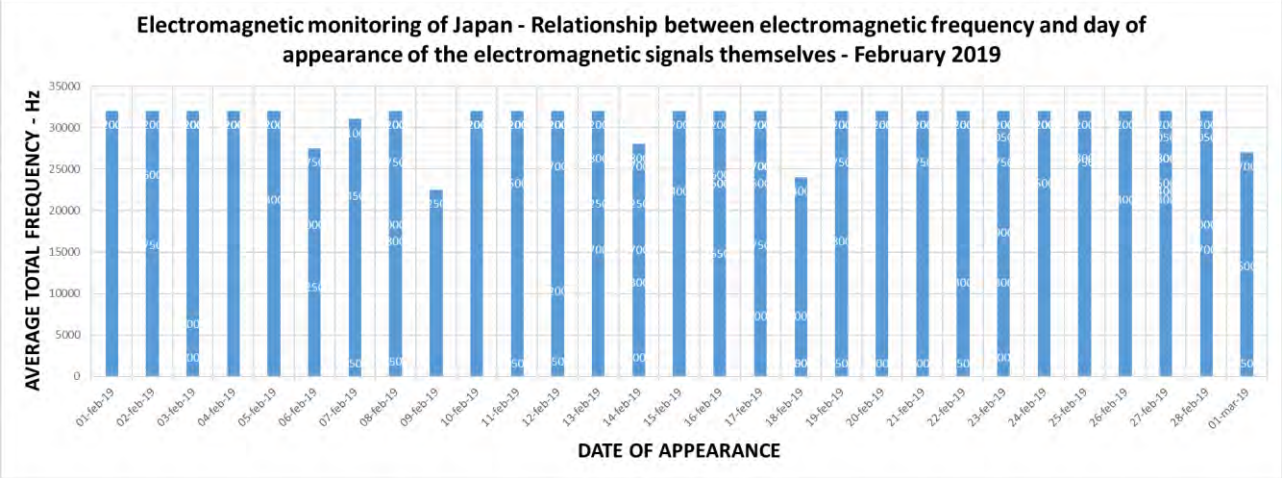

Figure 8 - Relationship between the number of radio anomalies that appeared during the study and their frequency distribution. Source: Radio Emissions Project. February 2019.

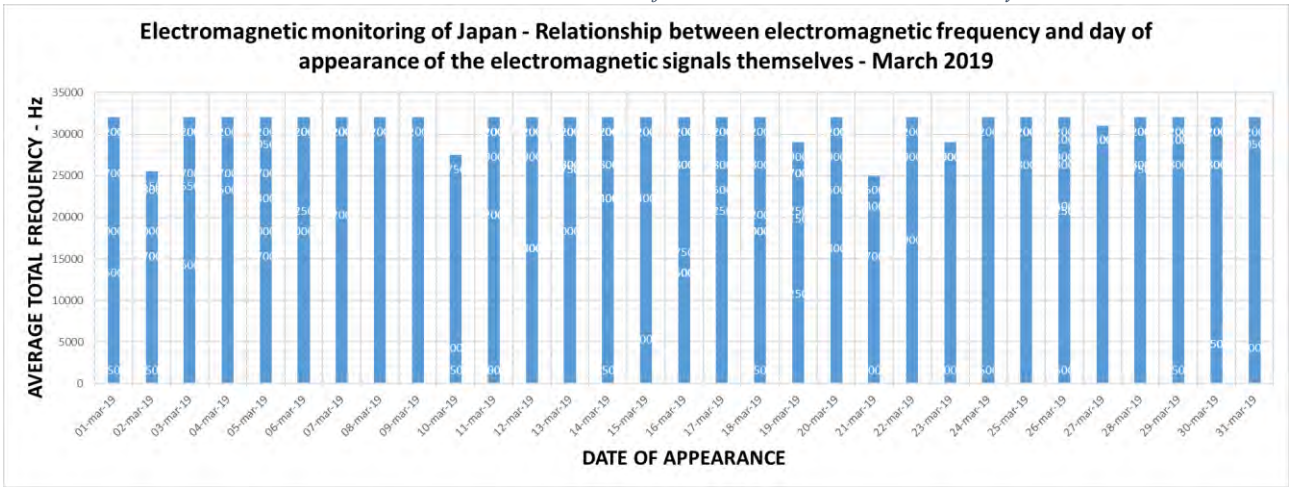

Figure 9 - Relationship between the number of radio anomalies that appeared during the study and their frequency distribution. Source:

Radio Emissions Project. March 2019.

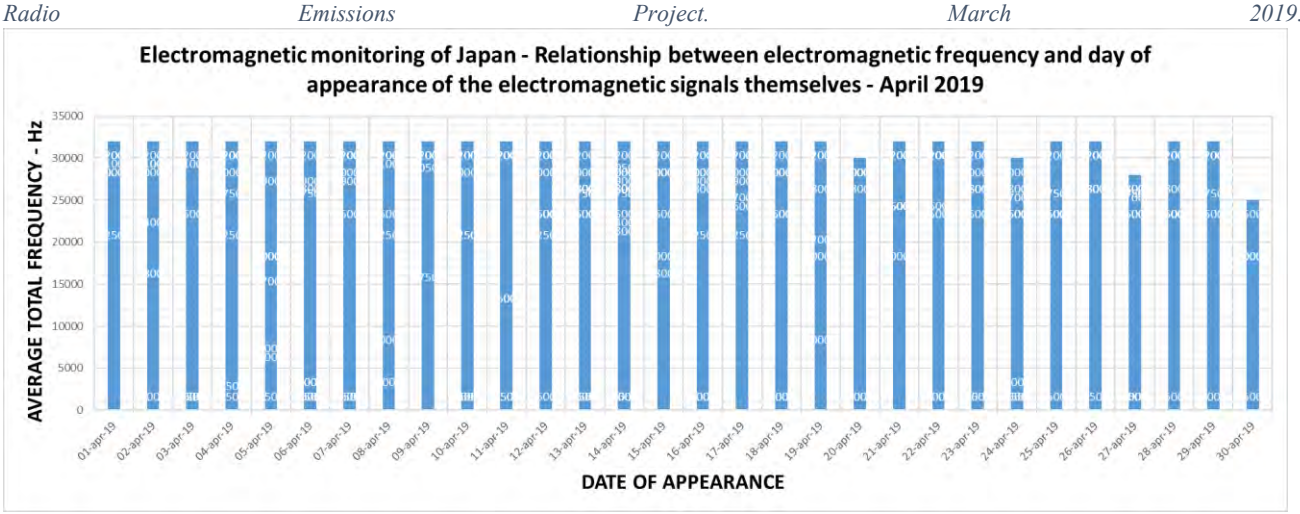

Figure 10 - Relationship between the number of radio anomalies that appeared during the study and their frequency distribution. Source: Radio Emissions Project. April 2019.

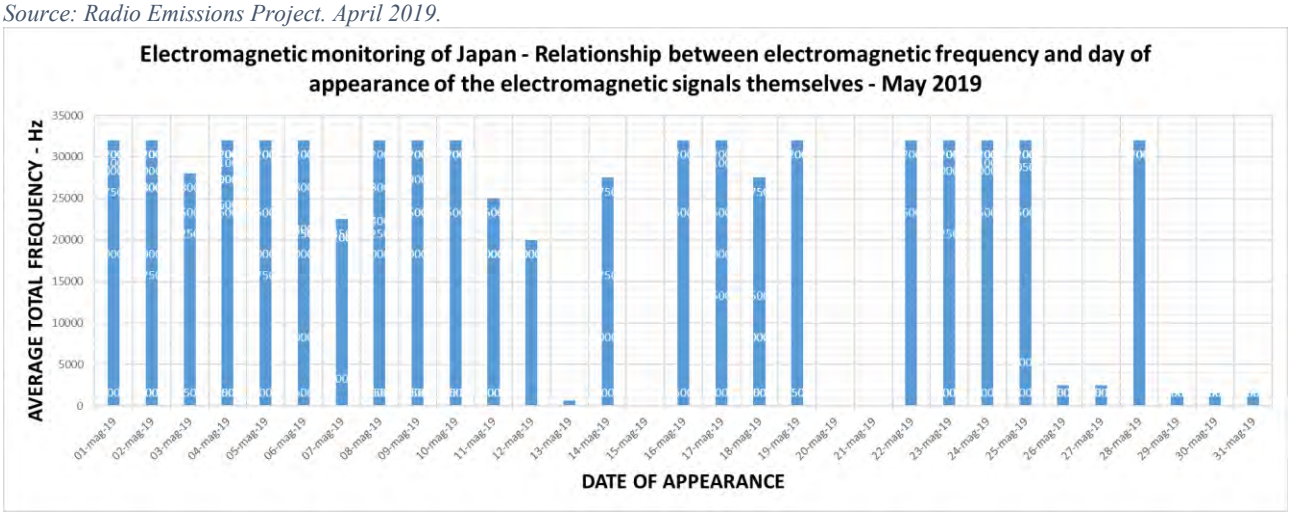

Figure 11 - Relationship between the number of radio anomalies that appeared during the study and their frequency distribution. Source: Radio Emissions Project. May 2019.

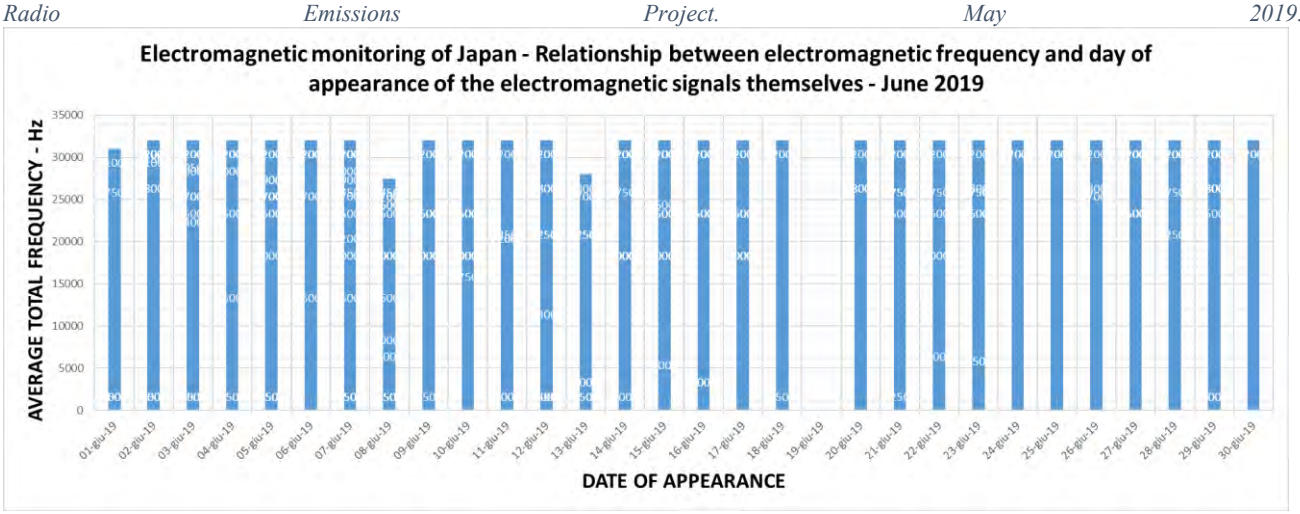

Figure 12 - Relationship between the number of radio anomalies that appeared during the study and their frequency distribution. Source:

Radio Emissions Project. June 2019.

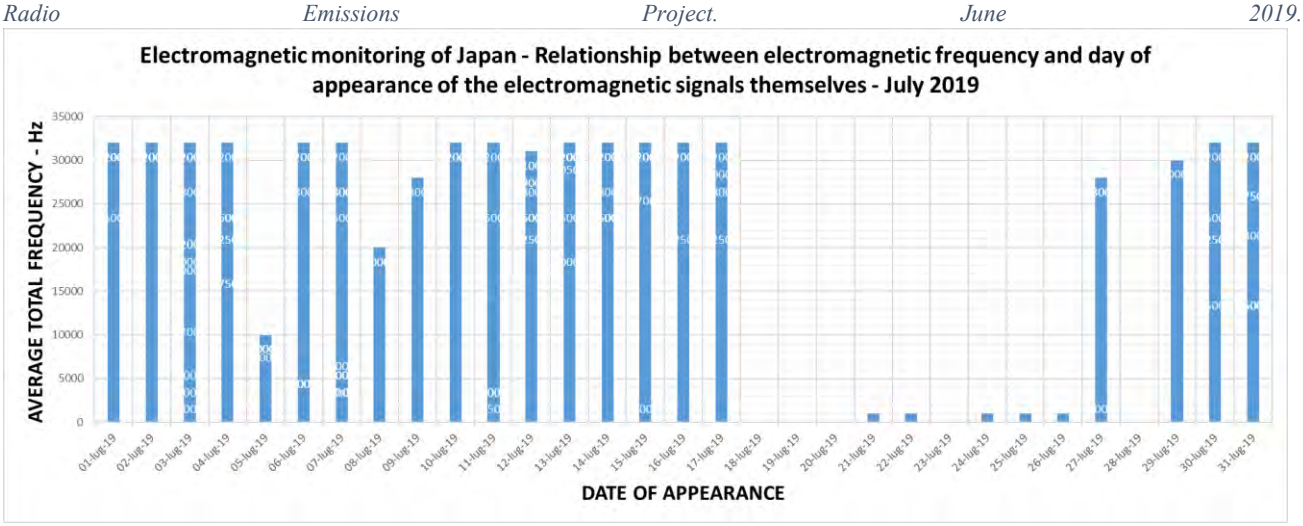

Figure 13 - Relationship between the number of radio anomalies that appeared during the study and their frequency distribution. Source: Radio Emissions Project. July 2019.

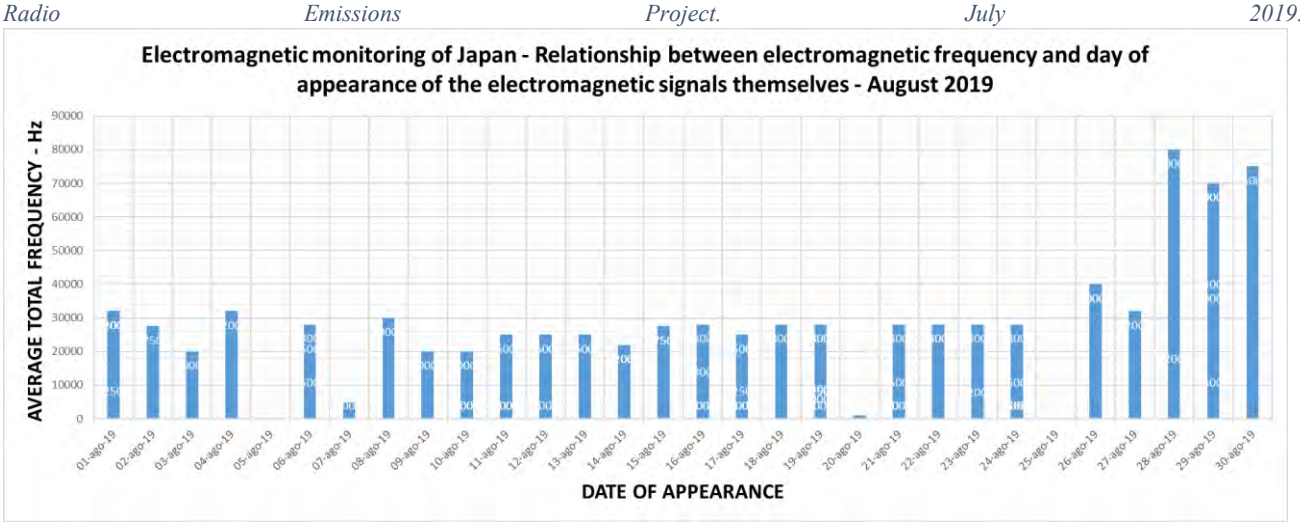

Figure 14 - Relationship between the number of radio anomalies that appeared during the study and their frequency distribution. Source: Radio Emissions Project. August 2019.

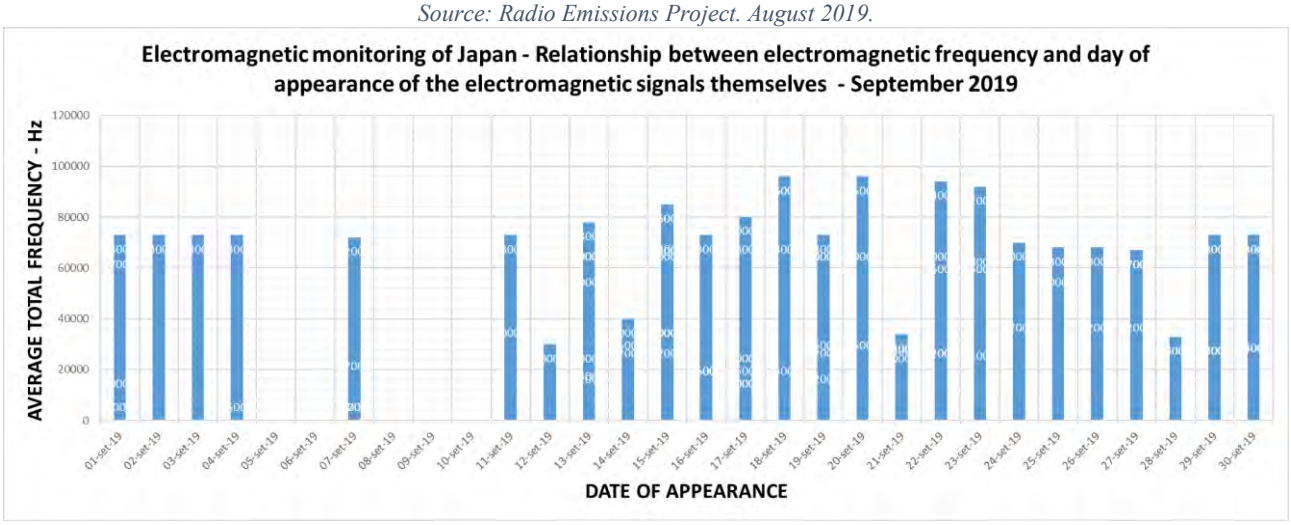

Figure 15 - Relationship between the number of radio anomalies that appeared during the study and their frequency distribution. Source: Radio Emissions Project. September 2019

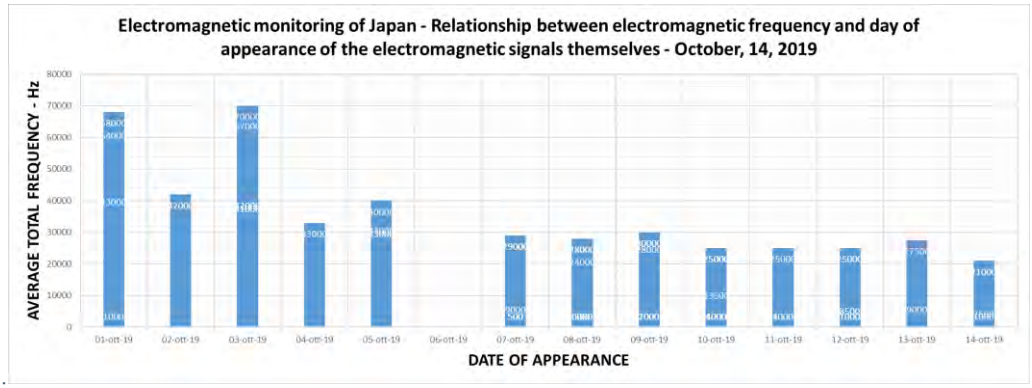

Figure 16 - Relationship between the number of radio anomalies that appeared during the study and their frequency distribution. Source: Radio Emissions Project. October 2019.

The study of the electromagnetic frequency of the radio-anomalies associated with the Japanese azimuth, shows us how there is the majority of electromagnetic emissions distributed over the entire electromagnetic band taken into consideration (0-32,000 Hz), coming from the monitored area.

In this context, it is possible to understand the behavior of these emissions on the time axis (as visible in Fig. 7, 8, 9, 10, 11, 12, 13, 14, 15, 16).

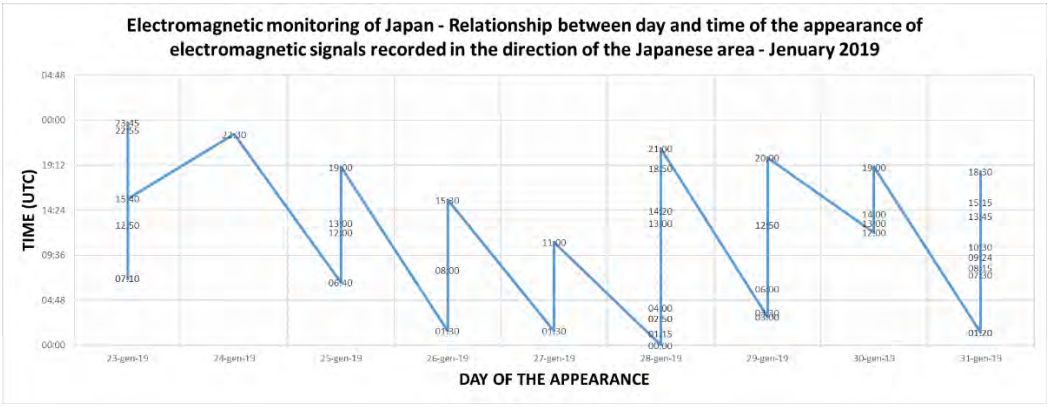

Fig. 17 - Relationship between number of anomalies, date and time of appearance compared to the period considered in the study. Source: Radio Emissions Project. January 2019.

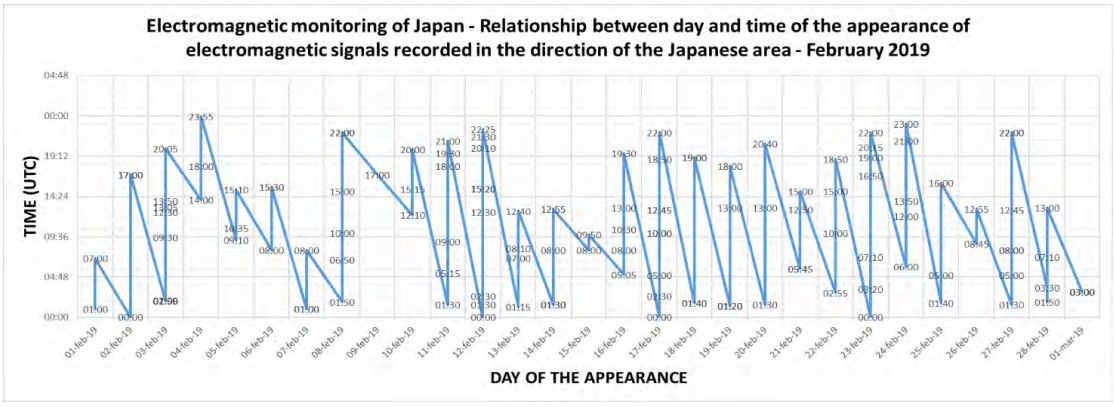

Figure 18 - Relationship between number of anomalies, date and time of appearance compared to the period considered in the study. Source: Radio Emissions Project. February 2019

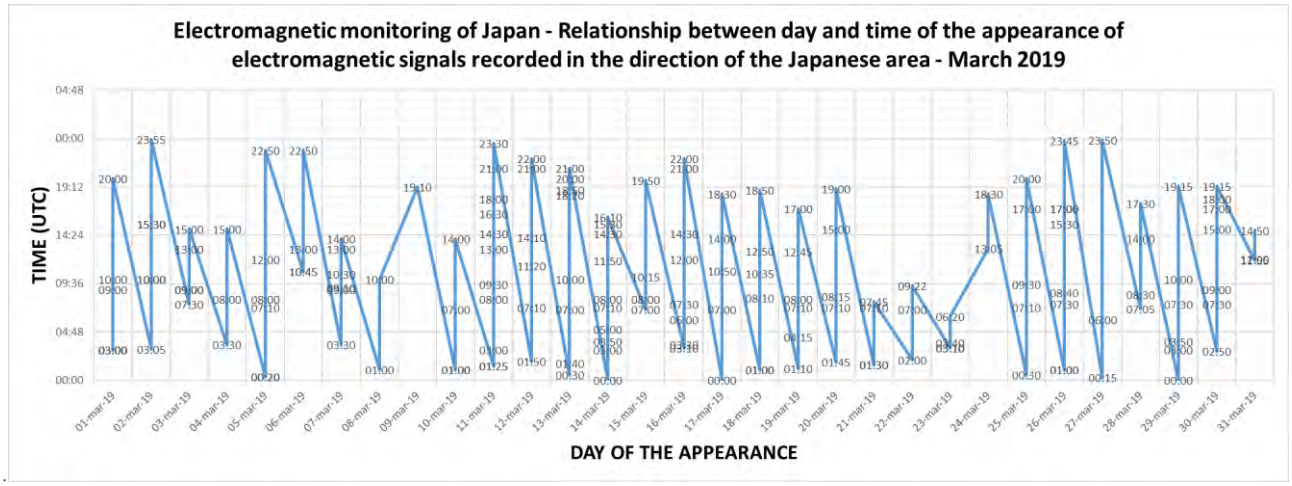

Figure 19 - Relationship between number of anomalies, date and time of appearance compared to the period considered in the study. Source: Radio Emissions Project. March 2019.

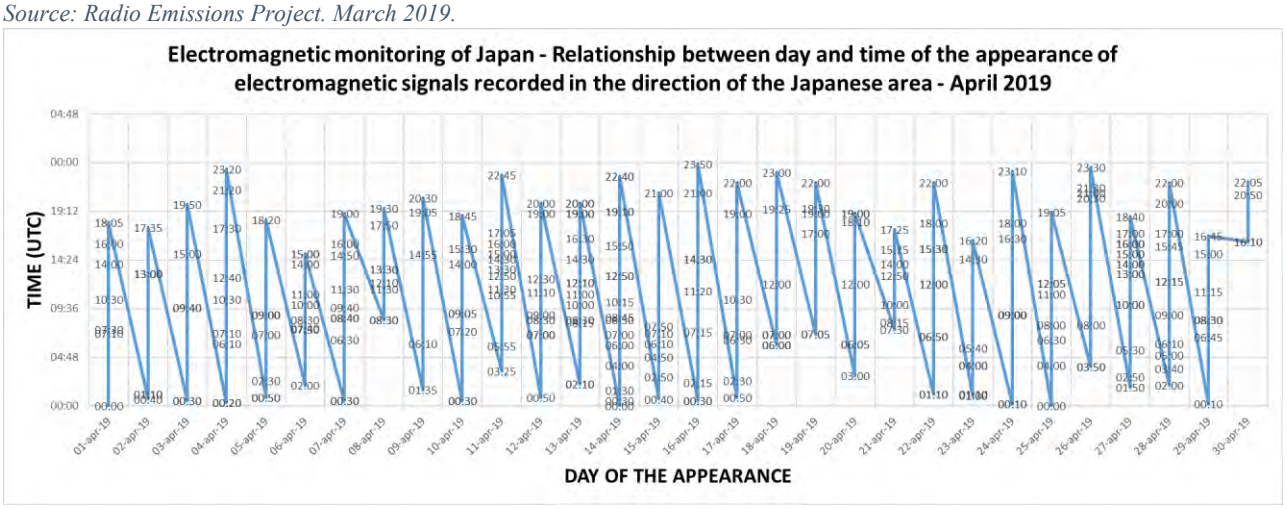

Figure 20 - Relationship between number of anomalies, date and time of appearance compared to the period considered in the study. Source: Radio Emissions Project. April 2019.

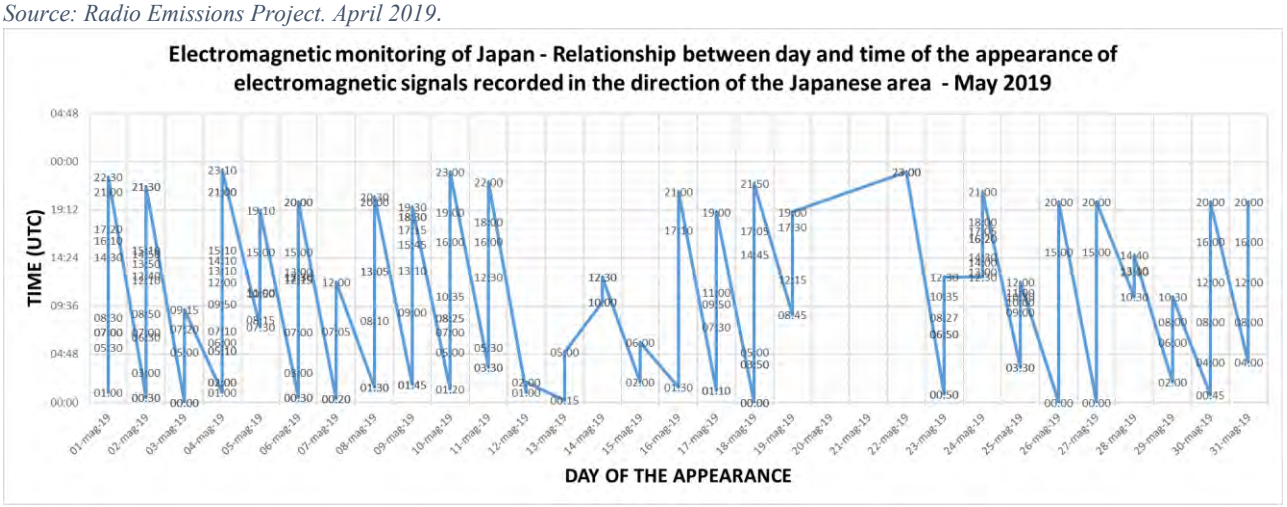

Figure 21 - Relationship between number of anomalies, date and time of appearance compared to the period considered in the study. Source: Radio Emissions Project. May 2019.

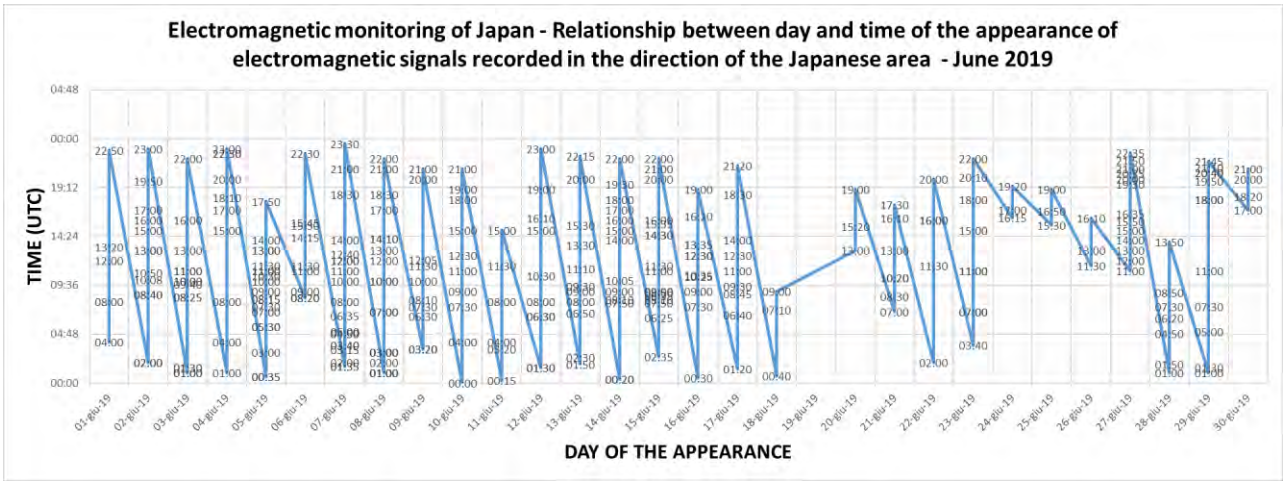

Figura 7 - Relazione tra numero di anomalie, data ed orario di comparsa rispetto al periodo considerato nello studio. Fonte: Radio Emissions Project. Giugno 2019.

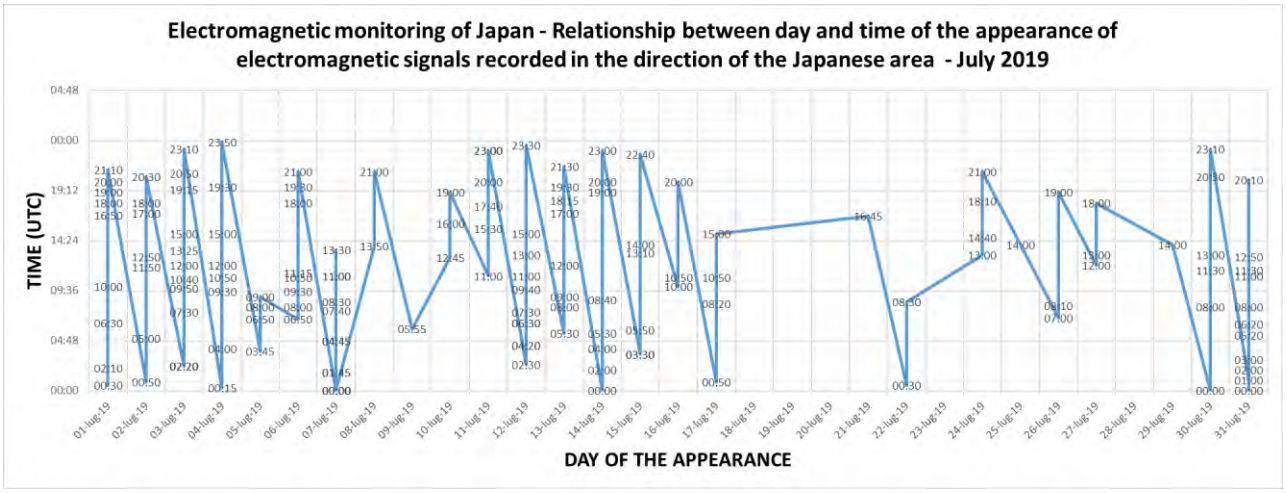

Figure 23 - Relationship between number of anomalies, date and time of appearance compared to the period considered in the study. Source: Radio Emissions Project. July 2019.

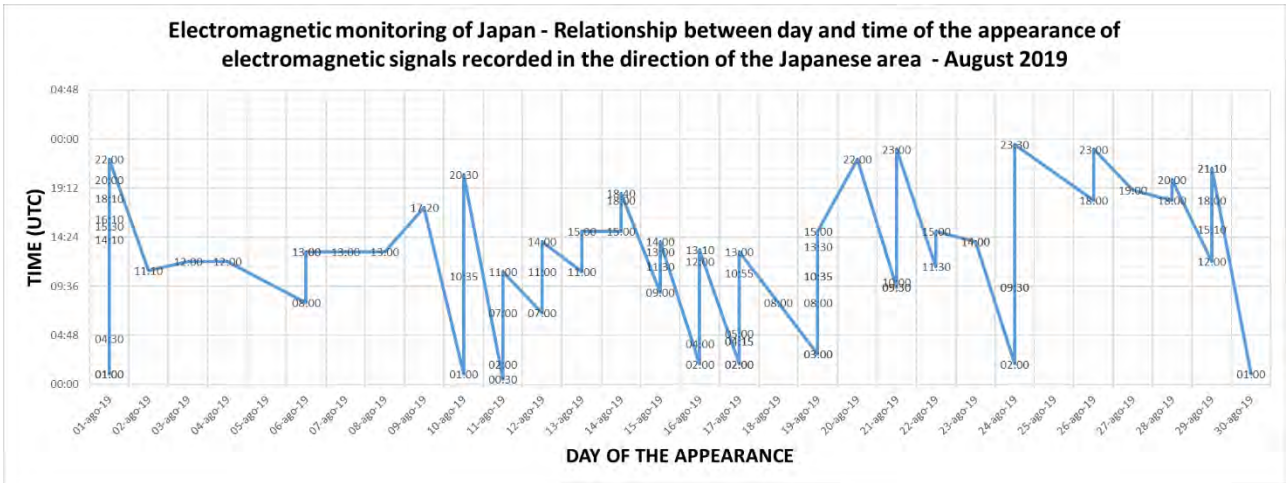

Figure 24 - Relationship between number of anomalies, date and time of appearance compared to the period considered in the study. Source: Radio Emissions Project. August 2019.

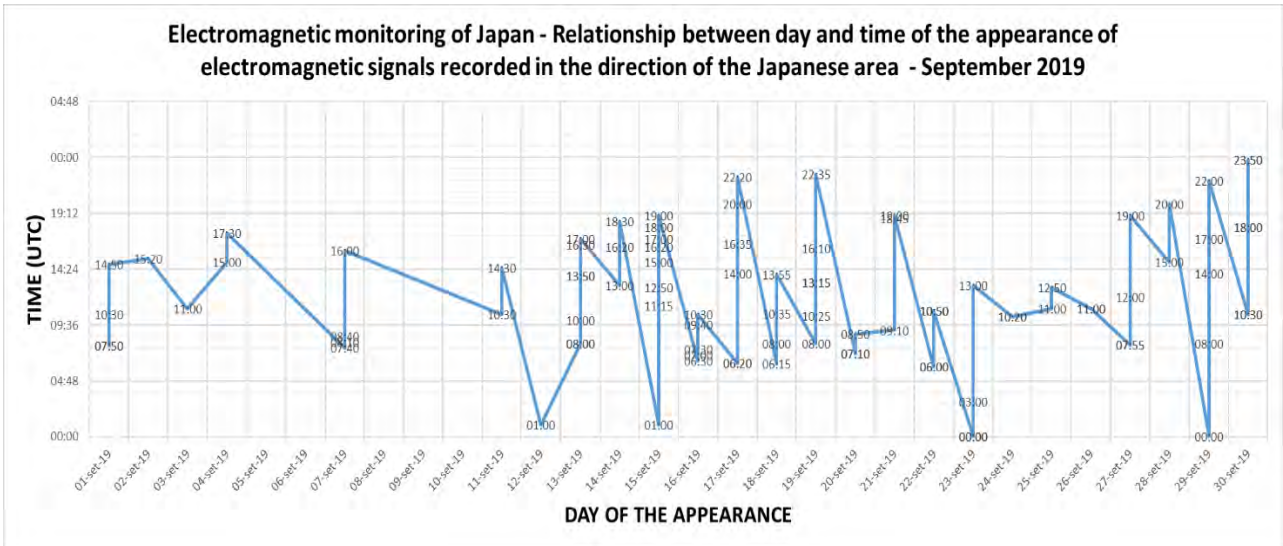

Figure 25 - Relationship between number of anomalies, date and time of appearance compared to the period considered in the study. Source: Radio Emissions Project. September 2019.

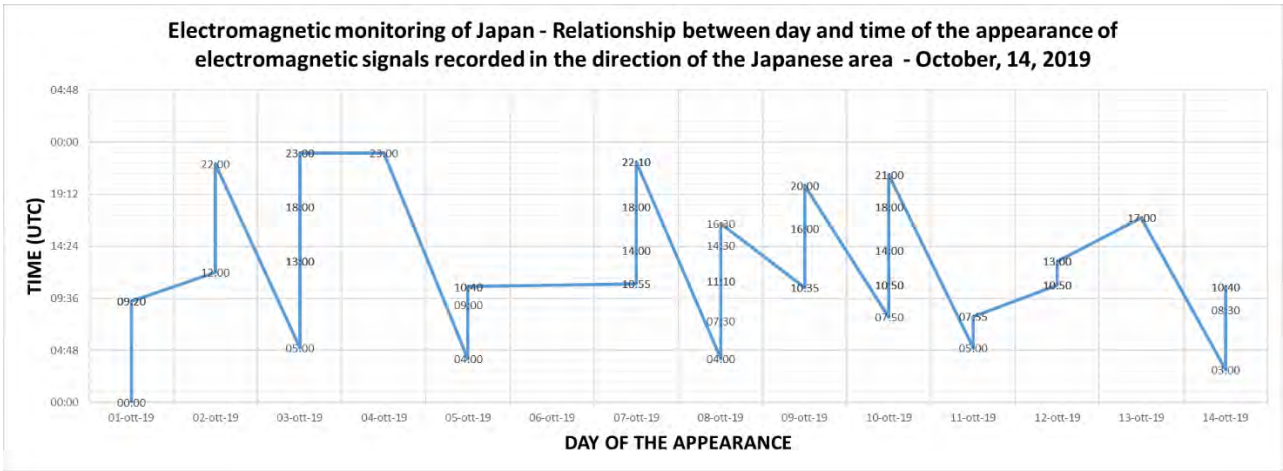

Figure 26 - Relationship between number of anomalies, date and time of appearance compared to the period considered in the study. Source: Radio Emissions Project. October 2019.

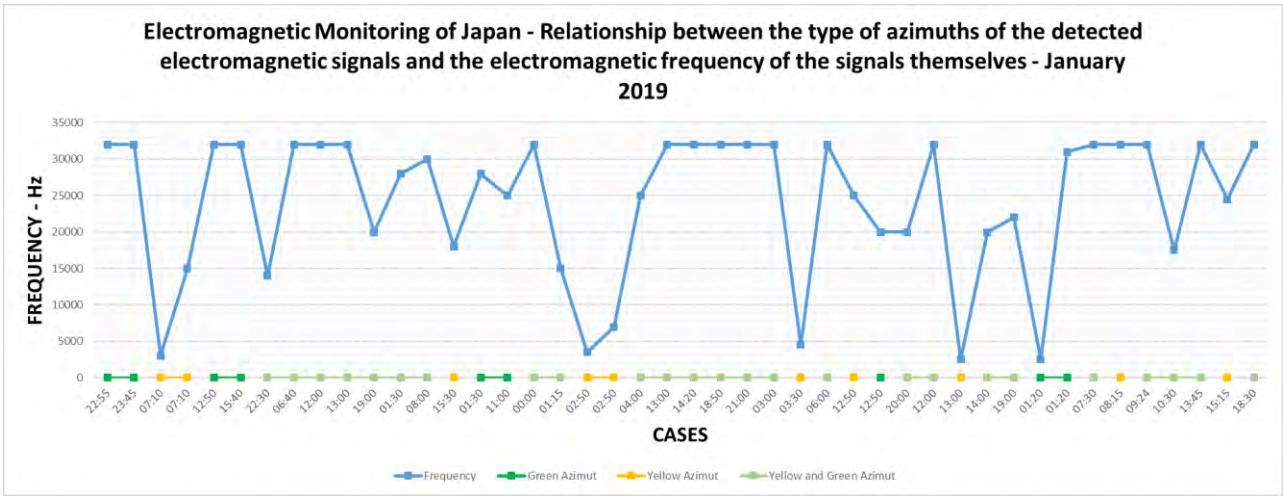

Fig. 27 - Relationship between the electromagnetic frequency of the signals received and their source azimuth. (green, green / yellow, yellow). Source: Radio Emissions Project. January 2019.

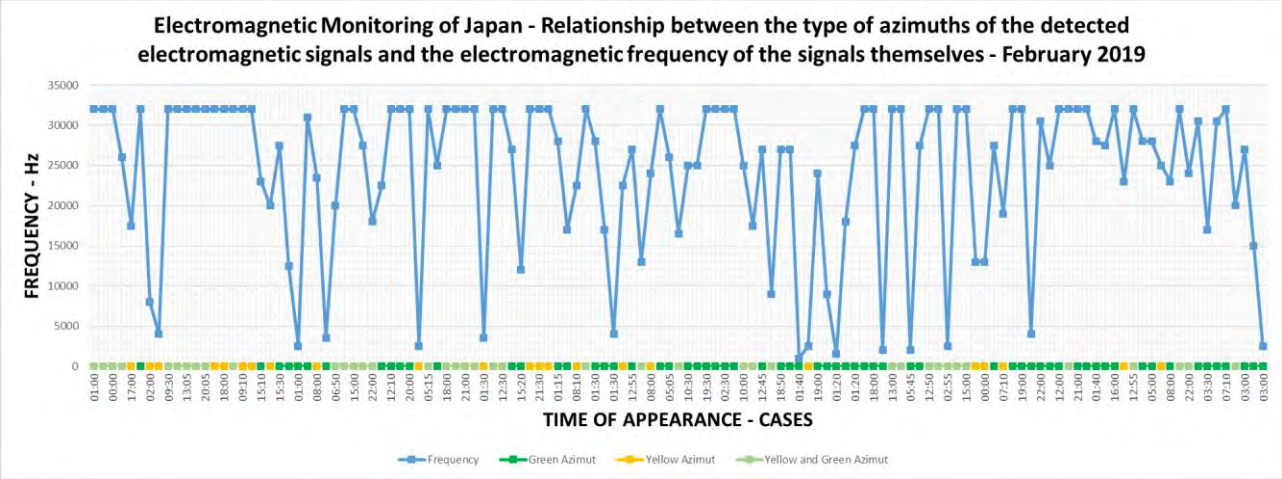

Fig 28 - Relationship between the electromagnetic frequency of the signals received and their azimuth of origin. (green, green / yellow, yellow). Source: Radio Emissions Project. February 2019.

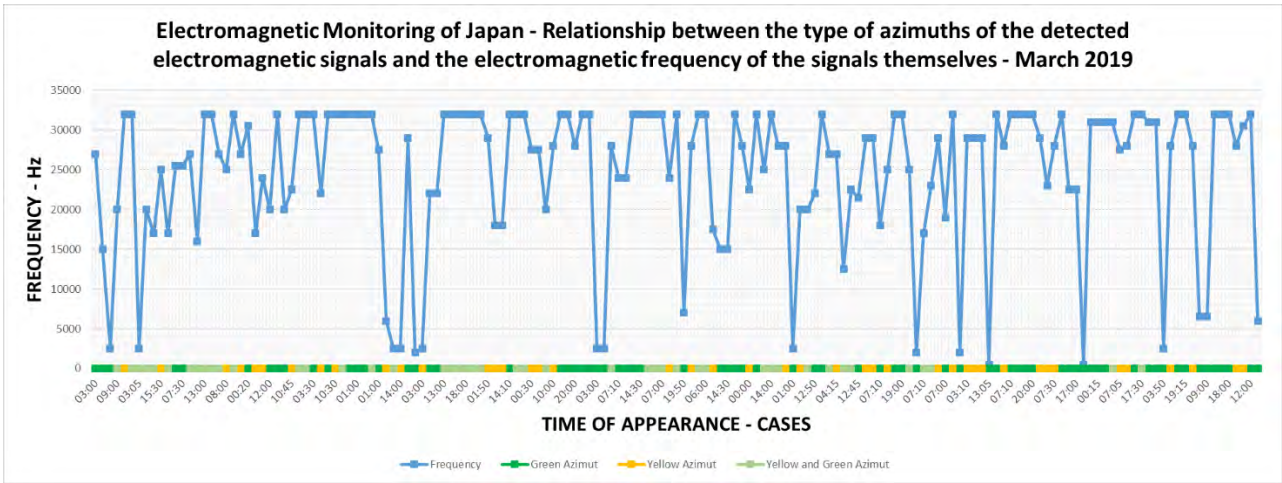

Figure 29 - Relationship between the electromagnetic frequency of the signals received and their source azimuth. (green, green / yellow, yellow). Source: Radio Emissions Project. March 2019.

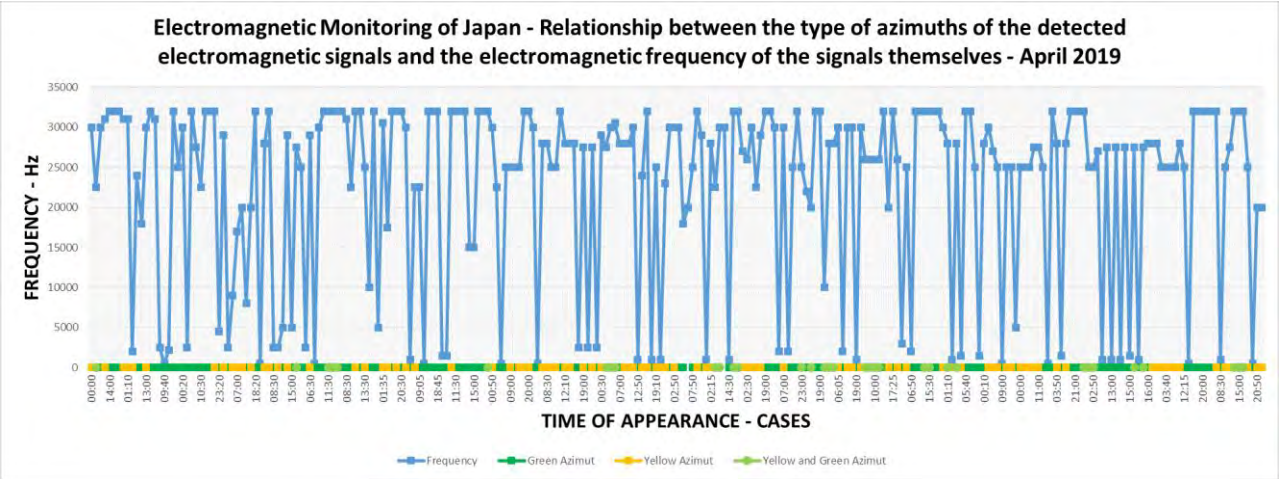

Figure 30 - Relationship between the electromagnetic frequency of the signals received and their origin azimuth. (green, green / yellow, yellow). Source: Radio Emissions Project. April 2019.

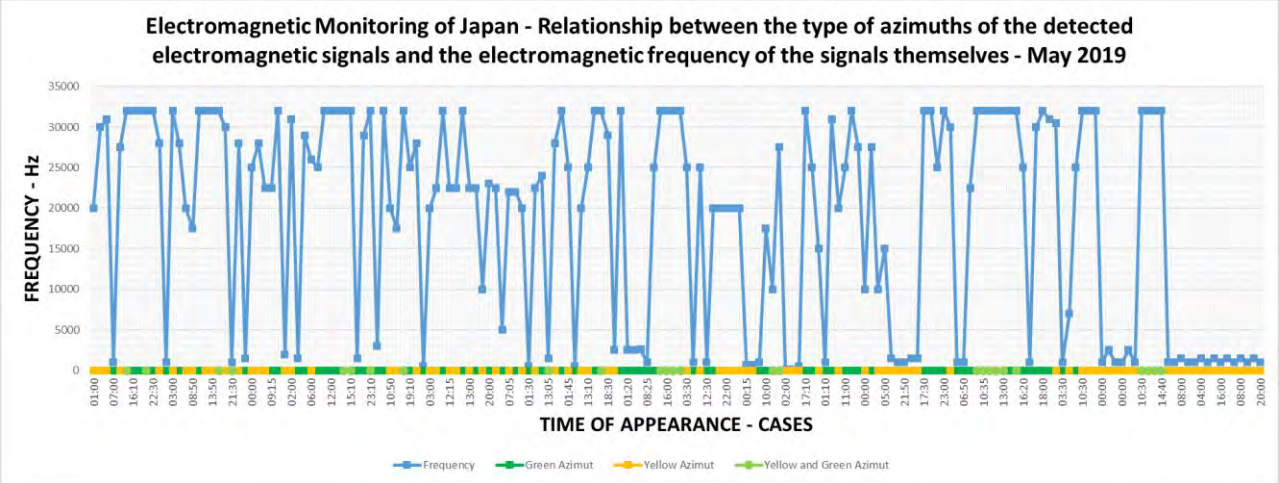

Figure 31 - Relationship between the electromagnetic frequency of the signals received and their origin azimuth. (green, green /yellow, yellow). Source: Radio Emissions Project. May 2019.

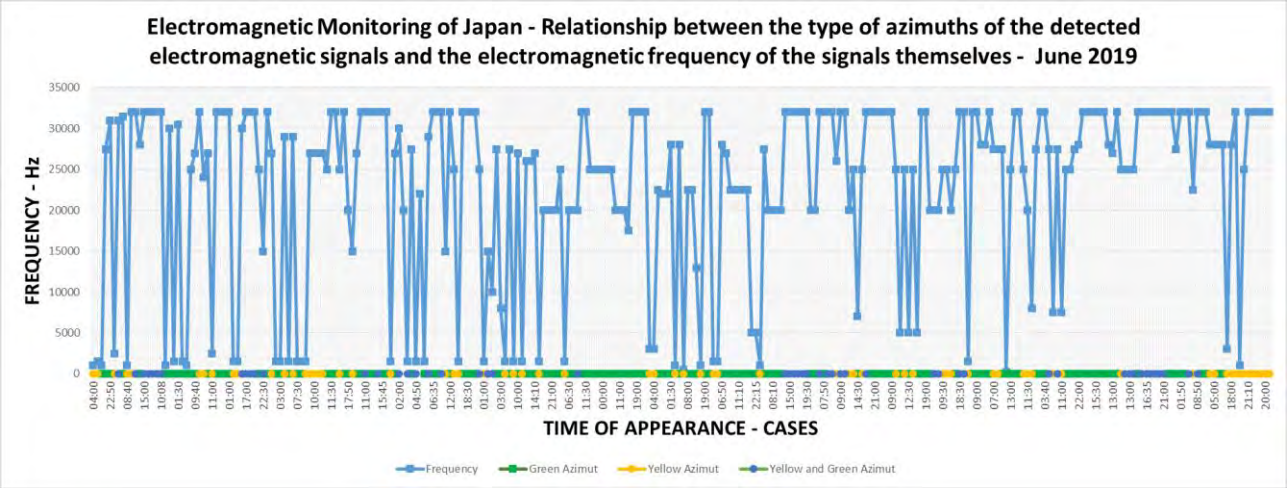

Figure 32 - Relationship between the electromagnetic frequency of the signals received and their source azimuth. (green, green / yellow, yellow). Source: Radio Emissions Project. June 2019.

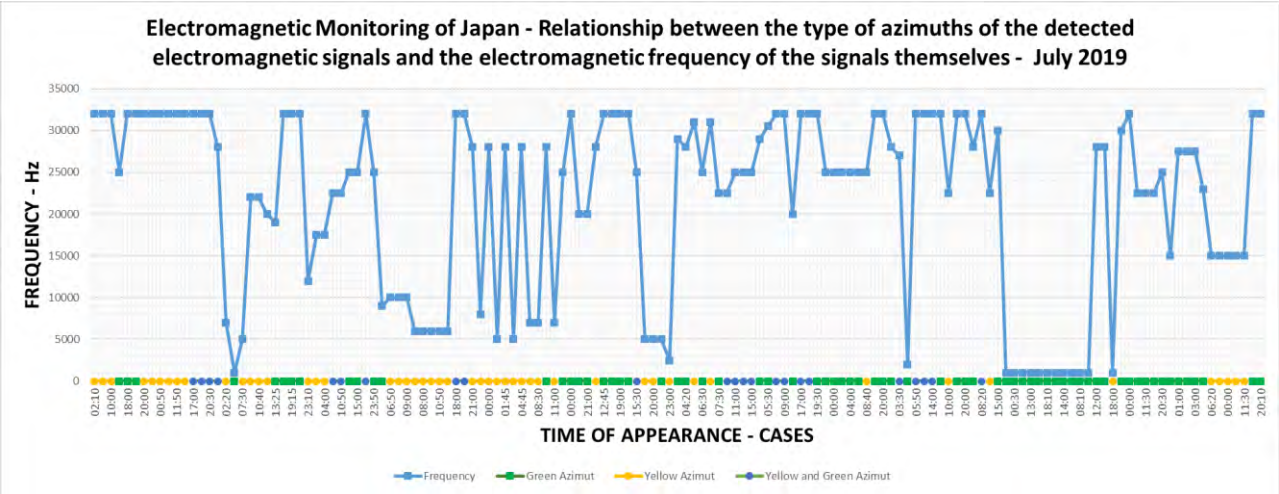

Figure 33 - Relationship between the electromagnetic frequency of the signals received and their azimuth of origin. (green, green / yellow, yellow). Source: Radio Emissions Project. July 2019.

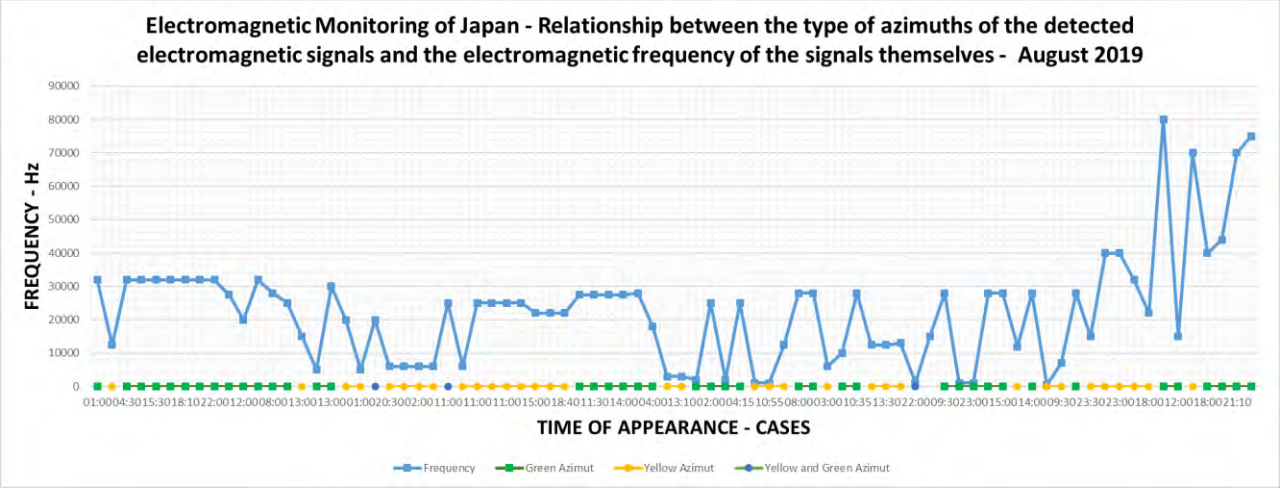

Figure 34 - Relationship between the electromagnetic frequency of the signals received and their source azimuth. (green, green / yellow, yellow). Source: Radio Emissions Project. August 2019.

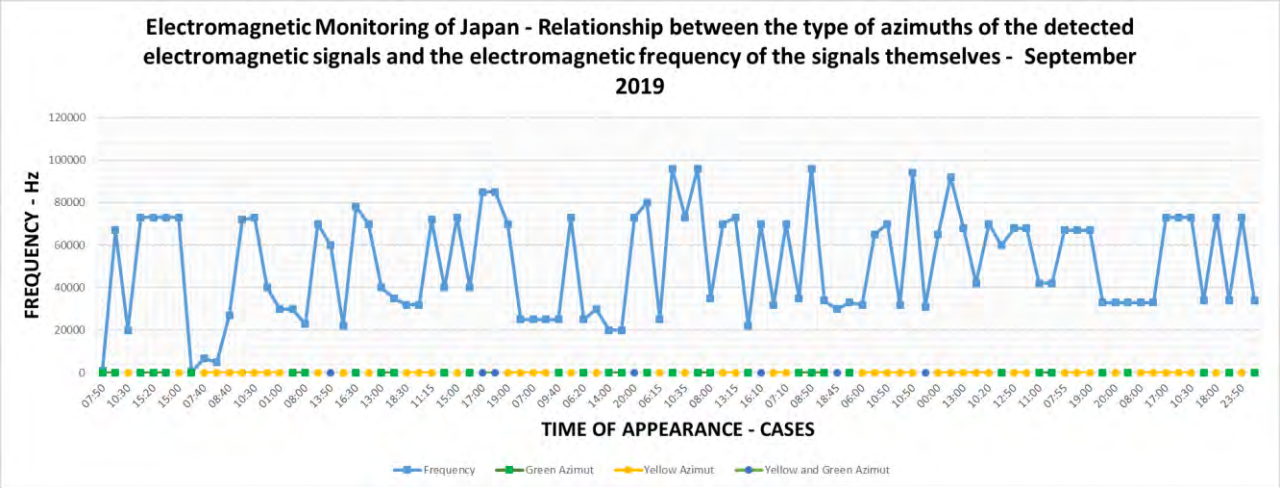

Fig. 35 - Relationship between the electromagnetic frequency of the signals received and their source azimuth. (green, green / yellow, yellow). Source: Radio Emissions Project. September 2019.

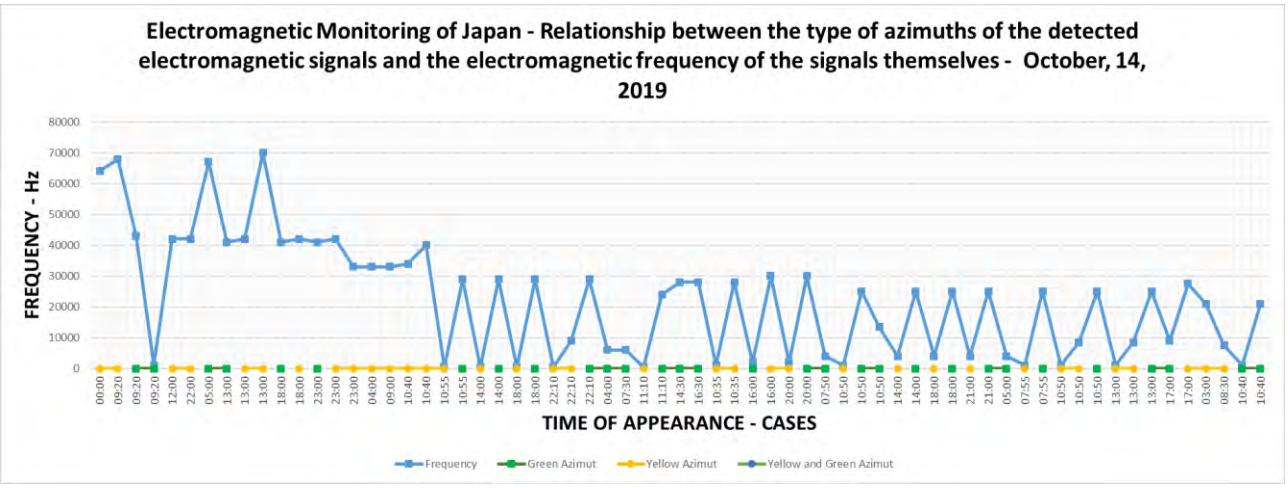

Figure 36 - Relationship between the electromagnetic frequency of the signals received and their azimuth of origin. (green, green / yellow, yellow). Source: Radio Emissions Project. October 2019.

The relationship between the electromagnetic frequency of the recorded signals and the distribution of the azimuths, from which these signals seem to come, is indicated by the graphs relating precisely to

the coloring of the azimuth and the peaks related to the electromagnetic frequency of the signals, extrapolated from the dynamic spectrograms in the study (as visible in Fig. 27, 28, 29, 30, 31, 32, 33, 34, 35, 36). In this case the yellow azimuth indicates the geographical center of Japan.

The relationship observed between the type of azimuth from which the electromagnetic signals seem to come and the distribution of Japanese earthquakes, tells us that the azimuth most commonly called is the yellow one, while many other appearances of electromagnetic signals seem to be those that come from the 'green azimuth. The data confirm that the signals from the Japanese area are those that seem to be generated in the direction of the center of this azimuth variation, which runs right in the center of Japan.

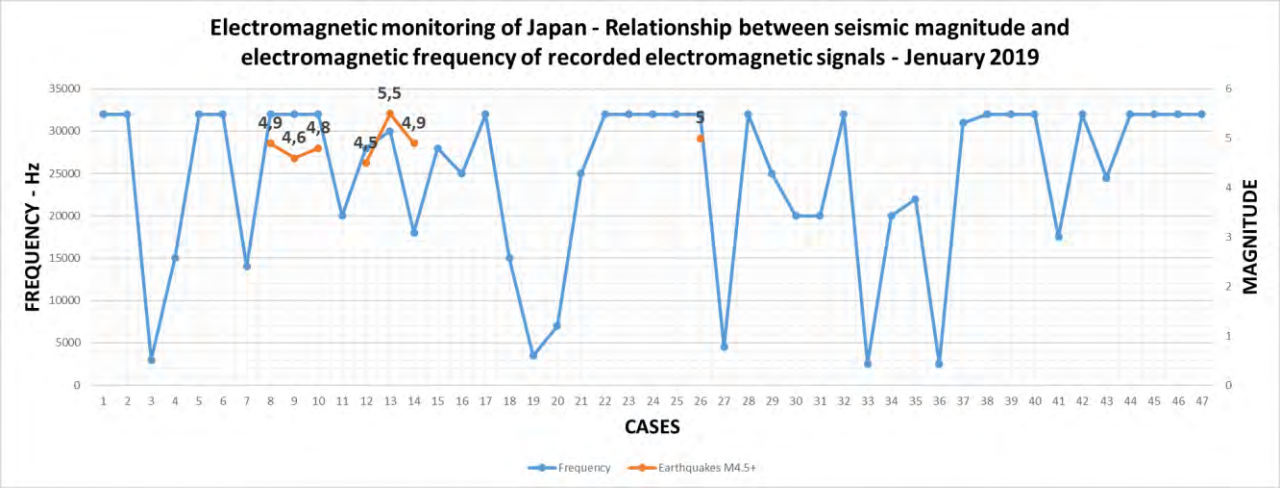

Fig. 37 - Relationship between the electromagnetic frequency of the signals received and the distribution of seismic events with magnitude M4.5 +. registered in January 2019 - Source Radio Emissions Project; USGS. January 2019.

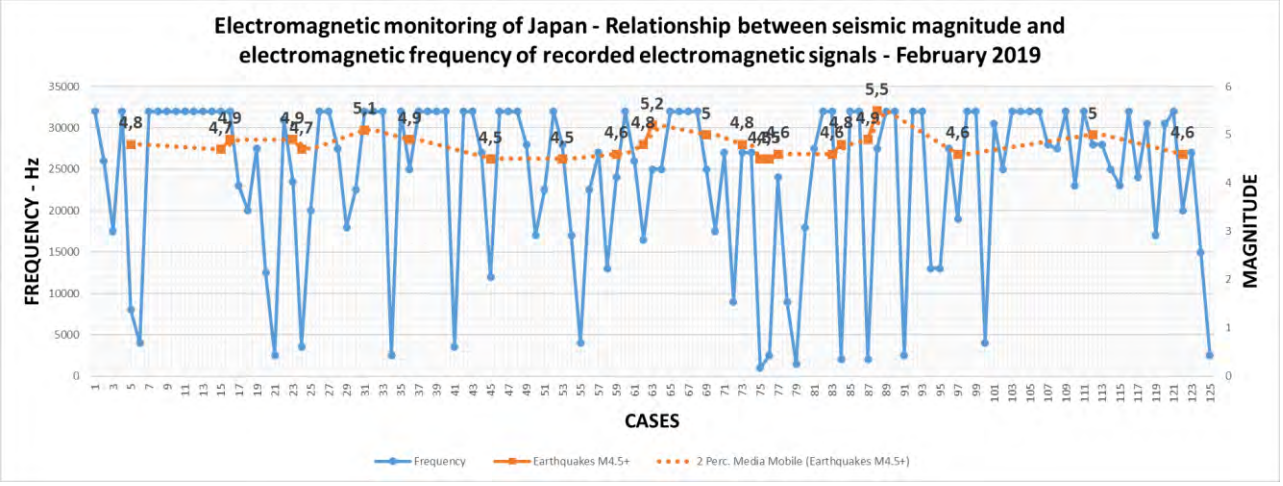

Figure 38 - Relationship between the electromagnetic frequency of the signals received and the distribution of seismic events with magnitude M4.5 +. registered in February 2019 - Source Radio Emissions Project; USGS. January 2019.

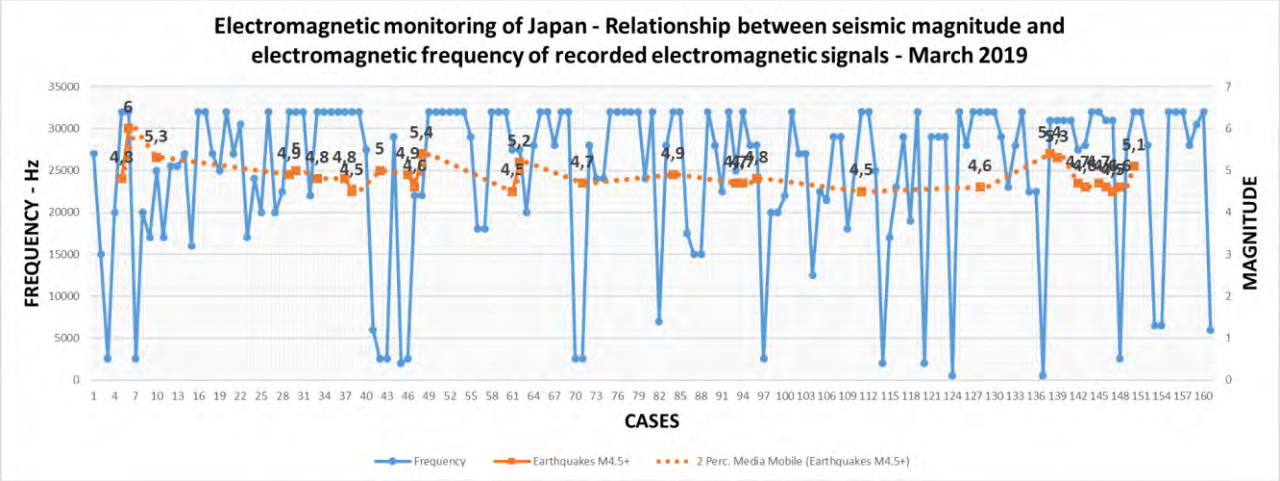

Figure 39 - Relationship between the electromagnetic frequency of the signals received and the distribution of seismic events with magnitude M4.5 +. registered in March 2019 - Source Radio Emissions Project; USGS. January 2019.

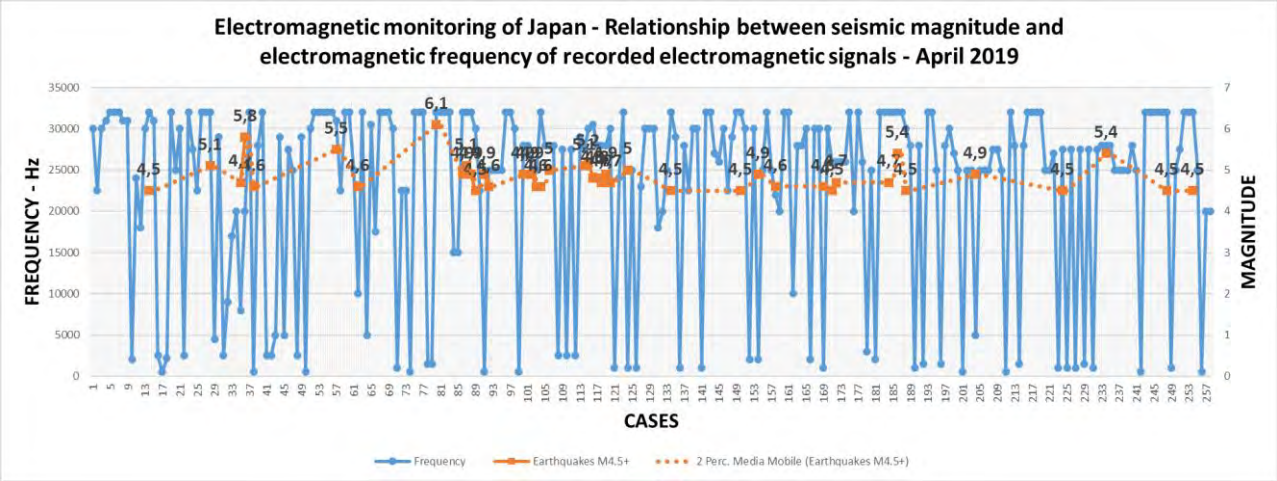

Figure 40 - Relationship between the electromagnetic frequency of the signals received and the distribution of seismic events with magnitude M4.5 +. registered in April 2019 - Source Radio Emissions Project; USGS. January 2019.

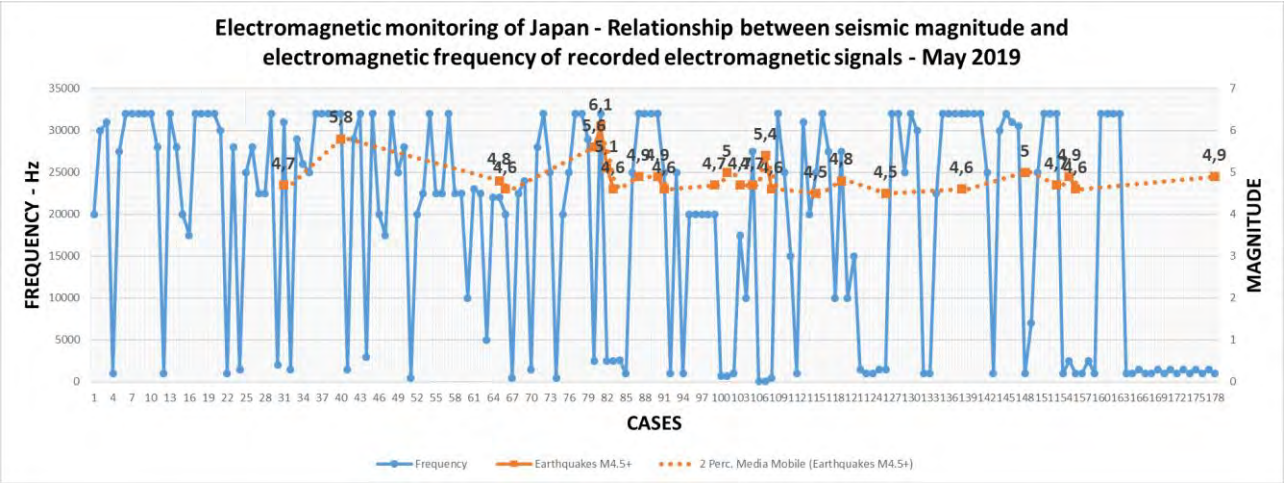

Figure 41 - Relationship between the electromagnetic frequency of the signals received and the distribution of seismic events with magnitude M4.5 +. registered in May 2019 - Source Radio Emissions Project; USGS. January 2019.

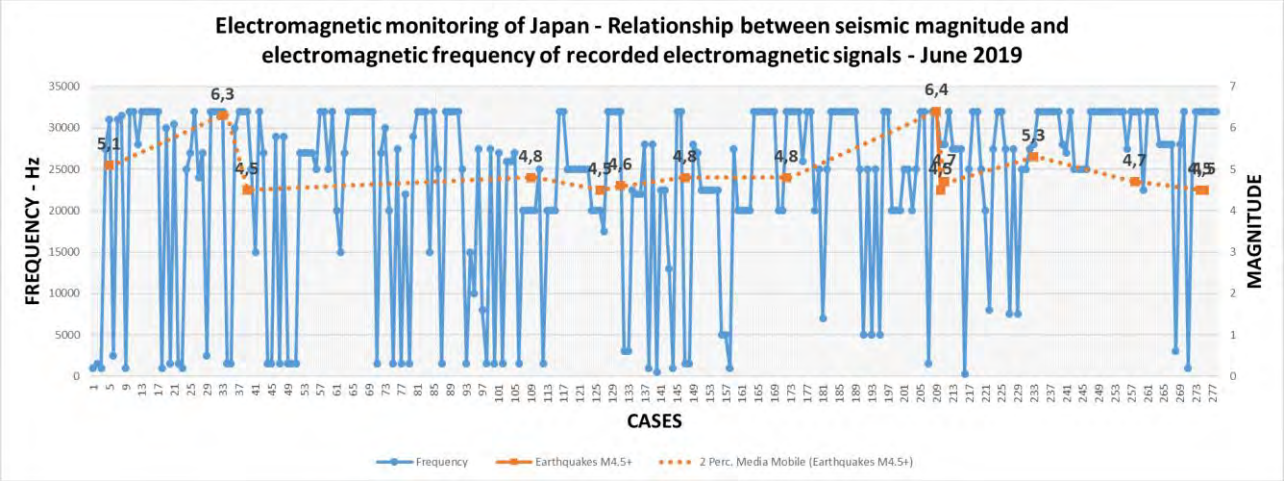

Figure 42 - Relationship between the electromagnetic frequency of the signals received and the distribution of seismic events with magnitude M4.5 +. registered in June 2019 - Source Radio Emissions Project; USGS. January 2019.

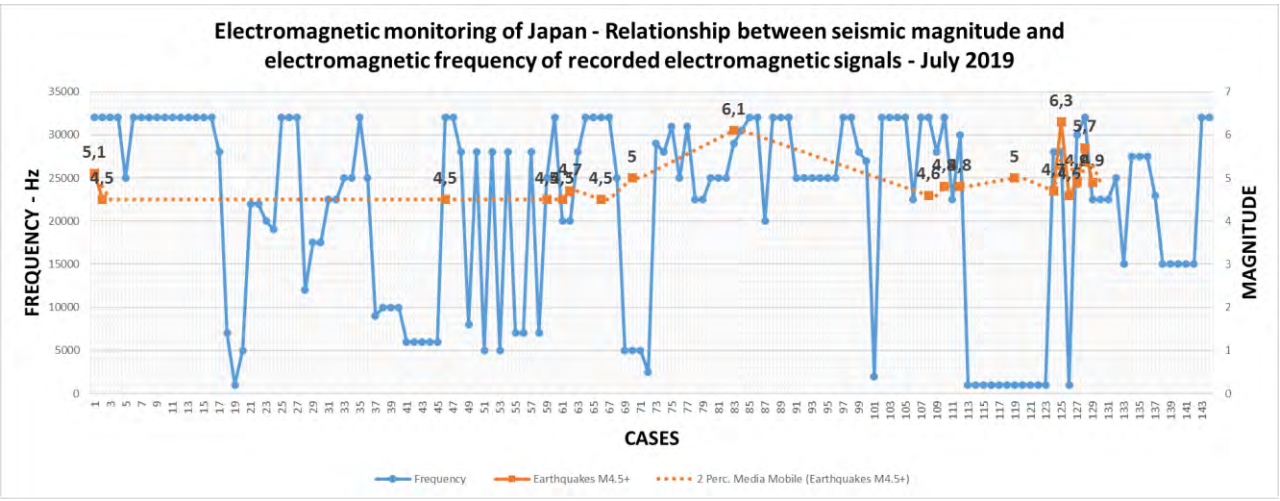

Figure 43 - Relationship between the electromagnetic frequency of the signals received and the distribution of seismic events with magnitude M4.5 +. registered in July 2019 - Source Radio Emissions Project; USGS. January 2019.

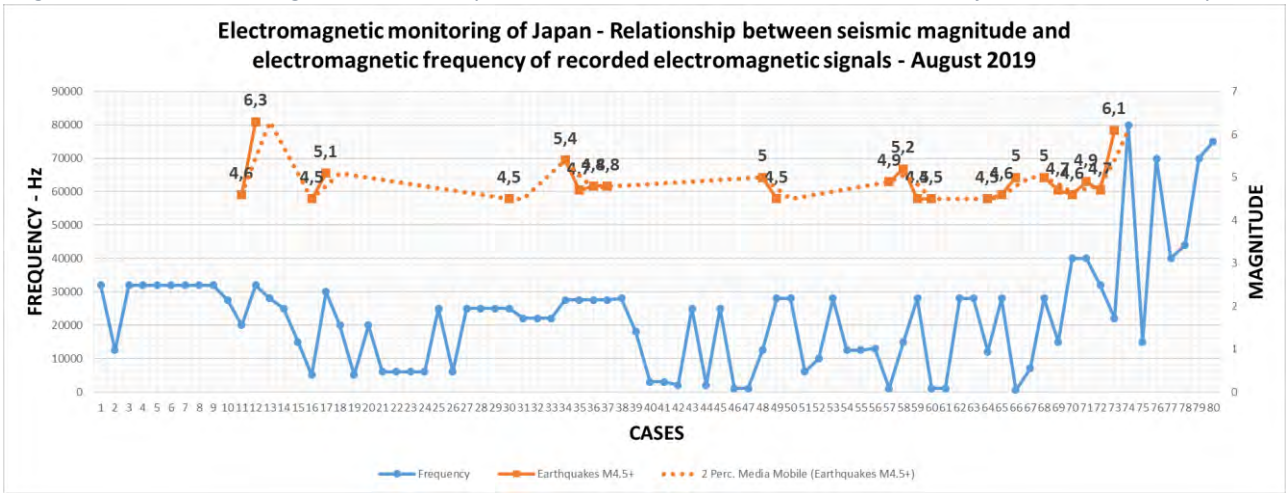

Figure 44 - Relationship between the electromagnetic frequency of the signals received and the distribution of seismic events with magnitude M4.5 +. registered in August 2019 - Source Radio Emissions Project; USGS. January 2019.

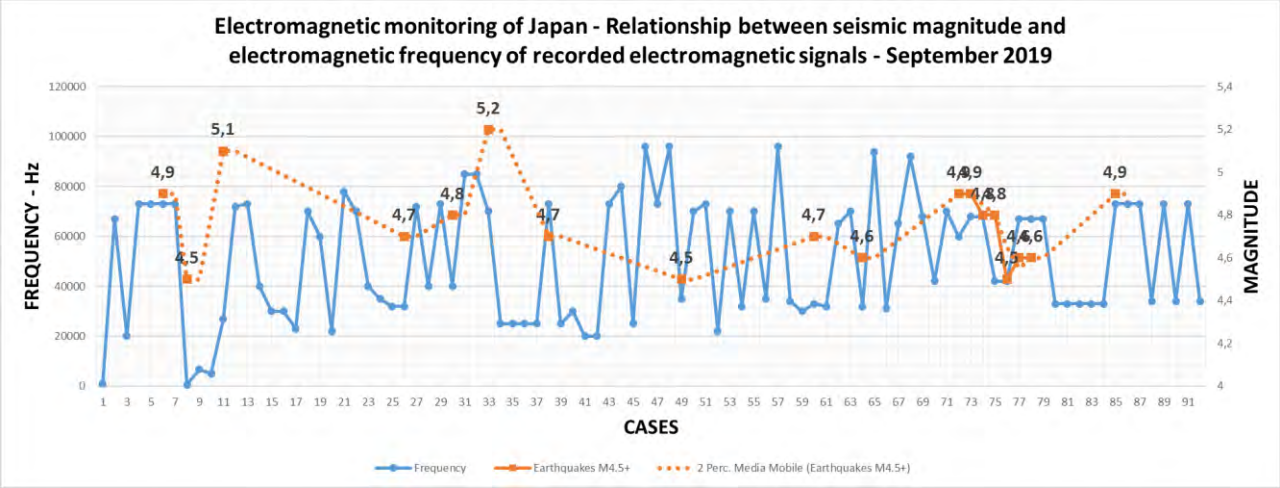

Figure 45 - Relationship between the electromagnetic frequency of the signals received and the distribution of seismic events with magnitude M4.5 +. registered in September 2019 - Source Radio Emissions Project; USGS. January 2019.

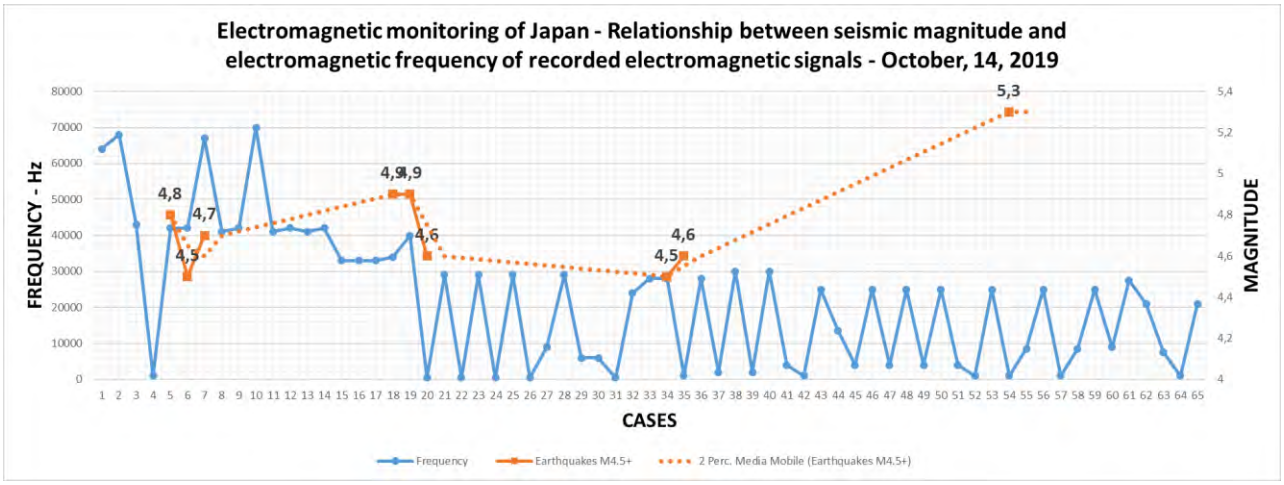

Figure 46 - Relationship between electromagnetic frequency of the received signals and the distribution of seismic events with magnitude M4.5 +. registered in October 2019 - Source Radio Emissions Project; USGS. January 2019.

The distribution of the electromagnetic frequency of the recorded signals, in relation to the temporal appearance of Japanese earthquakes with magnitude M4.5 +, indicates that seismic phenomena occur during electromagnetic increases that have appeared across the whole band (0-32 and 0-96 kHz), i.e. when the electromagnetic signals recorded by the RDF system are very extensive and exceed all other natural emissions present in the geomagnetic background (as visible in Fig. 37, 38, 39, 40, 41, 42, 43, 44, 45, 46) .

In this context, it is evident that the seismic magnitude follows the average frequency of the electromagnetic signals from the Japanese azimuth, in a directly proportional way. For the first time ever, the evidence from monitoring shows that there is a close relationship between crustal-type electromagnetic emissions and the occurrence of earthquakes of a certain magnitude.

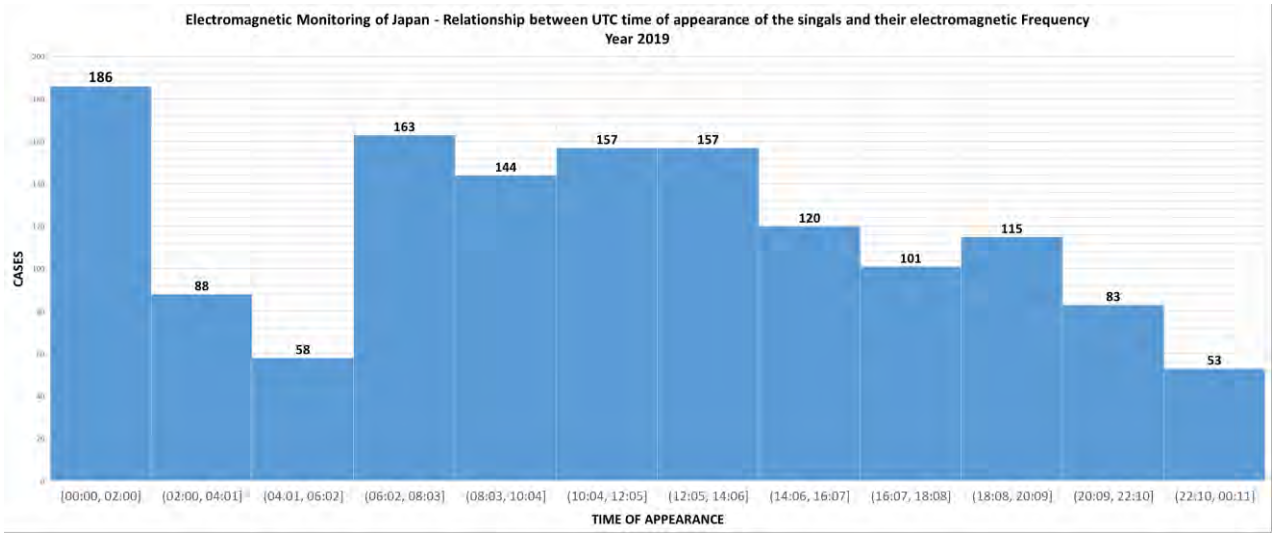

Figure 47 - Appearance of radio anomalies, with respect to the UTC time recorded by the RDF system developed by the Radio Emissions Project. The graph highlights well-distributed peaks and the number of radio anomalies associated with each group of hours considered within the study.

Scientific evidence shows that there are three substantial groupings of apparitions (electromagnetic signals - radio anomalies) well distributed, a first group is the one recorded between 00:00 UTC and 02:00 UTC, a second group is between 06:00 UTC and 14:00 UTC. A third and final grouping is found between 18:00 UTC and 20:00 UTC (Fig. 47).

The distribution of the hypocentral depth (Fig. 48) of the earthquakes that occurred in Japan, if related to the electromagnetic frequency of the radio-recorded anomalies by the RDF system, before the seismic events occurred, shows how, the deepest earthquakes were preceded by signals having an electromagnetic frequency distributed at a lower frequency, compared to earthquakes with a lower depth, preceded by signals distributed over the entire electromagnetic band.

As physics teaches us, the higher the frequency, the lower its propagation capacity through the planetary body, and vice versa. In this case, the data indicate precisely this phenomenon, where an electromagnetic frequency higher than the signals received before surface earthquakes have occurred.

This can be explained precisely thanks to the attenuation of the electromagnetic signal by the earth's crust: the greater the depth (in km), in which the electromagnetic emissions are generated, arising from local piezoelectric phenomena (electromagnetic dipoles determined by the distribution of electric charges, for the breaking of the crystalline lattice of rocks subjected to tectonic stress), and lower are the electromagnetic frequencies capable of reaching the ground level, to then be propagated in the earth-ionosphere cavity, and vice versa.

It will therefore be expected, as noted, that at a certain distance from these natural emitters (electromagnetic dipoles), the higher frequency emissions come from more superficially generated, therefore less attenuated, electromagnetic emissions, which are allowed to bounce off the ionospheric layers and reach thus far distant places, where they can then be received.

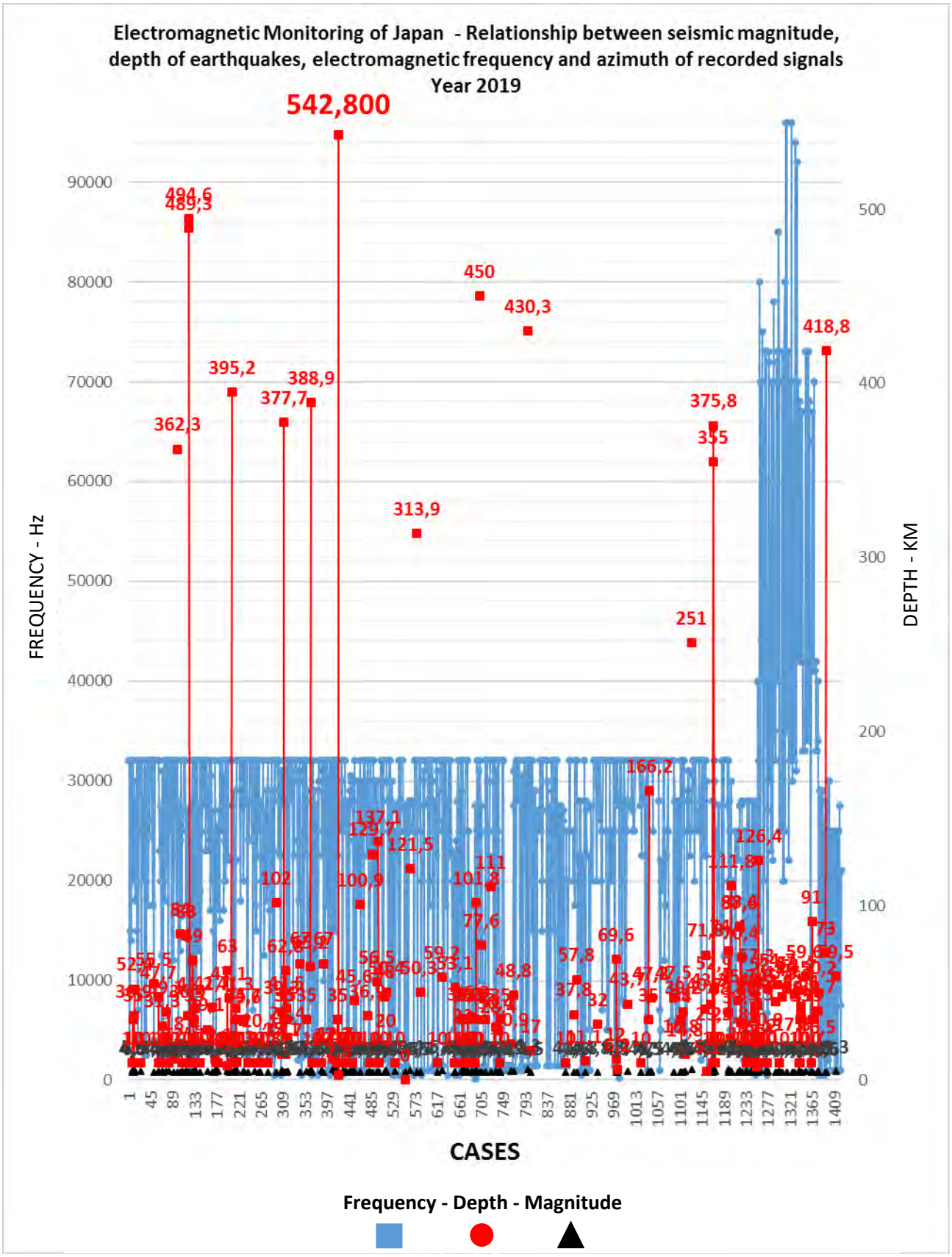

Fig. 48 - Relationship between the electromagnetic frequency of the recorded signals, the azimuth of origin in the direction of Japan and the distribution of the seismic events that occurred, with reference to their hypocentral depth and seismic magnitude. Source: Radio Emissions Project; USGS. Data from 2019.

6 – HYPOTHESIS

This important data strongly suggests that the emissions recorded by the monitoring system originated at the crustal level (in depth), precisely because the frequency distribution of the radio anomalies, compared to the seismic depth, shows that they follow the attenuation rules of propagation, better known as "fading by diffraction", due to the presence of physical obstacles, which in this case are represented by the layer of rocks in depth, just above the point where these signals are generated which acts as a filter, letting escape via the lower frequency electromagnetic frequencies, compared to those with higher frequency, depending on the depth of the emission point.

In this case even if these signals, to be detected thousands of kilometers away, seem to possess enormous powers in Watts, they do not only go to dissipate as a result of the "fading from soil reflection" which produces reflected waves which then go to added, with different phases, to the main wave, creating interference and random evanescence similar to "multipath fading", but in this case, thanks to seismic data, we know that this drop in frequency is associated with a lower seismic depth. Indicates that the lowering is substantially due to the depth of the electromagnetic emission in km, and not to the ionospheric fading phenomena.

In the face of this discovery, following the frequency characteristics of electromagnetic emissions, it is possible to partially understand their emission depth.

As regards instead the "phase shift" of the azimuth of the recorded signals (error in degrees with respect to the distance of origin of the signals themselves), we can certainly assume that this depends on the "multipath fading" which is a form of distortion of the electromagnetic signal which reaches its destination in the form of a certain number of replicas, out of phase over time, originating from the various paths (multipath) that the signal itself may have undergone during its propagation and summing up to each other in reception; moreover, each replica, having made its own path of a certain length and characterized by a different reflection on generally different surfaces, will therefore be subject to an attenuation in general different from that suffered by the other replicas. It is a typical problem of both fixed and mobile radio communications in a deterministic manner in the first case and with characteristics typical of a random process in the second case.

This would explain the azimuth error observed at a great distance, compared to the emissions coming from a few tens of kilometers away from the RDF detection station. These hypotheses are supported by the studies conducted by our team starting from 2017 (Straser et al., 2018).

7 – CONCLUSIONS

The data acquired with the RDF system have shown how it is possible to identify the direction of arrival of natural electromagnetic signals, and predict, with some precision when an earthquake can occur, along the azimuth indicated by the monitoring system.

In this context, the system if implemented can provide important information of a predictive nature in the field of seismogenesis, as well as providing suggestions on the evolution of the phenomena interconnected with the seismogenic phenomena that are at the basis of the seismic trigger. It is the duty of researchers to proceed along this field of research and invest efforts and economic funds for the realization of an integrated RDF system, even of a multiparametric type, that is, capable of correlating several types of data together.

REFERENCES

Cataldi, G., Cataldi, D., Rossi, R. and Straser, V., 2016. SELF-ELF Electromagnetic signals correlated to M5+ Italian Earthquakes that occurred on August 24, 2016 and January 18, 2017. NCGT Journal, vol. 5, no. 1, p. 134-143.

Cataldi, D., Cataldi, G. and Straser, V., 2017. SELF and VLF electromagnetic emissions which preceded the M6.2 Central Italy earthquake that occurred on August 24, 2016. European Geosciences Union (EGU), General Assembly 2017. Seismology (SM1.2)/Natural Hazards (NH4.7)/Tectonics & Structural Geology (TS5.5). The 2016 Central Italy Seismic sequence: overview of data analyses and source models. Geophysical Research Abstracts Vol. 19, EGU2017-3675.

Furumura T., Takemura S., Noguchi S., Takemoto T., Maeda T., Iwai K., Padhy S., 2011. Strong ground motions from the 2011 off-the Pacific-Coast-of-Tohoku, Japan (Mw = 9.0) earthquake obtained from a dense nationwide seismic network - Landslides, September, 8:333.

Straser, V., Cataldi, G. and Cataldi, D., 2015. Radio-anomalies: a tool for earthquake and tsunami forecasts. European Geosciences Union (EGU) General Assembly 2015, Natural Hazard Section (NH5.1), Sea & Ocean Hazard - Tsunami, Geophysical Research Abstract, vol. 17, Vienna, Austria. Harvard-Smithsonian Center for Astrophysics, High Energy Astrophysics Division, SAO/NASA Astrophysics Data System.

Straser, V., Cataldi, G. and Cataldi, D., 2016. SELF and VLF electromagnetic signal variations that preceded the Central Italy earthquake on August 24, 2016. NCGT Journal, vol. 4, no. 3, p. 473-477. Harvard-Smithsonian Center for Astrophysics, High Energy Astrophysics Division, SAO/NASA Astrophysics Data System.

Straser, V., Cataldi, G. and Cataldi, D., 2017. Seismic signals detected in Italy before the Nikol'skoye (off Kamchatka) earthquake in July 2017. NCGT Journal, vol. 5, no. 3, p. 391-396.

Straser V., Cataldi D., Cataldi G., 2018. Radio Direction Finding System, a new perspective for global crust diagnosis. New Concepts in Global Tectonics Journal, v.6, no. 2, June, p. 203-211.

Trembling Moon, its exosphere in comparison to atmospheres of Venus, Earth, and Mars and regolith layering.

Kochemasov G.G. IGEM of the Russian Academy of Sciences, 35 Staromonetny, 119017 Moscow, Russia, kochem.36@mail.ru

Abstract:

Low lunar gravity is not able to hold much atmosphere presumably created by degassing its solid body. Not like massive rocky planets-Venus, Earth, and Mars. They have atmospheres with their masses roughly proportional to their orbital frequencies (more frequency-more expelled volatiles from the planets depths by systematic wave shaking). Nevertheless, very thin exosphere is observed around the Moon. Its origin is related to the solar wind destructive action in the very thin surface film, meteorite impacts and, likely, due to constant trembling in the microwave diapason (modulated diapason due to the Moon orbiting around Earth and in Galaxy). By various methods in the lunar exosphere are found Argon 20000-100000 atoms in cm^{3}, helium 500-30000, neon up to 20000; sodium 70, potassium 17, hydrogen fever than 17 atoms in cm^3; methane and carbon also were found. There is a kind of equilibrium between supply of atoms from the solid lunar body and expelling them to space. Another result of constant trembling is in regolith layering.

Introduction:

The main point of the comparative wave planetology [1, 2] is: "Orbits make structures". This can be unfolded into four theorems: 1. Celestial bodies are dichotomous; 2. Celestial bodies are sectoral; 3.Celestial bodies are granular; 4. Angular momenta of different level blocks tend to be equal. Tectonic dichotomy or "wave 1-structure" or "2πR- structure" is easily observed on Earth, The Moon, and Mars as an opposition of pressed in "'oceanic" segments and bulging out "continental" ones [1-4].

There is well pronounced population of tectonic granules size of which depends on orbital frequencies of cosmic bodies. The higher frequency the smaller granule size, and, vice versa, the lower frequency the coarser grain. A sequence of well studied tectonic granule sizes is: photosphere πR/60, Mercury πR/16, Venus πR/6, Earth πR/4, Mars πR/2, asteroids πR/1…Pluto 62πR (not visible). Granules of Mars and asteroids coincide by size with the above described sectoring and segmentation. This row comprises various bodies: plasma, rocks, gases, ices, and different classes: star (aster), planet, satellite, asteroid. Only orbiting and rotation and their interactions play role.

As all cosmic bodies in Universe move in several orbits with very different orbiting frequencies they are affected by modulated waves. They appear as predicted by radio wave physics. The modulation is division and multiplication of the higher frequency by the lower one. As a result, along with main frequencies appear two side frequencies with corresponding them tectonic granules and radiations. Examples: Saturn, Pluto, the Moon, Titan, Ceres, Phobos, Churyumov-Gerasimenko comet core [5]. Very low orbiting frequencies of Galaxy and assemblies of galaxies in Universe modulate orbiting frequencies of smaller cosmic bodies forcing them to radiate short, fine and finest radio, X-ray and gamma rays and ether ("vacuum"). Lost mass and dark energy possibly are related to the shortest not yet measured oscillations.

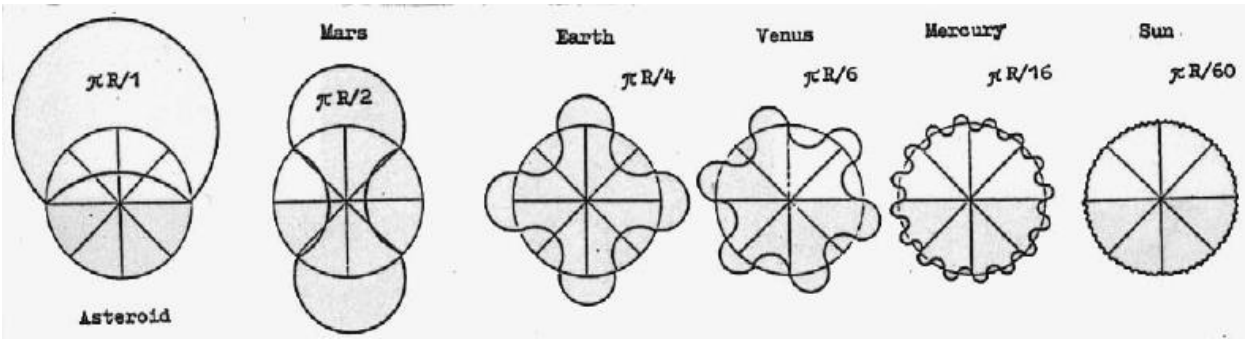

Fig. 1. Geometric models of wave warping planets, asteroids and Sun (aster). This row reflects growing orbital frequencies (for Sun-rotation) and compositions from plasma (Sun) through metal and rocks to ices. All sizes are brought to equal circles to stress importance of wave warping.

Observations and results:

It is commonly accepted that in formation of the very thin lunar atmosphere participate the solar wind, the UV radiation, steady bombardment of micrometeoroids. As a result, the whole spectra of elements was reported: alkali, rare gases, carbon, methane [6-9]. We suppose that to the listed agents should be added constant during billions of years trembling the satellite in the microwave diapason due to modulation of around Earth frequency by orbiting in Galaxy.

Fig.2. Lunar atmosphere rarely Observed 89830002_487197478613988_4927869822051522866_n.jpg.

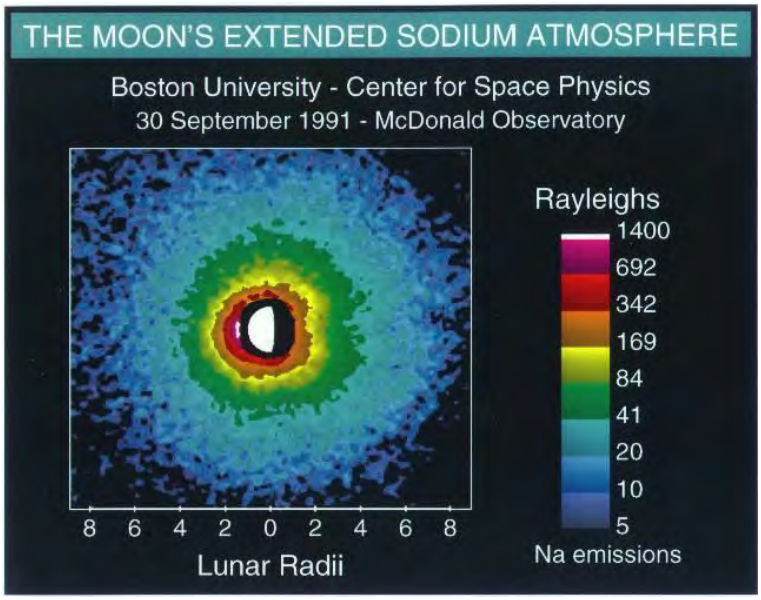

Fig. 3. The Moon's sodium atmosphere

Intersecting ripples of certain wavelengths and produced them tectonic granules are inversely proportional to the satellite main orbital frequencies (1/1 month – πR/4 and 1/1 year- πR/60 for the Moon) and calculated side frequencies (division and multiplication of the higher frequency by the lower one- πR/15 and πR/240) [6]. The granules can be observed on the lunar surface more or less pronounced. Often they are confused with impact craters but their even sizes and regular shoulder-to-shoulder disposition in lines and grids normally resolve the confusion.

Rare chances present the landings of the Chinese probes Chang'E 3 &4 on the Mare Imbrium and the South Pole Aitken Basin. Landing surface possibly cleaned by thruster jets of landing device revealed clear crossing lineation of a few centimeters spacing and produced them

granules. This very fine granulation fortunately can be calculated comparing it with a track of the Yutu' rover wheel. (about 10 cm wide) (Fig. 5, 6). An explanation of the granule size should be done with the above modulation procedure using two frequencies as was done for some celestial bodies earlier [3, 4, 10] The Moon main frequencies are 1/1 year and 1/1 month, the modulating Galaxy frequency is about 1/200 000 000 years. A scale is the Earth's orbiting period 1 year with the corresponding tectonic granule size πR/4 [1, 8].

Calculations for the Moon:

(1y. : 200 000 000y)πR = (1 : 200 000 000) 3.14 x 1738 km = 5.46 cm wave length for the circumsolar orbiting (or 0.46 cm wavelength for the around Earth orbiting). By the same galactic frequency modulation one obtains enigmatic metric radio waves for the Sun and decametric waves for Jupiter [4, 11]. Amalthea has 4.88cm (for the circumsolar frequency.), 0.0028mm (circumjovian frequency.), the Moon 5.46 cm (circumsolar frequency.), 0.46cm (circumterrestrial frequency) [4, 9, 11]. It is interesting that an enigmatic extra heat emission of Amalthea and its pronounced red color could relate to these calculated microwave and infrared emissions. Radio emission of the Moon at 2.5 cm wavelength was described in Berezhnoi et al., 2001 [12]. It is worth to note that well known radio wave and gamma-ray background observations are added by soft X-rays emitting from various celestial bodies – from cold comets to the hot Sun and measured by the Chandra X-ray Observatory [13].

The Chinese Chang'E-1 orbiter was equipped with a passive microwave radiometer (MRM) to measure the natural microwave emission from the lunar surface. The microwave emission, characterized by a frequency-dependent brightness temperature (TB), is related to the physical temperature and dielectric properties of the lunar surface. By measuring the brightness temperatures at different frequencies, detailed thermal behavior and properties of the lunar surface can be retrieved. The resulting maps show fine structures unseen in previous microwave maps that disregarded the local time effect. The new features revealed and their possible connections with the lunar geology were discussed. Daytime brightness temperatures are found to correlate well with TiO2 abundance by numerical analysis [14, 15].

In an earlier publication Chan et al. [14] indicated that resulting maps from the high frequency microwave channel show lunar topographic signatures with close similarity to those seen in Clementine's lunar topographic maps, while the low frequency channels reveal intriguing lunar surface properties not previously observed. Two characteristics displayed by the filtered brightness temperature maps are discussed: in the high frequency maps the existence of an anti-correlation between daytime and nighttime brightness temperature deviations in certain regions (especially in the lunar maria), and in the low frequency maps the appearance of cold spots which correspond with the hot spots observed in the infrared during lunar eclipses.

Thus, some relationship between lunar microwave emission and the geological background was discussed earlier [12, 14,15]. In the present work we show existence of the fine crossing rippling of the lunar surface at the microwave lengths and its origin indicating at galactic structuring trace.

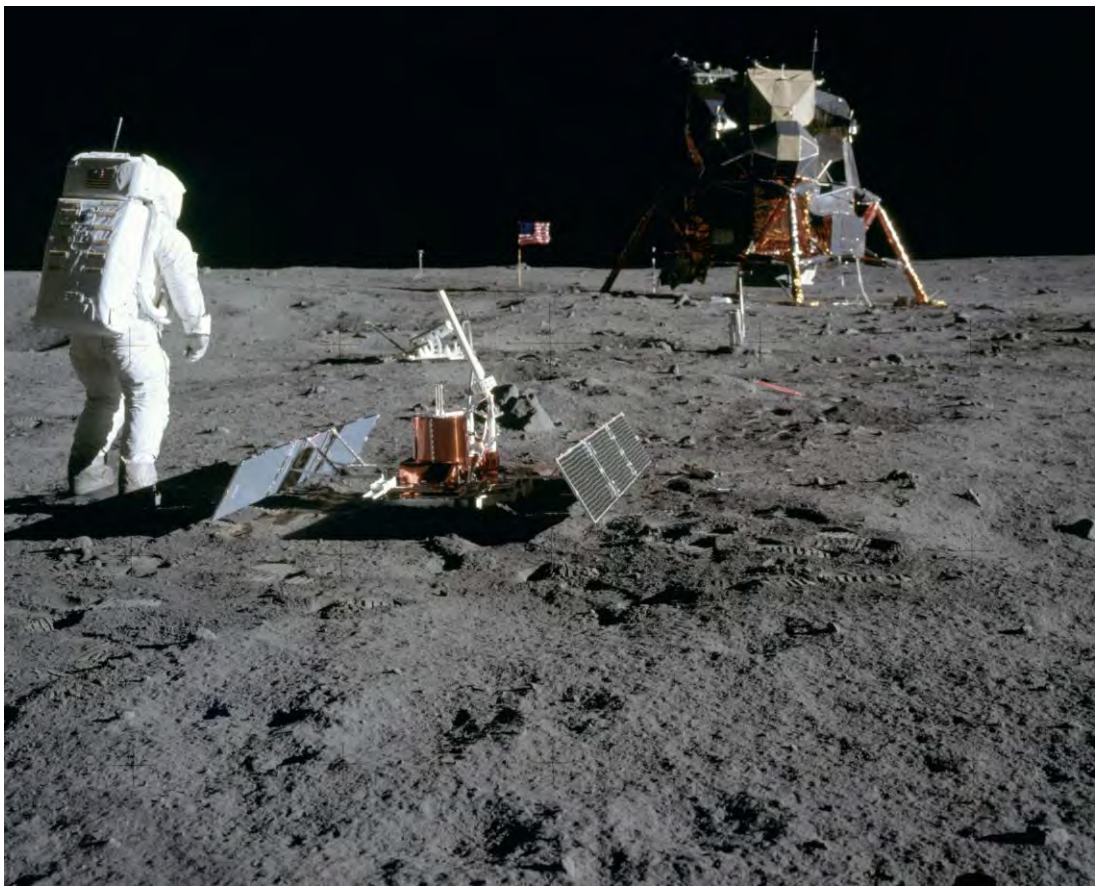

Fig. 4 Buzz Aldrin on the Moon. Apollo-11 mission. Intersecting regolith lineations are visible

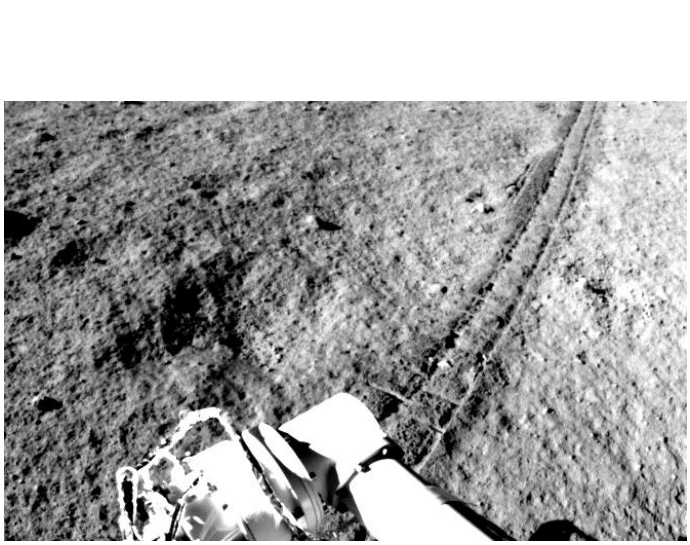

Fig. 5 (left). Yutu-1 rover wheel track on Mare Imbrium surface clearly showing fine intercrossing lineations (centimeters spacing). A portion of Chang'E 3 image 00.
Fig. 6 (right) Yutu-2-wheel-tracks-350x350-. Intercrossing regolith lineations in the South Pole Aitken Basin.

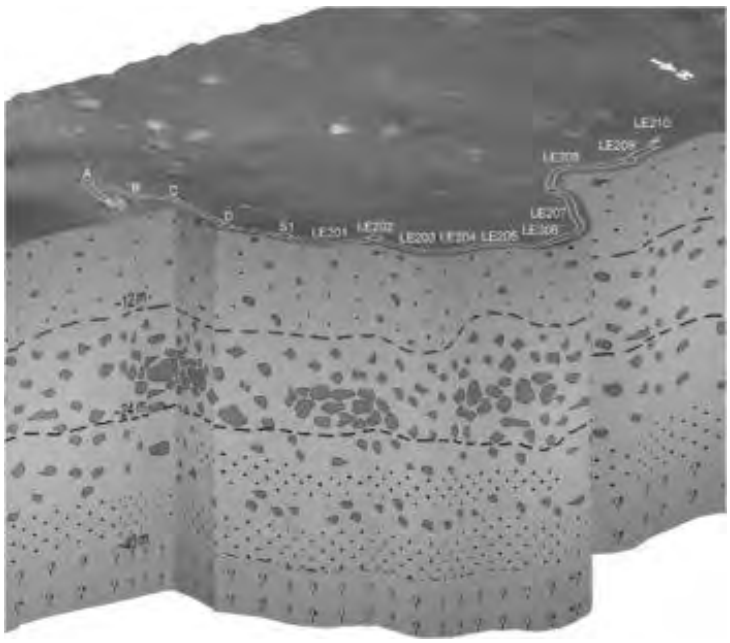

Fig. 7 Regolith layering. (F3.large_-350x307.jpg. Data of Chang'E-4). Vertical section.
Another important result is the fine microwave trembling observed within the Moon regolith causing its layering.

Similar fine cm-size crossing rippling is clear in images of the Chang'E-4 (Fig. 5, 6) and the Apollo 11 (Fig. 4). Thus, this modulation process, involving orbital frequencies of the Moon and Galaxy, is observed at the northern and southern lunar hemispheres as well as in the near and far lunar sides. Now, one might speak about the whole Moon modulation event. It is worth to note that the same approach is applied to calculating frequencies of the Martian global dust storms (joint consideration of the rotation and orbiting of Mars-spin-orbit coupling) [5, 16].

Another important result is the fine microwave trembling observed within the Moon regolith is cousing its layering. The recent data of the Chang -4 show that in the SPA Basin along track of the rover the regolith cover is layered: the upper about 12 m are composed of finer fragments than the full of larger fragments underlying layer (24 m, Fig.7) This might be explained in that upper finer fragments are predominantly less dense that the lower larger ones composed of intergrowths silicates with native iron [17].

A role of the wave trembling and "sweeping out" volatiles is vividly demonstrated at comparison of the wave granulation and atmospheric masses of three rocky planets: Venus, Earth, and Mars. Planetary atmospheres as inseparable parts of planetary geospheres have close structural and compositional ties with underlying solid formations. Atmospheres are produced by solid bodies as a result of their outgassing ("sweeping out" volatiles) that apparently is tied to their oscillations and tectonic granulations [18, 19]. Intensity of "sweeping" out volatiles of planets increases with frequency of their wave "shaking" that is in an inverse correlation with their orbital frequencies. The comparative wave planetology having stated that "orbits make structures" finds that two fundamental properties of all celestial bodies are most important for their structuring: movement and rotation. All bodies move in non-circular Keplerian elliptic (and parabolic) orbits that imply periodic acceleration changes and appearance of inertia-gravity forces producing warping waves. Individual for any body waves whose lengths are inversely proportional to their orbital frequencies produce tectonic granules: higher frequency – smaller granule, lower frequency – larger granule. The Atmospheres following row shows increasing granule sizes (a half of a wavelength): Venus $\pi R/6$, Earth $\pi R/4$, Mars $\pi R/2$ [2, 3,18,19, 20]. One may say that Venus is tectonically "fine-grained", Earth "medium-grained", Mars "coarse-grained". The wave produced granulation and known atmospheric masses indicate that fine-grained Venus is more thoroughly shaken out and released of its volatiles (degassed) than Earth and Mars. The atmospheric masses increase from Mars through Earth to Venus as ~ 0. 01 : 1 : 90

(mass ratios). This is proved not only by its massive atmosphere containing a large amount of nitrogen but also by a very low ratio of radiogenic to primordial argon (Venus 1, Earth 300, Mars 3000) [21].

Conclusion:

An interaction between the higher frequencies lunar orbits in the Solar system and much lower Galactic rotation frequency (modulation of the first by the second) reveals additional side frequency in the microwave range. The lunar constant trembling in this range, revealed by cosmic devices and revising surface images, brings out results in supplying by volatile elements and compounds (even by methane) thin exosphere and layering the regolith with thickness of about several tens of meters. Thus, the lunar microwave trembling has two-fold global results in its sparse atmosphere and in the regolith layer.

References:

[1] Kochemasov, G.G. (1998) Tectonic dichotomy, sectoring and granulation of Earth and other celestial bodies. Proceedings of the International Symposium on New Concepts in Global Tectonics, "NCGT-98 TSUKUBA", Geological Survey of Japan, Tsukuba, Nov 20-23, 1998, 144-147.

[2] Kochemasov G.G.(1999) Theorems of wave planetary tectonics. Geophys. Res. Abstr. V.1, №3, P.700;

[3] Kochemasov G.G. (2001) On one condition of further progress in lunar studies // First Convention of Lunar Explorers, 8th to 10th March, 2001, Programme and Contributed Abstracts, Palais de la Découverte, Paris, France, p. 26

[4] Kochemasov G.G. (2002) Radiowaves and tectonic dichotomy: two sides of one coin // Geophysical Research Abstracts, Vol. 4, 2002, European Gepphysical Society XXVII General Assembly, Nice, France, 21-26 April 2002

[5] Kochemasov G.G.(2018) Modulated wave frequencies in the Solar system and Universe // Universal Journal of Physics and Application 12(4): 68-75, Doi: 10.13189/ujpa.2018.120402.

[6] Cook J.J.C, S.A. Stern, P.D. Feldman, G.R. Gladstone, K.D. Retherford, C.C.C.Tsang (2013)New upper limits on numerous atmospheric species in the native lunar atmosphere// Icarus, v. 225, 681-687.

[7] Hodges R.R. Jr. (2016) Methane in the lunar exosphere: Implications for solar wind carbon excape // Geophys. Res. Lett, v. 43, 6742-6748.

[8] Killen R.M., W.-H. Ip, (1999) The surface-bounded atmospheres of Mercury and the Moon // Rev. Geophys., v 37, 361-406.

[9]Yokota Sh., Terada K., Saito Y., Kato D., Asamura K., Nishino M.N., Shimizu H.(2020) KAGUYA observation of global emissions of indigenous carbon ions from the Moon // Science Advances, 06 May 2020, v. 6, no.19,aba 1050. DOI: 10.1126/sciadv.aba 1050.

[10] Kochemasov G.G. (2003) Universe of oscillations: sound-radiowaves-gamma-rays-ether // Geophysical Research Abstracts, Vol. 5, 02159, 2003;

[11] Kochemasov G.G. (2008) Wave modulations in the Solar system bodies and their radio emissions // Geophysical Research Abstracts, Vol. 10, EGU2008-A-01272, 2008. SRef-ID: 1607-7962/gra/EGU2008-A-01272, EGU General Assembly 2008.

[12] Berezhnoi A.A., Bervalds E., Khavroshkin O.B., Ozolins G., Shevchenko V.V, Tsyplakov V.V. (2001) Radio emission of seismic origin from the Moon at 25 mm during the Leonid 2000 meteor shower // First Convention of Lunar Explorers, 8th to 10th March, 2001, Programme and Contributed Abstracts, Palais de la Découverte, Paris, France, p. 2.

[13] Bhardwaj A. , Gladstone G. R. , Elsner R. F. et al.(2002) Soft X-Ray emissions from planets and moons // ESLAB 36: Earth-like planets and moons, Programme and abstract book, ESTEC, Noordwijk, The Netherlands, 3-8 June 2002, Abstract # 23.

[14] Chan K.L., Tsang K.T., Kong B., Zheng Y-C. (2010) Lunar regolith thermal behavior revealed by Chang'E-1 microwave brightness temperature data // EPSL, v. 295, (1-2), 2010, 287-291.
[15] Zheng Y.C., Tsang K.T., Chan K.L., Zou Y.L., Zhang F., Ouyang Z.Y. (2012) First microwave map of the Moon with Chang'E-1 data: the role of local time in global imaging // Icarus, 2012, v. 219, issue 1, 194-210.
[16]Shirley J.H. (2017) Orbit-spin coupling and the circulation of the Marian atmosphere // Plan. Space Sci., 141, 1-16. 10.1016/j.pss.2017.04.006.
[17] Kochemasov G.G.(2019) Possible Fe-metal enrichment areas in the SPA Basin //Developing a New Space Economy (2019), 5024 pdf.
[18] Kochemasov G.G. (2006) Outgassing of planets in relation to their orbital frequencies // EUROPLANET-2006 Sci. Conference, Sept.22-26, 2006, Berlin, EPSC Abstracts, Vol. 1, EPSC2006-A-00043, CD-ROM.
[19] Kochemasov G.G.(2012) Atmospheres of Venus, Earth, and Mars: their masses and granulations in relation to orbits and rotations of the planets // Comparative Climatology of Terrestrial Planets, 8008 pdf.
[20] Kochemasov G.G. (2009) A regular row of planetary relief ranges connected with tectonic granulations of celestial bodies // New Concepts in Global Tectonics Newsletter, # 51, June 2009, 58-61.
[21] Pollack J.B. and Black D.C. (1979) Implications of the gas compositional measurements of Pioneer Venus for the origin of planetary atmospheres // Science, v. 205, #4401, 56-59.

NCGT Short Communication

Heat transfer causing epicenter and volcanic eruptional transition

Fumio Tsunoda
agatsuma.terao@gmail.com

High temperature zone (Super Plume) from the outer core at 4000?

Fluctuations of the earth's axis indicate the existence of liquid in the center of the earth which is said to be the 4000? molten outer core. The thermal structure model of the earth is based on mantle tomography technology (Obayashi, 2009). The Obayashi model is explained in 17 images and commentary in the front page published in Tsunoda (2009). The molten part extends from the 4000? outer core, which is the heat source of the earth, to the South Pacific Ocean (Fig. 1). Figure 1 is an image of Obayashi's model, illustrated by Tsunoda et al (2013). Fukao (1992) first pointed out this high temperature heat transfer path. This heat transfer path is called Super Plume (called SP for short).

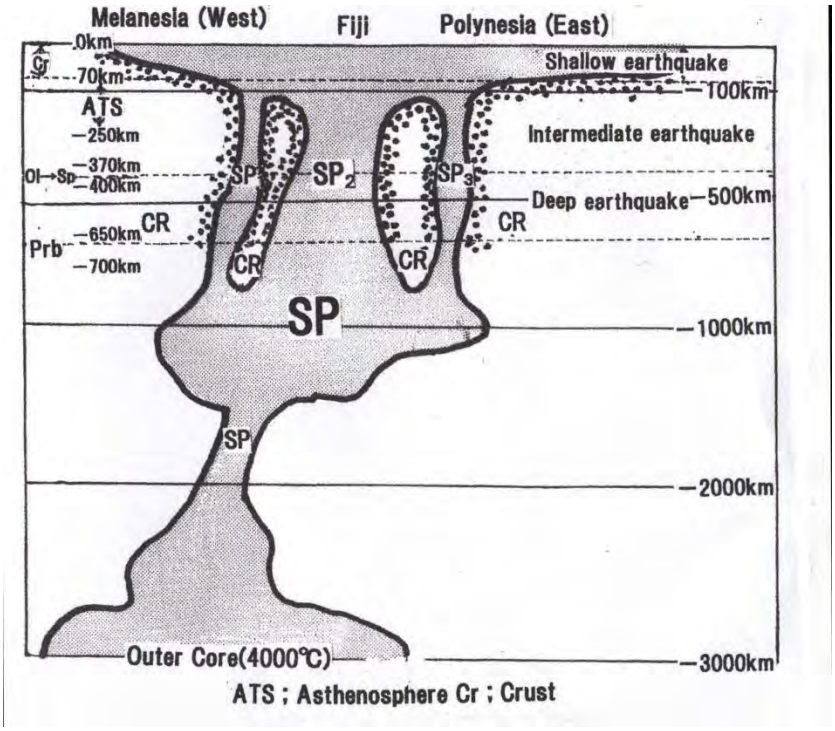

Figure1 Huge heat transfer path (Super plume, SP) Tsunoda et al (2013) Figure 1-1b (Southwest Pacific SP) is simplified and quoted

Seismic zone classification of the Upper Mantle

If the gray part in Fig.1 is a hot and molten SP, seismic waves do not occur there. However, if the white part (CR in Fig. 1) is a cold rock layer, there will be an increase in temperature and expansion and destruction will occur, causing an earthquake. The dotted area in Fig. 1 represents the epicenter zone. Thus, there are seismic zones classified as follows: at depths of 720~300km is a deep earthquake zone, from 300~70km is a medium depth earthquake zone, and from 70~0km is a shallow earthquake zone (Kikuchi, M., 2003; Fig. 1). There are three regions where these phenomena occur the southwestern Pacific (time series [Table 1(1), Fig. 2] along longitude 180E, Meridian line), Southeast Asia (time series along longitude 150E

[Table 1 (2), Fig. 2]) and the Far East (time series along longitude 120E, [Table 1 (3), Fig. 2]) (See figure 2a of Tsunoda et al (2013).

Fig.2 Earthquake-eruption time series by area in the Pacific region

Table 1(1) is the Melanesian and Polynesian areas, (2) is a Far East Asia, (3) is a Southeastern Asia

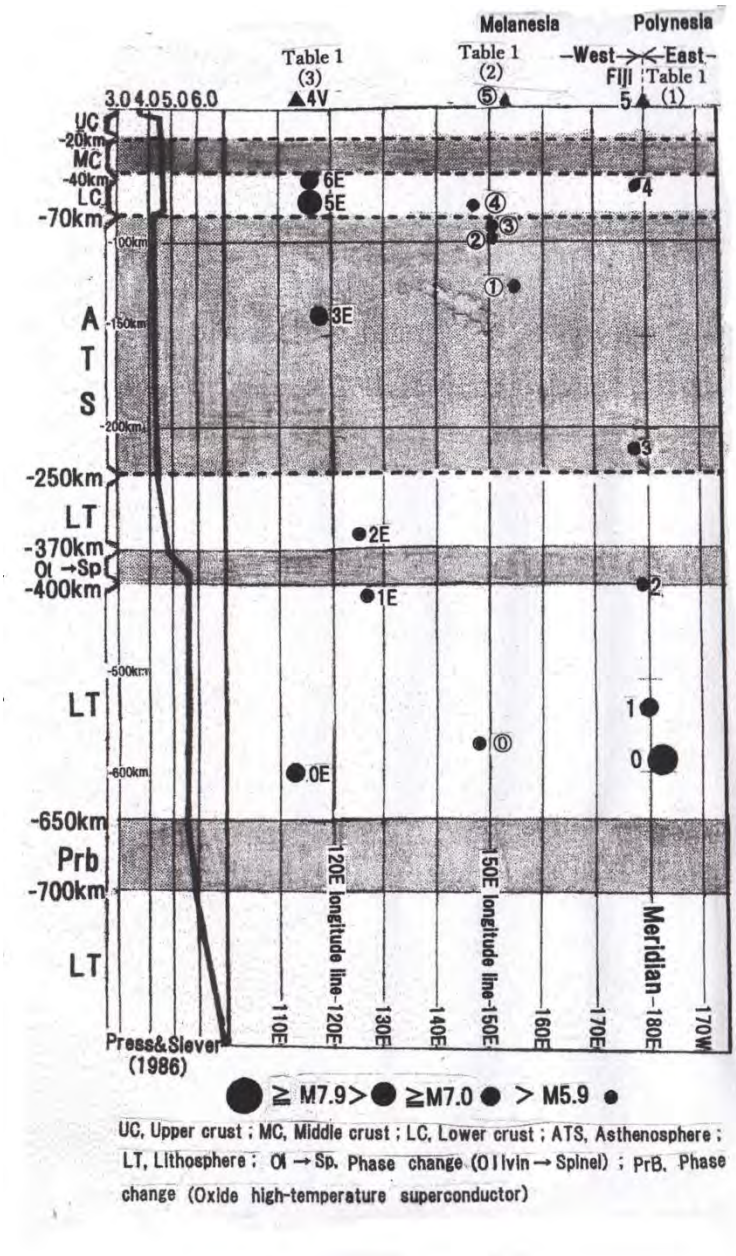

Figure 2 Earthquake-eruption time series by area in the Pacific region Table 1(1) is the Melanesian and Polynesian areas, (2) is a Far East Asia, (3) is a Southeastern Asia

Earthquake-eruption time series caused by massive heat transfer along the SP Thermal energy flow from the outer core is constantly flowing from SP to SP2. On September 6, 2018, the energy flow caused a huge M7.9 earthquake at 670km underground SP (Table 1, [1]). Heat flow from the outer core raised the temperature of the rock layer at that depth, causing thermal expansion and destruction. In other words, it is this M7.9 earthquake which is the point of ?670km in Figure 1. Furthermore, this extreme heat flow continued to rise for a week and

erupted to the Whakari/White Island volcano of New Zealand's North Island. The deepest earthquake occurred twice a year since then. These two heat sources caused a VEI (Volcanic Explosivity Index) 02 eruption of White Island volcano on December 09, 2019. Earthquakes and eruptions occur alternately in the time series or occur at the same place and on the same day. These indicate that heat flow is considered to be the energy source for both earthquake time series and eruptions.

Earthquake-eruption time series along the smallest amount of heat flow A small M4.5 earthquake occurred 567km underground in Vostok (Russia) in the Far East (?E, '19/01/13, 50N 148E, M4.5). A weak heat flow generated a continuous time series of M4 earthquakes thereafter (?E, '19/02//11 ~?E, '19/02/17). And finally, there was a slight volcanic fumarolic activity. In other words, Raikoke volcano emitted a steam and gas plume with ash ('19/06/22, 48N 153W, Kurile Russia), However, when a deep M6.3 earthquake occurred due to a strong and high heat flow ('19/11/20, Ozermovskiy Russia, 53N 153E, ?496km, M6.3), a large shallow earthquake ('20/03/25, Kuril'sk Russia, 48N 157E, ?57km, M7.5 earthquake) and violent volcanic activity occurred ('20/07/15~21, Kamchatka Russia, Karymsky volcano, 54N 159E, emitting a gas and steam plume containing ash). From the above, it can be said that the strength of heat energy flow determines the magnitude and strength of volcano seismic activity. Earthquake-eruption time series in Southeast Asia where volcano-seismic activity is active From Southeast Asia, spreading to Melanesia, volcano-seismic activity is active, and thermal energy is abundant. The time series of volcano-seismic activity from the end of 2018 to the beginning of 2019 began with heat supply from SP2. First, the heat flow that generated the earthquake (M7.9 on '18/09/06) along SP2 produced a volcano just above it one week later. For about a month after that, seven M6 earthquakes along SP2 occurred due to the heat flow. Such heat supply caused the asthenosphere to heat up and swell, causing a ?03E earthquake and a ?04V eruption (Fig.1 (3)). Large earthquakes ?5E and ?6E were generated due to the heat energy that could not be consumed in the inactive ?04 eruption.

Problems related to heat flow From 2016 to 2019, there were large deep earthquakes in the Upper Mantle, but the eruptions were weak (Tsunoda, 2019). This indicates that the amount of heat radiation during this period (DE15 by Tsunoda, 2019) was scanty and the sea water temperature was low. As we have already seen, the greater the number of deep earthquakes, the greater the heat energy capacity. On the contrary, if the deep earthquakes are small and scarce, the heat energy capacity is also small. If the seawater temperature is low, the Pacific high will not develop. This may be the cause of Japan's long rainy season this year (2020).

Acknowledgment Mr. Matt, W. proofreads the paper, I thank you very much.

Table 1. Time series from continuous epicenter to eruption

(1) Earthquake-eruption time series along a large-capacity heat transfer path (SP)

6V	19/12/09	New Zealand North Island Whakari/White Island Volcano	VEI (Volcanic Explosivity Index) 02		
6E	'19/10/21	Vanuatu	19S 178W	?231km	M6.6
5E	'19/09/01	Fiji	20S 178W	?581km	M6.6
4E	'19/05/30	Tonga	21S 176W	?177km	M6.0
3E	'19/01/26	Fiji	?588km	M6.2	
2E	'18/12/23	Tonga	20S 175W	?113km	M6.4
1E	'18/09/30	Fiji	18S 179W	?550km	M6.0

1V	18/09/12	New Zealand Whakari/White Island volcano	37S 177E	Gas and steam emission	
0E	‘18/09/06	Suva Fiji	18S 179W	?670km	M7.9

(2) Earthquake – eruption time series along the heat transfer path with the smallest capacity

?V	‘19/06/22	Kurile Russia	48N 153E	Raikoke volcano	
?E	‘19/02/17	Shikotan Russia	43N 146E	?57km	M4.5
?E	‘19/02/14	Kuril’sk Russia	45N 151E	?75km	M4.6
?E	‘19/02/13	Kuril’sk Russia	45N 151E	?101km	M4.9
?E	‘19/02/11	Ozernovskiy Russia	51N 156E	?136km	M4.9
?E	‘19/01/13	Vostok Russia	50N 148E	?567km	M4.5

(3) Earthquake-eruption time series of Southeast Asia with active volcano seismic activity

?6E	‘19/01/06	Tobelo Indonesia	2N 126E	?43km	M6.6?
?5E	‘18/12/29	Philippine	5N 126E	?60km	M7.0
?4V	‘18/10/3~4?’18/12/16	Indonesia	1N 124E	Soptan volcano	Ash explosion
?3E	‘18/12/01	Soumulaki Indonesia	7S 128E	?136km	M6.4
?2E	‘18/11/30	Manado Indonesia	2N 124E	?331km	M4.6.
?1E	‘18/11/21	Dili East Timor	6S 126E	?409km	M4.6
?01E	‘18/11/04	Sapod Philippine	7N 123E	?600km	M6.6
?0V	‘18/09/12	New Zealand	Whakari/White Island volcano	37S 177	Gas and steam emission
?00E	‘18/09/06	Suva Fiji	18S 179E	?670km	M7.9

References

Blot, C. and Choi, D. R., 2004, Recent devastating earthquakes in Japan and Indonesia viewed from the seismic energy transmigration concept. NCGT Newsletter, no.33, p. 3-12.

Fukao, Y. (1992) Seismic tomogram of the earth’s mantle: geodynamic implications: Science, v. 258, N.5082, 625-630.

Kikuchi, M. (2003) Real-time Seismology. Tokyo University Press, Tokyo, 222p (in Japanese).

Mogi, K., 1968, Migration of seismic activity. Bull. Earthq. Res. Inst., 46, 53-74.

Obayashi, M. (2009) Temperature of the Earth’s interior revealed by mantle tomographic technology. Model images and explanations for different depths of frontpieces published in Tsunoda (2009).

Obayashi, M. Yoshimitsu, J. Sugioka, H. Ito, A. Isse, T. Shiobara, H. Reymond, D. and Suetsugu, D., 2016, Mantle plumes beneath the South Pacific superswell revealed by finite

frequency P tomography using regional seafloor and island data. Geophysical Research Letters, 43(22), 11628-11634.

Smithsonian Institution National Museum of National History, 2020, Global Volcanism Program, volcano.si.edu/database/search_eruption_results.cfm

Tsunoda, F. (2009) Habits of earthquake: Time and place of occurrence and their migrate paths., Kodansha Ltd., ??Shinsho, 480-1 C, Y-876, Tokyo, 190p (in Japanese)

Tsunoda, F., Choi, D.R and Kawabe, T. (2013) Thermal energy transmigration and fluctuation. NCGT journal V.1, no.2, www.ncgt.org, 65-80.

Tsunoda, F. (2019) One idea of the heat transfer in the Upper Mantle. NCGT Journal, V7, No.3, NCGT Short Communication, 148-151.

United State Geological Survey (2020) Earthquake Hazards Program, Search Earthquake Catalog, https://usgs.gov/

BOOK REVIEW

The Hidden History of Earth Expansion told by researchers creating a Modern Theory of the Earth, edited by Stephen W. Hurrell, Hardback edition ISBN:13 9780952260387, 2020, OneoffPublishing.com.

By : Louis Hissink

This new book sets out to show that earth expansion theory, contrary to popular belief, remains a plausible scientific explanation for the Earth's observed surface structure. The book may take a couple of days to read and starts with a long introduction by Stephen Hurrell, the editor, followed then by fourteen chapters devoted to each researcher or team's theories justifying their model of Earth expansion. Each chapter starts with a short biography of the chapter author(s), followed by the description of the particular evidence the author(s) believe(s) supports earth expansion theory. The book concludes with a comprehensive reference and index. There are also interesting personal anecdotes of the author(s) journeys along the earth expansion theory path, and how they coped with the plate tectonics mafia.

Most of the ideas described in this book assume the standard cosmological gravitational model though two authors, John B. Eichler and Vedat Shehu, widened their analysis to include an additional role for electrical plasma, but gravity theory itself was not reviewed. This is interesting, because the proposed mechanics of earth expansion flatly contradict the standard mechanism of gravitational accretion. I would have thought disproving gravitational accretion would logically confirm earth expansion.

Earth expansion theory, like plate tectonic theory, developed from the idea of continental drift, popularised by Alfred Wegener during the early 20th century, when it was realised that the Americas and Europe-Africa could be joined together if the Atlantic ocean was removed. This continental "match" was interpreted before geoscience knew anything about the structure of the ocean floors, but which was also ridiculed since "everyone" knew the Earth was cooling and shrinking at the time. It is also became clear using geographical origami to refit the continents back in time was not possible on the present size of the Earth, and it took some time before it was realized that it could be done if a smaller earth was assumed. The book's introduction thus describes in some detail the progress of expanding earth theory from Wegener's time until the present, especially after WWII when mapping of the world's ocean floors started.

One of the puzzles involved gigantic dinosaurs that the book's editor, an engineer, realised could not have lived on today's Earth, since the gravitational force is too high. This led to the realisation that gravity had to have been much lower during the Mesozoic Era, and his argument is described in Chapter 8. This led to the heresy that gravity at the Earth's surface seemed to have increased over deep, or geological, time though from a cosmological position, somewhat difficult to explain under the umbrella of the Big Bang cosmology. As mentioned above, no author seems to have thought of questioning gravity itself.

The first chapter is essentially a description of the genesis of Hugh S. Owen's "Atlas of Continental displacement from the late Triassic - Early Jurassic (200 Ma) to the present". A full explanation of the problems associated with map projections and the various hypothetical cul de sacs researchers find themselves in during research. The author argues that expansion must also involve subduction to maintain sphericity; this conclusion is bound to be controversial.

Chapter 2 deals with Cliff Ollier's memories and ideas about the expanding Earth theory, and how the Pacific Ocean is younger than Atlantic Ocean (p.109, and relates interesting anecdotes of the various expanding Earth researchers he worked with and personally knew). Ollier raises the fundamental problem of new basalt formation and dyke swarms, specifically the provenance of the various basalts and suggests dyke intrusions occurred into the crust up to the Mesozoic when sea floor spreading then starts and dyke emplacement shifted to the newly forming sea floors. Mafic dykes are essentially the infilling of extensional stress regimes in the crust which can only be caused by an inflating or expanding Earth.

Chapter 3 details Karl Heinz Jacob's ideas from a self-organising system model, and his belief that earthquakes, volcanic activity, earth expansion and electricity were interconnected. He describes the antipathy mainstream geology has to the technical challenges of plate tectonics.

Chapter 4 by James Maxlow is a well-reasoned explanation of earth expansion using geotechnical origami. It is the standard reference model though continued discoveries of new ocean floor structures will necessitate revisions of the model. As with all expanding earth hypotheses, gravity and mass formation remain problematical.

Chapter 5 - Jan Koziar presents an interesting and intriguing historical account of Earth Expansion theorising in Poland and the difficulties the author faced with geological orthodoxy. There are many references to Koziars many papers, all accessible via the internet and well as the large number of photos of the active Earth Expansion group over the years. Of interest is his criticism of Popper and Kuhn concerning scientific relativism and the emergence of scientific paradigms.

Chapter 6 - Stefan Cwojdzinski becomes a bit more philosophical and describes the development of scientific monopoly by later generations of students who were never exposed to the previous generation's ideas about contentious scientific ideas, science being about competition of ideas, not ideological monopolism. As with the other authors in this volume, he considers earth expansion requires the formation of matter in the core, since there seems to be insufficient sources of energy in the Earth to permit expansion.

Chapter 7 - Carl Strutinski traces the development of geological theory during communism in Romania and its eerie continuation under the plate tectonics mafia. The author introduces the role of weak electric fields in producing lithological layering and the associated theory Variscan orogens. Notes that variations in gravity affected the biosphere.

Chapter 8 - Stephen W. Hurrell, in which he considers the necessity for a lower value of gravity for the dinosaur problem. The author also edited the volume under review.

Chapter 9 by John B. Eichler approaches earth expansion in terms of plasma physics, but assumes a gravitational accretion model coupled with a plasma mechanism. It seems universally accepted that the gravity force has increased over time but only include mass creation inside the earth, which remains a serious problem for expansion theories.

William Erickson introduces the idea of a volumetrically pulsating Earth during which expansion results in continental drift and reduction in gravity, when dinosaurs appeared during the breakup of Pangea. The asymmetric expansion implied by the Atlantic ocean, requires subduction elsewhere to maintain the Earth's sphericity is necessary.

Chapter 11 by David Noel describes how the author was led to expanding earth model when studying the anomalous distribution of nuts or flora. This led to the notion of neutron decay and its inferred effects based on the assumption that planets might be the end product of neutron star evolution.

Chapter 12 by Khan and Tewari is a review of plate tectonics and earth expansion, in which they argue the impossibility of subduction, and that so called plate collisions cannot form subduction planes. They noted the discovery of Precambrian rocks near the crust of the Mid-Atlantic Ridge as a serious problem for plate tectonics. They also noted the latest work showing subcontinental India did not collide with the Himalayas and that floral and faunal evidence contradicts plate tectonics but is expected for expanding earth theories.

Chapter 13 - Vedat Shehu introduces the idea that the Earth's core is similar to that of the Sun, and could be extrapolated to galaxy scaled analogs. Earth expansion is thus inferred from the emittance of energy and matter from the core via plume mechanics to spreading ridges that later formed the oceans. The author sees the Earth as part of a universal expanding cosmological system.

Chapter 14 - Richard Guy, describes his observations of receding sea levels as a young man, as evidenced by the Roman roads in Wales that followed the old coast but were now 2 miles inland. In North America land splitting, and increasing area remains a problematical issue for real estate development. However the expansion rates are a lot higher than inferred by geophysical measurements.

All in all, this latest book is a timely addition to Expanding Earth theory, and it is pretty obvious our understanding of tectonics, whether global or local, remain incomplete. The book is highly recommended.

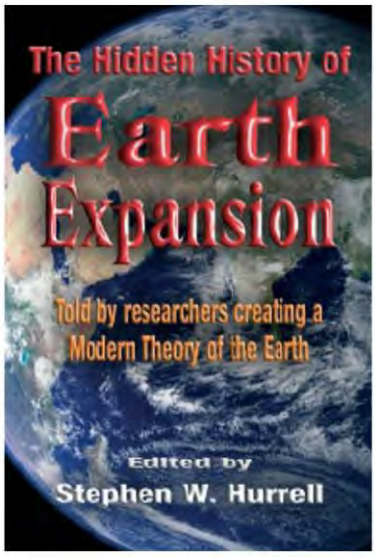

The Hidden History of Earth Expansion:
Told by researchers creating a Modern Theory of the Earth

Edited by Stephen W. Hurrell. With chapters by: Hugh G. Owen, Cliff Ollier, Karl-Heinz Jacob, James Maxlow, Jan Koziar, Stefan Cwojdziñski, Carl Strutinski, John B. Eichler, William C. Erickson, David Noel, Zahid A. Khan and Ram Chandra Tewari, Vedat Shehu and Richard Guy.

Format: Hardcover
ISBN: 9780952 26038 7
Pages: 472
Figures: 219
Publisher: Oneoff Publishing.com
Recommended Price: £28 UK, $36 US, $49 CAD, €33 EU, $55 AUS
Publication date: 14 May 2020
Available: All good bookshops worldwide, including: Amazon (UK, US, AU, CA, BR, DE, ES, FR, IN, IT, JP, NL, SG), BookDepository, Barnes&Noble, Bol.com, Buecher, Thriftbooks, Target, Hive, Alibris, Abebooks, Walmart, Fishpond, Libris, Blackwell, Waterstones, Adlibris, Booktopia, Opentrolley, Bertrand, Wook, Mercadolibre

Erratum

Pavel Kalenda, Ivo Wandrol, Karel Frydrýšek, Vítězslav Kremlík (2018): Calculation of solar energy, accumulated in the continental rocks. NCGT, Vol. 6, No.3, 347-380.

Two errors were found in the mentioned paper, published in the NCGT in 2018. Both eliminated each other and then the data analysis and results of the paper remained unchanged. Changes are highlighted by yellow:

2.2. Relationships for the heat sources on the surface (f_2)

The Earth´s crust can be thought of as a half-space. The Fourier-Kirchhoff heat equation can be used for the evaluation of the temperature distribution from the surface to the depths on condition that the half-space is homogeneous and isotropic medium, which does not contain any heat source.

Berger´s model of thermoelasticity (Berger, 1975; Kalenda, et al., 2012; Frydrýšek et al., 2012) considers elastic half-space with defined horizontal coordinates x and z, and with the vertical coordinate (depth) y. The model is designed as a 2-D model with the axes x, y, because all of the variables are symmetric with respect to the horizontal axis z. The additive surface temperature is determined by the harmonic wave with the amplitude T_0 $/K/$, the angular speed ω $/rad\ s^{-1}/$, and the wave number k $/m^{-1}/$

$$\Delta T(x,t) = T_0 e^{i(\omega t + kx)}, \qquad /8/$$

We can solve the equation for determination of the thermal field at the depth h. The x-coordinate can be neglected due to symmetry of the thermal field ($x = 0$) and for clarity, and the variable y can be changed to h. Then the thermal field can be described by the equation (see also Mareš et al., 1990)

$$\Delta T(h,t) = T_0\, e^{-h\sqrt{\frac{\omega}{2a}}} \cos\left(\omega t - h\sqrt{\frac{\omega}{2a}}\right). \qquad /9/$$

Carslaw and Jaeger (1959) derived in Chapter II (p. 50) a simplified solution of the equation for the linear heat flow. This equation can be then simplified for conducting heat from the surface as

$$\frac{dG}{dt} = a\,\frac{d^2G}{dh^2} \quad . \qquad /10/$$

where $G(h,t)$ $/K/$ is the scalar function, which describes the temperature distribution between borders of the stick or layer. The function $G(h,t)$ can be written in the form

$$G(h,t) = T_{h,t_0} + \frac{1}{2}\, c_1\, h^2\, \Delta T_{h_0,t_0} + c_2\, t\, \Delta T_{h_0,t_0} \quad , \qquad /11/$$

where c_1 $/m^{-2}/$, c_2 $/s^{-1}/$ are constants. After the substitution into /10/ we obtain

$$c_2\ \Delta T_{h_0,t_0} = a\, c_1\, \Delta T_{h_0,t_0} \quad . \qquad /12/$$

If $c_2 = a\, c_1$ is true according to /12/, then the function /11/ is the solution of /10/ and we can write

$$G(h, t+\Delta t) = G(h,t) + c_2\, \Delta t\, \Delta T_{h_0,t_0} \quad . \qquad /13/$$

The function $G(h, t+\Delta t)$ could be formally written as $G(h, t+\Delta t) \approx T_{h,t_0+\Delta t}$. If we sign $c_2\, \Delta t \approx b_h$ $/1/$, then /13/ could be written as

$$T_{h,t_0+\Delta t} = T_{h,t_0} + b_h\, \Delta T_{h_0,t_0} \quad . \qquad /14/$$

2.3. Total temperature changes at the depth *h* at the time *t*

The function f_1 at the depth h according to the equation /7/ will have a form

$$f_1(T_{h,t}, \Delta t) = \widetilde{T_h} + \Delta T_{h,t_0}\, e^{-a_h.\Delta t} \quad , \qquad /15/$$

The function f_2 will have a form according to the equation /14/. Then the relationship /1/ can be rewritten for the time $(t_0 + \Delta t)$ in the form

$$T_{h,t_0+\Delta t} = \widetilde{T_h} + \Delta T_{h,t_0}\, e^{-a_h.\Delta t} + b_h\, \Delta T_{h_0,t_0} \quad , \qquad /16/$$

where a_h $/s^{-1}/$ and b_h $/1/$ are material constants, which depend on the specific place and time increment only. They should be evaluated by the measurement.

The relationships derived above show that when the material characteristics of the environment do not change, or changes are very slow (from the calculation point of view), then the temperature changes at the depth h depend only on the temperature changes on the surface.

Based on **Figure 1** and the equation /16/ it is evident that for the time Δt, the temperature in the monitored cube at the depth h will change. The heat from the cube will transfer to the surroundings if the temperature in the cube is higher than the average temperature in the surroundings, while part of the heat difference from the surface will go to the depth h. For the calculation, it is necessary to determine the value of the coefficients a_h and b_h through the measurement of temperatures for a reasonably long period in time steps Δt.

The other Chapters, data analysis and results are not affected.

Acknowledgments

We would like to thank an unknown reviewer under the nickname "melsor" who discovered these errors.